ENHANCED CONTAMINANTS REMOVAL FOR PAPER RECYCLING BY ADSORPTION DEINKING AND NEW FLOTATION METHODS

A Dissertation
Presented to
The Academic Faculty

by

Xiaotang Du

In Partial Fulfillment
of the Requirements for the Degree
Doctor of Philosophy in the
School of Chemical & Biomolecular Engineering

Georgia Institute of Technology
August, 2017

ENHANCED CONTAMINANTS REMOVAL FOR PAPER RECYCLING BY ADSORPTION DEINKING AND NEW FLOTATION METHODS

Approved by:

Dr. Jeffery S. Hsieh, Advisor
School of Chemical & Biomolecular Engineering
Georgia Institute of Technology

Dr. Dennis W. Hess
School of Chemical & Biomolecular Engineering
Georgia Institute of Technology

Dr. Sven H. Behrens, Advisor
School of Chemical & Biomolecular Engineering
Georgia Institute of Technology

Dr. Preet Singh
School of Materials Science & Engineering
Georgia Institute of Technology

Dr. J. Carson Meredith
School of Chemical & Biomolecular Engineering
Georgia Institute of Technology

Date Approved: July 20th, 2017

To my family, friends and others who share the same values as me

求是 创新

Seeking the Truth and Pioneering New Trails

ACKNOWLEDGEMENTS

I would like to express my sincere thanks to my advisor Dr. Jeffery Hsieh for his support, advice, and significant time commitment to my research while at Georgia Tech. He is not only a Ph.D. advisor, but also a mentor for career and life. I would also like to give my special appreciation to Dr. Sven H. Behrens and Dr. J. Carson Meredith who shared the responsibilities as a thesis advisor when Dr. Jeffery Hsieh was appointed as Emeritus Professor, especially for their continuous support, inspiring input and valuable feedbacks throughout the last two years of my Ph.D. study. Finally, I would like to thank my committee members, Dr. Dennis W. Hess and Dr. Preet Singh, for committing their time to serve on my thesis committee.

I also wish to extend my thanks to my research group members. Specifically, I would like to thank Daniel T. Lee and Yi Zhang for introducing me to Dr. Jeffery Hsieh's and Dr. Sven H. Behrens's research group, respectively. Grateful thanks are also extended to all the current and former group members in the Behrens lab, Songcheng Wang, Joohyung Lee, Joana Tsao, Abiola Shitta, Maritza Mujica, Scott Essenmacher and others, the moments we spent together inside and outside the lab will be an unforgettable time for me.

I would also like to thank the undergraduate researchers who have been of great help for the past five years: Chang-Gun An, Daniel Rodriguez, Sandunie Liyanagamage, Xing Zheng, Deonte Fletcher, Ryan K. Baptiste, Jonathan C. Pang, Jin Bae, Brandan D. Brown.

I would also like to express my gratitude to my friends Jilai Ding, Tao Zhu, Yang Zhang, Ke Liu, Zhihao Ding, Ruizhi Sun, Haiwei Zhao, Miao Yu, Xu Du, Zihao Qu, Shuai Tan, my

mentors and colleagues during my internships at Kimberly Clark and Enzymatic Deinking Technologies Anita Neidert, Kaiyuan Yang, Vladimir Quinones Silva, Jianhua Ma, and my partners from consulting club and other volunteer activities Chenghao Ge, Abhirup Mukherjee, Xuetian Ma and Aida Demissie. You all have shaped me who I am today.

Lastly, I would like to express my deepest thanks and gratitude to my parents and my entire family for their endless love and support. They selflessly encouraged me to accept new challenges, explore new possibilities and pursue my dreams. This journey would not have been possible if not for them, and I dedicate this milestone to them.

TABLE OF CONTENTS

LIST OF TABLES

LIST OF FIGURES

LIST OF SYMBOLS AND ABBREVIATIONS

γ	Surface tension/Interfacial tension
θ	Contact angle
Θ	Surface coverage
Γ	Surface molar concentration
c_{eq}	Bulk concentration
D	Diffusion coefficient
r	Radius
ΔG	Desorption energy
ΔE	Energy barrier
ϕ_b	Energy barrier between particles and pristine interfaces in RSA model
ϕ_s	Energy barrier from blocking effect in RSA model
Φ	Total energy barrier in RSA model
ϕ	Energy barrier based on DLVO interactions in RSA model
ERIC	Effective residual ink concentration
EC	Ethyl cellulose

SUMMARY

Paper recycling industry is facing new challenges from contaminants that are not compatible with fiber cleaning processes. These contaminants cause problems in fiber quality and process runnability. For example, the contaminants show detrimental effect on fiber optical property and physical strength. In this thesis, two types of contaminants, hydrophilic inks and microstickies that are well known in paper industry were chosen to be studied. Compared with traditional offset inks, new generations of hydrophilic inks show long shelf life, fast turnaround, on-demand printing capabilities, and exceptional print quality. These advantages result from the submicron size, strongly negative surface charge and hydrophilic surface wettability, and all of them become disadvantages from the paper recycling perspective. For example, hydrophilic inks cannot be removed by flotation deinking because of the strong repulsion force with air bubbles, and hydrophilic surface wettability. In addition, the submicron ink particles redeposit irreversibly in the fiber lumen.

As part of my research in deinking, we developed a method to establish a quantitative understanding of the problem. Specifically, we determined which fraction of the residual in found on fiber surfaces was actually bound to the surface, and which fraction was merely redeposited there during pulping the paper formation. This is a very important step because both of them remain on fiber surfaces after pulping but with different mechanisms, and a quantitative understanding is necessary to prioritize and develop a separation strategy targeting the component that is more problematic. The method shows that about 16% of original ink is bound on the fiber surface, 32% redeposits to fiber surface, and 52% stays

in water phase as free ink after pulping, which guides us to prioritize redeposited ink over bound ink. The shift of residual ink on fiber from bound ink to redeposited ink was also observed when increasing the pulping consistency, which allows us to remove bound ink and redeposited ink simultaneously. Adsorption deinking is a potential solution for redeposited ink control because ink particles are removed from the system right after detachment from fiber surfaces, and chitosan showed a higher ink adsorption capacity than cellulose fiber, which is the fundamental reason why chitosan can adsorb ink particles in the presence of fiber. The kinetic study showed that about half of ink particles were adsorbed by chitosan within the half an hour pulping time. Finally, the efficacy of chitosan adsorption deinking was proved in paper deinking experiments and the paper ISO% Brightness was 5 points higher with a 70ppm reduction in ERIC.

After developing strategies to solve the quality problem, we then focused on methods to remove free ink particles in water phase from pulp slurry with different modifications to the standard flotation process, including electric treatment and oil-coated bubbles. The electric treatment alone induced ink agglomeration and showed high selectivity of ink over fiber through electroflotation mechanism with 20% reduction in ERIC. Graphite as the anode material showed a higher ink removal efficiency material than stainless steel because dissolved heavy metal ions from stainless steel leads to ink redeposition through electrocoagulation during electric pretreatment, and to higher yield loss during flotation. The redeposition of ink to fiber is strong and cannot be reversed by washing. However, the flotation itself showed a similar deinking efficiency as electric pretreatment followed by flotation. It is hypothesized that the ink particles removed by electric pretreatment are also

removable via traditional flotation. Thus it is important to be cautious about this problem when applying electric pretreatment.

Since the electric treatment did not show significant benefits over traditional flotation, another alternative modification to flotation, oil-coated bubble flotation, was studied fundamentally and its application in hydrophilic ink deinking was proven qualitatively. In order for a particle to adsorb on the interface, it has to diffuse to the interface, potentially overcome an energy barrier, and adsorb on the interface to from a stable contact angle. There are three fundamental benefits from oil-coated bubbles: one related to *fluid dynamics* giving oil-coated bubbles a longer residence time, one related to faster *adsorption kinetics* caused by a reduction in the energy barrier, and one related to favorable *thermodynamics* of particle adsorption resulting from the higher wetting affinity of hydrophilic particles for oil-water interfaces compared to gas-water interfaces. Particle adsorption kinetics is the focus of my study because the adsorption process is kinetically controlled due to the short life of air bubble, and the adsorption energy barrier during flotation is presumably dominated by the interactions between particles and pristine interfaces. The particle adsorption kinetics was probed by dynamic interfacial tension measurement and the early stage energy barrier was calculated by fitting kinetic models. The oil-water interface always shows faster adsorption kinetics, and a lower energy barrier than the air-water interface for all conditions studied in this thesis. Moreover, we found that *electrostatic* particle interaction with air-water and oil-water interfaces has similar magnitude, whereas nonelectrostatic interactions such as the London-van der Waals interaction with air-water and oil-water interfaces are quite different. The resulting overall difference in the energy barrier to particles adsorption at the air-water interface and oil-water interface was detected

and quantified. This finding is consistent with the theoretical prediction that the van der Waals interaction between air and particles across water is repulsive, whereas the corresponding particle-oil interaction across water is attractive. This fundamental study illustrates an alternative method to improve flotation efficiency by modifying air bubbles instead of modifying the properties of ink particles. The application of this concept in deinking was demonstrated using a custom-designed flotation cell capable of generating both oil-coated and uncoated bubbles, and a better deinking performance was observed for oil-coated bubble flotation.

A detailed study on microstickies measurement and agglomeration was also performed. Previous research on stickies was confined to deposition in the paper machine, and the deposition of stickies on cellulose fiber and its detrimental impact on paper strength was proven in this thesis. A cellulosic model surface was prepared to establish a quantitative understanding in the deposition of stickies on cellulose fibers. The effects of different polymers on the agglomeration and deposition of microstickies were investigated, and a new agglomeration method based on electric treatment was developed and it improved the screenability of microstickies by 50%.

CHAPTER 1. INTRODUCTION

1.1 Paper recycling and deinking

Recycling has been an important part of paper industry in the United States and the rest of the world for the past decades and will become more important in future years. The main goal of paper recycling is to minimize the environmental impact of the paper industry by preventing the accumulation of paper in landfills as well as reducing energy usage. Statistically, recycling one ton of paper could save 17 trees, 4000 kilowatt hours of energy (64%), 7000 gallons of water (58%) and 3.3 cubic yard of landfill space compared with producing paper from blank fiber.

More than 60% of the paper consumed in the US is recycled, and the global demand for recycled fibers is still growing at a rate 2% per year in the next decades[1]. Based on a report by Environmental Protection Agency[2], there were about 254 million tons of municipal solid waste generated in the United States in 2013 and 87 million tons of the waste were recycled which was equivalent to 34% recycling rate as shown in Figure 1-1. Among all the municipal solid waste, paper and paperboard contribute to the largest amount and account for 69 million tons (27% of all the solid waste) with 67% recycling rate. Around 46 million tons of paper and paperboard were recycled in 2013 which accounted for 50% of all recovered municipal solid waste. Thus, paper and paperboard play the most important role in both municipal waste generation and waste recovery.

Although the paper recycling rate reaches 67%, a lot of areas still need to be improved because there is a big discrepancy in recycle rate between paper from different sources. For

example, in 2015, 33.7 million tons of paperboard containers were produced with 93% recycling rate. However, in the same year 19 million tons of printing-writing papers were supplied with only 59% recycling rate. Thus, it is necessary to study the current paper recycling technology for printed paper in order to improve the paper recovery rate.

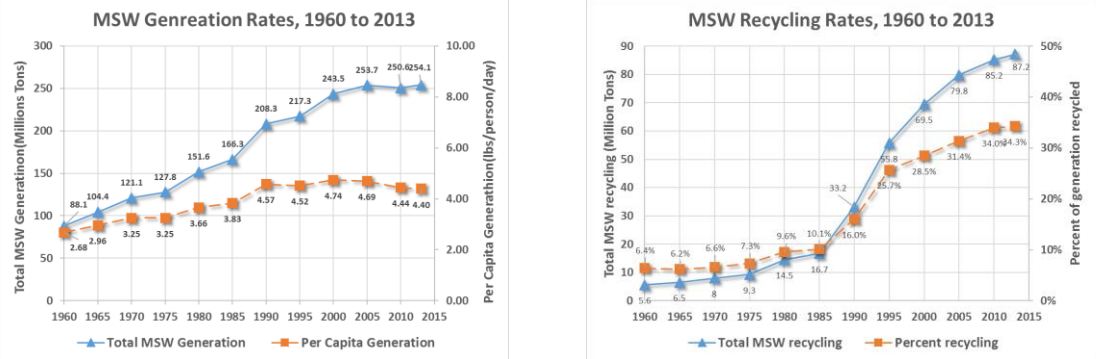

Figure 1-1 Municipal waste (left) generation (right) recycling rates from 1960 to 2013.

To make usable recycled paper products, any ink that has been printed onto the paper must be removed. There are three steps in the paper recycling process, including pulping, deinking and papermaking. During pulping, fiber networks are broken down by external mechanical force with the help of deinking chemicals. In the meantime, ink particles also detach from fiber surfaces and release to aqueous phase. The deinking chemicals include oleic acid, sodium silicate, hydrogen peroxide, sodium hydroxide, and calcium chloride.

Sodium hydroxide could swell the paper fibers and improve the ink detachment in an alkaline condition. Additionally, sodium silicate acts as a dispersant, which improves detachment of the ink from the paper fiber and prevents ink redeposition[1]. Finally, oleic acid complexes with calcium ions and acts as a coagulant to agglomerate ink particles to around 10 microns which is more suitable for separation by flotation.

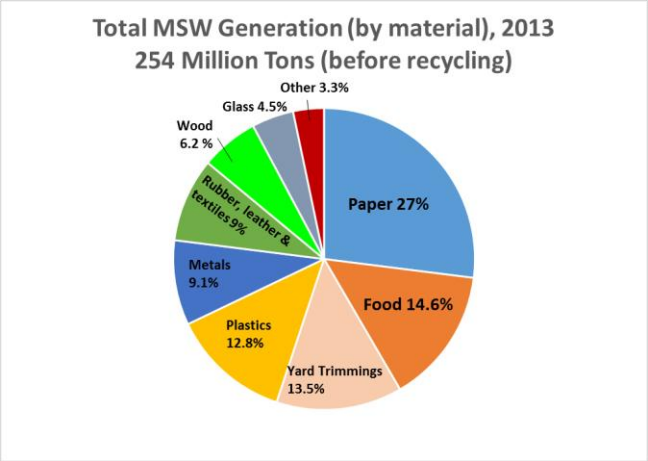

Figure 1-2 Total municipal solid waste generation by materials in 2013.

Figure 1-3 Recycling rates of selected materials in 2013.

After pulping, the pulp slurry will go through either flotation deinking or washing deinking. The purpose of deinking is to remove contaminant particles like inks or stickies released into water during pulping. Flotation process highly relies on the hydrophobicity of particles and its ability to form strong interaction with air bubbles, which are blown into the flotation cell. The air bubbles lift the inks to the surface and form a thick froth that can be removed.

The optimal particle size for flotation deinking is around 10 microns. During washing deinking, the fiber slurry is diluted to 0.02% consistency followed by thickening through a screen. This process is most useful for removing particles smaller than about 30 microns. Compared with flotation deinking, it is more effective to remove hydrophilic or small particles. However, it only has 70% yield compared with 90% yield of flotation deinking.

1.2 Hydrophilic inkjet ink deinking

Compared with traditional printing technology, inkjet printing technology with hydrophilic ink shows some advantages including fast turnaround, on-demand printing capabilities, and exceptional print quality[3-9]. In addition, hydrophilic printing inks also eliminate environmental and health concerns from the volatile organic compounds present in the solvent of traditional inks[10-11]. However, the flotation deinking operations that have worked very efficiently in the past are facing new challenges due to the increased use of hydrophilic ink printing on industrial scales, which is not compatible with flotation deinking[12]. Specifically, the gaps between hydrophilic ink properties and flotation requirements are caused by small ink particle size, hydrophilic surface property and strong surface charge, and it is important to develop a solution and bridge the gaps in order to maintain and grow the recycling levels as is desired.

1.2.1 Ink formulation, size distribution, wettability and surface charge

Ink is a complex system which is composed of solvents, pigments, resins and other additives like lubricants, surfactants. For traditional inks, the solvent is hydrocarbon which allows for good flow and drying after printing[13]. However, there is a transition to water as a new solvent for environmental and health concerns, which also sets new requirements

in pigments and resins. In order to achieve a long shelf life and good printing quality, pigment particles have to be well dispersed in the solvent. But traditional pigment particles are too hydrophobic to be stabilized in water and the pigment particles are modified by polymers like acrylic resins to solve the problem[14-15]. Although this modification could improve the stability of ink particles in water, it also causes deinking problems during paper recycling because of its small ink particle size, hydrophilic surface property and strong surface charge[16-17].

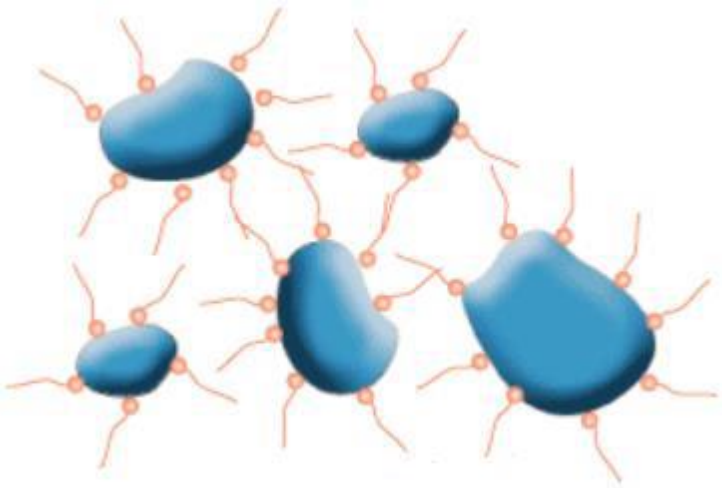

Figure 1-4 Illustration of ink pigment stabilization in hydrophilic inks.

The particle size of hydrophilic ink is 0.04 μm to 2 μm after pulping, which is much smaller than the flotation requirement 10-200 μm. This is caused by the necessity to achieve high stability during ink production and storage, and the ink particles are modified by hydrophilic polymers. As a result, the modified inks are highly dispersed and fail to agglomerate to a reasonable size for flotation during deinking operations[18-21]. Besides the tiny size of hydrophilic inks, the surface hydrophilicity and strongly negative surface charge are two other reasons why the interaction between ink particles and air bubbles is

weak[8]. For example, the zeta-potential of ink particles in alkaline condition is -40mV and there is a strong electrostatic repulsion force between ink particles and air bubbles.

These problems cause only a small amount of hydrophilic ink to be removed through the current deinking operations in recycling mills[12]. The lack of removal of hydrophilic ink reduces the quality of the final paper product due to decreased optical properties. In addition, since water loop in paper mill is closed, the inkjet ink will also accumulate in the filtrate of the mill and decease the quality of other recycled pulp, making hydrophilic ink printed paper unusable for many recycled paper products (newsprint, printing paper, etc.) [8]. Due to these concerns, recycling plants generally only accept recycled paper sources that contain little to no hydrophilic ink printed paper products[12].

1.2.2 Ink redeposition

It has been well-known that hydrophilic ink would redeposit into the fiber lumen or onto fiber surfaces[8, 22-26]. The redeposition into the fiber lumen is caused by the small size of ink particles and mainly occurs during pulping[22]. This redeposition can be eliminated by optimizing pulping conditions like time and consistency[26]. In contrast, the redeposition onto fiber surfaces occurs during paper formation and can be controlled by removing metal ions. Thus, the redeposition process can be prevented by increasing the electrostatic repulsion[23].

1.3 Current research progress in deinking

Since the invention of inkjet printing, the undeinkability of these hydrophilic inks has caused concerns, but has not been a major problem for the industry due to the very low

proportion of paper products printed using inkjet printing. However, the popularity of these printing options has increased significantly in the past decade and will continue to overtake traditional offset printing market share in the future. Because of this, there has been a large amount of research done to mitigate these issues. Some of the successful efforts include optimization of pulping conditions for hydrophilic inks[21, 27-30], neutral deinking and coagulants[25-26, 31-34], enzyme deinking[35-38], and adsorption deinking[39-44].

1.3.1 Optimization in pulping conditions

Previous researches have showed that the pulping of hydrophilic ink printed papers only requires the first few minutes and longer pulping time beyond that had a negative effect on optical properties[28-29]. The relationship between mixing energy and optical properties followed a similar trend that an increase in mechanical energy from mixing led to the redeposition of hydrophilic flexographic ink[19, 22, 26].

The optimization of the pulping conditions by reducing pulping time and decreasing pulping energy could decrease redeposition of ink in the fiber lumen, but the optimal conditions would only apply to 100% pigmented ink stocks because the optimal conditions for hydrophilic inkjet inks are inadequate for traditional inks[8, 27-29]. Thus, the operating conditions would have to be compromised between the two because the paper mills recycle a mixture of hydrophilic ink prints and offset prints, which would greatly reduce effectiveness of the technique on improving pigmented ink removal.

Fractional pulping is a newly developed technique that focused on optimizing pulping conditions of hydrophilic ink and hydrophobic ink. The pulping stage was stopped at a short interval followed by a washing step to remove hydrophilic inks. And the paper fibers

collected after washing was pulped again to make sure offset inks can be detached from fiber surfaces. This pulping-washing cycle was performed multiple times[21, 45]. Although this method could mitigate the problems in pulping conditions of recycling hydrophilic and offset inks, the deinking process requires extensive washing, leading to unacceptable yield loss[19, 32, 46-47], high water usage and high ink concentration in water[8].

1.3.2 Neutral deinking and coagulation

Both neutral deinking and coagulation focused on the methods to increase the ink size and avoid redeposition into fiber lumen. As mentioned earlier, the ink particles are anionic charged in an alkaline condition. Thus a neutral pulping condition or coagulants could decrease the electrostatic repulsion force between ink particles and increase the particle sizes[31, 48]. The filtrate darkening effect was dramatically improved because larger ink particles can be retained into fiber network easily during paper formation. However, this method not only reduced repulsion forces between ink particles, but also between ink particles and fibers. As a result, more ink particles redeposited onto the fiber surfaces[25]. In addition, neutral pulping cannot remove traditional offset ink so it is necessary to have another alkaline dispersion and flotation to remove offset ink afterwards[26, 32]. Coagulants and flocculants have also been shown to have little effect on the deinking efficiency of inkjet inks and additionally cause large increases in yield losses[24-25, 49].

1.3.3 Enzymatic deinking

There has been some success by using enzymes for deinking of different kinds of inks including inkjet inks, flexographic inks, offset inks and toners[35-36, 50-51]. There are

mainly two different mechanisms for enzymatic deinking, including hydrolysis of cellulose or hemicellulose, and decomposition of ink particles directly. For example, cellulase or hemicellulose can randomly cleave enzyme-specific cellulose bonds in order to remove ink particles that cannot be detached from fiber surfaces[52]. Another benefit of cellulase based enzyme is to free entrapped inks from fiber network by creating spaces. In contrast, lipase has been shown to hydrolyze the polymer component in toner inks and allow the pigments to detach from the fiber surface. However, the enzyme treatment efficiency is influenced by type of ink particles and substrates[37]. For example, over 85% of the toner ink was removed during enzymatic deinking operations. But less than 15% removal of the ink was achieved with the same procedure followed for offset newsprint or hydrophilic ink deinking. Thus, although very high ink removal efficiencies can be achieved in lab conditions, the ink composition is unknown in industrial applications and would be difficult to treat with this method[8, 37].

1.3.4 Adsorption deinking

Although adsorption is a widely-used technology for separation, it is still a very new idea for deinking. Adsorption deinking has been shown successful for offset inks through plastic and nylon beads[39, 44, 53], and the influence of surface tension and charge was recently studied[39-40]. For example, Ravi studied the balance between deinking chemicals and polymer beads and he found polyethylene terephthalate beads had the best newsprint deinking performance[39]. Compared with flotation deinking, this new deinking method could dramatically reduce the water consumption by 90% and energy consumption by 20%[41, 43]. However, the It is still questionable whether adsorption deinking could solve the problem of hydrophilic inkjet ink. In addition, the adsorbents separation and

regeneration are challenges for its application potential in industry. Based on previous knowledge, ink particles are negatively charged in water. Thus, adsorbents with cationic surface charge are good candidates for hydrophilic ink removal through electrostatic attraction.

1.4 Oil coated bubble for flotation

Traditional flotation technology relies on the attachment of particles to gas bubbles and the formation of particle-bubble aggregates. These aggregates rise to the surface and the froth layer is skimmed off to remove the particles from the flotation cell. Thus, the flotation process can be described by three independent steps, including the collision between particles and gas bubbles, the attachment of particles to bubbles, and the stability of the particle-bubble aggregates[54-55]. Specifically, the particle-bubble attachment process can be further divided into three steps: the thinning of the liquid film to a critical thickness, the rupture of the film and formation of the three-phase contact nucleus, and the expansion of the contact nucleus to form a stable three-phase contact line[56]. If the particles are hydrophilic like minerals or hydrophilic ink particles, the separation performance of traditional flotation process is notoriously poor, and hence at least one of the three steps to particle attachment must be impeded.

The addition of oil droplets into flotation has gained some success in the past. For example, Ralston[57-58] showed that oil droplets stabilized by polymers could effectively separate calcite particles from fine quartz gangue. Kusaka also investigated the role of isooctane in quartz fines recovery with liquid-liquid extraction process with and without the presence of surfactants[59-60]. However, due to the large amount of oil consumed during the

flotation, this is not an economical method unless the oil can be further cleaned and recycled.

1.4.1 Oily bubble flotation

In order to solve the problem of large oil consumption, a new flotation methods by air bubbles coated by a thin oil layer was invented, and the application of this novel technology in minerals separation was investigated. Liu first studied the effect of reactive oily bubbles (bubbles covered by a thin layer of oil containing oil-soluble collectors) in silica, sphalerite and galena recovery[61]. Here, the contact angle values between mineral particles and reactive oily bubbles are also much more favorable (*i.e.* closer to 90º, implying stronger attachment) than those for regular air bubbles, pointing at an improved collecting power. The foaming properties and film thickness of different organic solvent and their mixtures were studied by Tarkan[62-64]. He found that 25:75 hexadecane/heptane is the best candidate for oily bubble bitumen flotation because of the high stability of the foams. Another useful observation is the ability of a low concentration of silicone oil (3 ppm) in promoting the foam stability through solvent surface tension reduction. Su and Zhou further expanded the application of oily bubble flotation in bitumen, apatite, dolomite and bastnaesite recovery through kerosene oil with 100ppm fatty acid[65-68]. Besides its application in mineral recovery, Gomez also applied silicone oil coated air bubbles to improve the deinking efficiency[69].

Although these studies showed the higher separation performances of oil-coated bubbles in mineral flotation and deinking, the fundamental reason for this improvement has not

been understood. We are therefore motivated to study the particle adsorption kinetics on pristine air-water and oil-water interfaces.

1.4.2 Benefits of thin oil layer for particle attachment: kinetics perspective

The attachment of particles onto oil coated bubbles during flotation is similar to the formation process of Pickering emulsion, where particles adsorb to oil-water interface to stabilize emulsions. Thus, the advantages of oil coated bubble over regular bubbles during flotation are caused by the difference in particle adsorption processes between oil-water interface and air-water interface.

The thermodynamics of this adsorption process has been well understood and the energy benefit can be calculated by Equation 1.1.

$$\Delta G = -\gamma_0 \pi r^2 (1 - |\cos\theta|)^2 \quad \textbf{(1.1)}$$

In this equation, γ_0 is the surface (interfacial) tension of the pristine interface, θ is the three-phase contact angle of the particle with the fluid-fluid interface and r is the particle radius. This energy can exceed thermal energy by several orders of magnitude for large particles (>20nm) and the particles can be considered irreversibly adsorbed to the interface. If the particles are small (<5nm), the desorption energy is on the order of thermal fluctuation (kT) and the adsorption process is reversible as in the case of surfactants. However, due to the short life of bubbles during flotation, the adsorption process is kinetics controlled. Thus, it is important to study the particle adsorption kinetics at interfaces, especially the energy barrier.

1.4.2.1 Reversible adsorption kinetics models

Most of the models on particle adsorption kinetics are directly taken from surfactant adsorption kinetics, and this is valid for small particles. Comprehensive introductions to surfactant adsorption behaviors on interfaces were reviewed by Eastoe and Chang[70-71] so only a short summary is presented in this section.

The most classical quantitative model for surfactant adsorption was reported by Ward and Tordai[72]. According to this model,

$$\Gamma(t) = 2\sqrt{\frac{D}{\pi}}(c_{eq}\sqrt{t} - \int_0^t \frac{c_i(\tau)}{\sqrt{t-\tau}})d\tau) \quad \textbf{(1.2)}$$

where Γ is the molar surface concentration, c_{eq} is the bulk concentration, c_i is the concentration at the sublayer and τ is a dummy variable of integration.

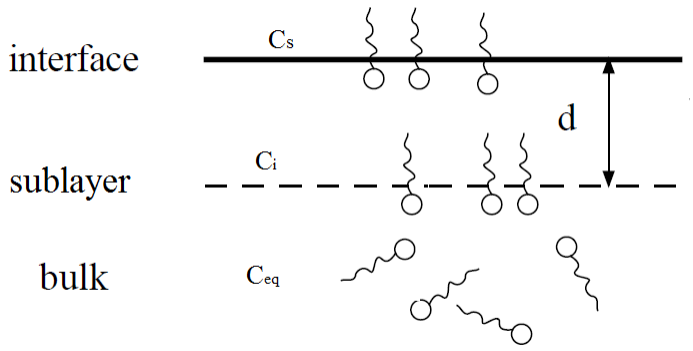

Figure 1-5 Diffusion diagram of surfactants from the bulk to the interface through a sublayer.

The first term on the right-hand side represents the diffusion of monomers from bulk to the interface, and the second term on the right-hand side shows the back diffusion. An

important assumption in this model is that the adsorption process is diffusion-controlled. Thus, the adsorption energy barrier equals zero and the time required for the solute to transfer from the bulk to the subsurface is much longer than the time required for equilibration between the surface and the subsurface. However, this equation is unsolvable due to the convolution integral in back-diffusion. So it was difficult to apply this model to surface tension profile until asymptotic solutions were developed by Fainerman[73].

At the early stage ($t \to 0$) there is no back diffusion, and the back-diffusion term thus vanishes. Equation 1.2 can be written as

$$\Gamma = 2c_{eq}\left(\frac{Dt}{\pi}\right)^{0.5} \tag{1.3}$$

At the start of adsorption, the surface coverage is low and Henry's isotherm can be applied:

$$\gamma - \gamma_0 = -nRT\Gamma \tag{1.4}$$

where n=1 for non-ionic surfactants, n=2 for ionics. Substituting Equation 1.4 into Equation 1.3 gives

$$\gamma(t) = \gamma_0 - 2RTc_{eq}\sqrt{\frac{Dt}{\pi}} \tag{1.5}$$

On the other hand, at later stage ($t \longrightarrow \infty$) the subsurface concentration is very close to the bulk concentration and $c_i(\tau)$ may be factored out of the integral. Then Equation 1.2 becomes

$$\Gamma(t) = 2\sqrt{\frac{D}{\pi}}(c_{eq}\sqrt{t} + c_i(t-\tau)^{0.5}\Big|_0^t) \quad \textbf{(1.6)}$$

Equation 1.6 can be rearranged to

$$\Delta c_{t\to\infty} = c_{eq} - c_i = \Gamma\sqrt{\frac{\pi}{4Dt}} \quad \textbf{(1.7)}$$

Combining Equation 1.7 with Gibbs equation for adsorption (Equation 1.8), the late stage approximation can be stated as Equation 1.9

$$\left(\frac{d\gamma}{d\ln c}\right)_{T,P} = -nRT\Gamma \quad \textbf{(1.8)}$$

$$\gamma(t) = \gamma_\infty + \frac{RT\Gamma_\infty^2}{c_{eq}}\sqrt{\frac{\pi}{4Dt}} \quad \textbf{(1.9)}$$

where γ_∞ is surface tension during equilibrium and Γ_∞ is the molar surface concentration at steady state.

However, in a lot of systems the species adsorption energy barrier exists and the adsorption kinetics is controlled by two processes in series. The first one is the diffusion of the species from the bulk to a sublayer and this process follows Fick's law of diffusion. The second one is the transport of the species from the sublayer to the interface.

An important study of mixed diffusion-kinetic control model has been given by Liggieri et al.[74]. They introduced an "apparent" diffusion coefficient D_{eff}, where

$$D_{eff} = D\exp(-2\frac{\Delta E}{k_B T}) \quad \textbf{(1.10)}$$

ΔE represents the adsorption energy barrier. All the other terms in Ward and Tordai (Equation 1.2) were kept the same, and the modified equations with a potential adsorption barrier is

$$\Gamma(t) = 2\sqrt{\frac{D_{eff}}{\pi}}(c_{eq}\sqrt{t} - \int_0^t \frac{c_i(\tau)}{\sqrt{t-\tau}})d\tau) \quad \textbf{(1.11)}$$

Again, this equation is unsolvable, and it is necessary to apply asymptotic solutions developed by Fainerman[73] to calculate the effective diffusion coefficient and compare it with the Stokes-Einstein diffusion coefficient to get the energy barrier.

This method has been applied extensively to study the adsorption kinetics of surfactants [75-79]; more recently, its application was extended to solid particles[80-84] and microgels[85-87]. For example, Kutuzov[83] studied the adsorption thermodynamics and kinetics of trioctylphosphine oxide (TOPO) stabilized cadmium selenide (CdSe) nanoparticles at the toluene-water interface. The effective diffusion coefficients were calculated by fitting early-stage or late-stage interfacial tension curves to Equation 1.5 or Equation 1.9, respectively. The adsorption energy barrier was obtained by comparing effective diffusion coefficient with Stokes-Einstein diffusion coefficient by Equation 1.12.

$$D_{eff} = D_{S-E}\exp(-\frac{\Delta E}{k_B T}) \quad \textbf{(1.12)}$$

He found the effective diffusion coefficients from both early stage analysis to be smaller than the diffusion coefficient from Stokes-Einstein law, and the and n coefficient from the late stage analysis to be even smaller, which is consistent with the energy barrier at the early stage of adsorption being dominated by particle-interface interactions, and the energy barrier at late stage adsorption being governed by particle-particle interactions. The values of the two energy barriers were around 1.5kT and 6kT, respectively. Ferdous[81-82] and Fang[80] also observed a shift from diffusion-controlled early stage adsorption kinetics to kinetic-controlled late stage adsorption of modified gold particles, and graphene-oxide.

1.4.2.2 Irreversible adsorption kinetics models

However, since the model was originally developed for reversible adsorption, it can only be applied to nanoparticle system where the desorption energy is in the same order of magnitude with thermal energy (kT). This is only valid for systems studied by Kutuzov and Ferdous where the particle sizes are smaller than 10nm. Bizmark[88] showed that the traditional asymptotic solutions of Ward and Tordai theory are problematic for irreversible adsorption by studying the adsorption kinetics of ethyl cellulose at air-water interface. The effective diffusion coefficient is greater than Stokes-Einstein diffusion coefficient by several orders of magnitude. They developed a new model to analyze the initial decay of surface tension, which is given by

$$\gamma(t) = \gamma_0 - 2N_A|\Delta G|c_{eq}\sqrt{\frac{Dt}{\pi}} \qquad \textbf{(1.13)}$$

The new model is identical to the classical model (Equation 1.5) if $\Delta G = k_B T$. However, if $\Delta G \gg k_B T$, the classical model will overestimate the effective diffusion coefficient,

yielding an effective diffusion coefficient far greater than the reference value from the Stokes-Einstein law. Dugyala[89]and Gyulai[90] further combined the modified model Equation 1.13 with Equation 1.12 to calculate the early stage energy barrier for particles adsorption onto fluid-fluid interfaces. Dugyala[89] investigated the adsorption kinetics of silica nanoparticles onto a decane-water interface at different salt concentrations and showed that the early stage adsorption barrier can range from 7kT to 10kT. This study proved the importance of electrostatic interactions in the adsorption kinetics especially in highly charged particle systems.

If the particle size is greater than 20nm, the desorption energy will be much greater than thermal energy which implies an irreversible adsorption. In the past decade, Adamczyk[91] developed the fundamental adsorption model based on generalized random sequential adsorption theory at solid-liquid interfaces and Bizmark[88, 92] recently expanded its application to fluid-fluid interfaces. Random sequential adsorption theory assumes that the particles are adsorbed sequentially and randomly on the free space of the interface and two adsorbed particles cannot overlap. In addition, the desorption of the adsorbed particles from the surface, and the diffusion of the adsorbed particles on the surface, are neglected in random sequential adsorption theory but are taken into consideration in generalized random sequential adsorption. In this model, the mass conservation equation for one dimensional transport can be written as

$$\frac{\partial c}{\partial t} = \frac{\partial}{\partial x}\left[D(x)\exp(-\frac{\Phi}{k_B T})\frac{\partial}{\partial x}\left[c\exp(\frac{\Phi}{k_B T}) \right] \right] \qquad \textbf{(1.14)}$$

$$\Phi = \varphi + \varphi_s \tag{1.15}$$

$$\varphi_s = -k_B T \overline{B}(\Theta) \tag{1.16}$$

The diffusion coefficient in Equation 1.14 is the position-dependent diffusion coefficient, and overall energy barrier Φ is assumed to be the summation of energy barrier ϕ based on DLVO interactions and energy barrier ϕ_s from (steric) blocking effects as in Equation 1.15. The energy barrier from blocking effect can be related to generalized blocking function $\overline{B}(\Theta)$ by Equation 1.16, where Θ is the fractional coverage of the interface.

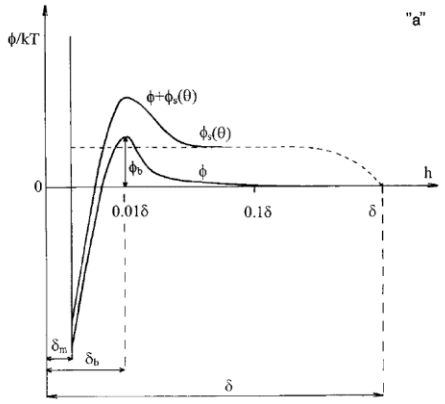

Figure 1-6 Schematic presentation of the energy profile.

The Equation 1.14 can be integrated with quasi-steady state assumption to get

$$-j = k_a c \overline{B}(\Theta) \tag{1.17}$$

$$k_a = \frac{e^{\Phi(\delta)/kT}}{\int_{\delta_m}^{\delta} \frac{e^{\phi/kT}}{D(x)} dx} \tag{1.18}$$

In Equation 1.18, δ_m is the position of the energy minimum (corresponding to interfacial particle attachment).

Then based on Equation 1.18, the mass balance for adsorbed particles on the interface gives

$$\frac{1}{S}\frac{d\Theta}{dt} = k_a c\overline{B}(\Theta) \quad \textbf{(1.19)}$$

where S is the characteristic cross section of a particle (in the case of spheres $S = \pi r^2$).

At late stage when $\Theta \to \Theta_{max}$, the generalized blocking function for spheres can be written as

$$\overline{B}(\Theta) = 2.32(1-\Theta/\Theta_{\max})^3 \quad \textbf{(1.20)}$$

Combining Equation 1.19 with Equation 1.20 and integrating gives

$$\Theta = \Theta_{\max} - \frac{K_1}{\sqrt{(\pi r^2 N_A c)^2 Dt}} \quad \textbf{(1.21)}$$

$$K_1 = \Theta_{\max}\left(\frac{\Theta_{\max} N_A c_{eq} \pi r^2 D_{S-E}}{4.64 k_a}\right)^{1/2} \quad \textbf{(1.22)}$$

Next, we can use the following two Equations to correlate Θ with γ

$$\gamma = \gamma_0 - \frac{\Theta}{\pi r^2}|\Delta G| \quad \textbf{(1.23)}$$

$$\gamma_\infty = \gamma_0 - \frac{\Theta_{\max}}{\pi r^2}|\Delta G| \quad \textbf{(1.24)}$$

Finally, we can get Equation 1.25 by combing Equation 1.22, 1.23 and 1.26 together

$$\gamma(t) = \gamma_\infty + \frac{K_1|\Delta G|}{(\pi r^2)^2 N_A c_{eq}}\sqrt{\frac{1}{Dt}} \quad \textbf{(1.25)}$$

Equation 1.25 and Equation 1.9 show the same relationship between γ and t that $\gamma \sim t^{-1/2}$ when the adsorption process is close to reach equilibrium. And it is possible to calculate K_1 and k_a based on the slope of $\gamma \sim t^{-1/2}$ plot. After that, the maximum value of the interaction energy ϕ from particle-interface DLVO interactions, ϕ_b can be approximately calculated from Equation 1.26. To summary, the overall strategy of this method to estimate the energy barrier between particles and pristine interfaces (also early stage energy barrier) is to calculate k_a from late stage slope analysis and then get ϕ_b based on Equation 1.26.

$$k_a \cong \frac{D_{S-E}}{r}\sqrt{\frac{\varphi_b}{\pi k_B T}}\exp(-\frac{\varphi_b}{k_B T}) \quad \textbf{(1.26)}$$

Bizmark[88] firstly reported this method and validated it through the adsorption of ethyl cellulose (EC) onto air-water interface. He showed that the ethyl cellulose-interface energy barrier is 3.1 $k_B T$ and 5.9$k_B T$ for 89nm and 42nm EC particles, respectively. In a later publication[92], he also proved that the EC-interface energy barrier does not change with salt concentration as long as the concentration is lower than the critical coagulation concentration of EC. This conclusion is counter-intuitive because the screening effect of salts should reduce the electrostatic interactions between particles and the interface.

Bizmark's method was also adopted by Nelson et al.[93] to study the interfacial behavior of iron oxide-poly(ethylene-glycol) at decane-water interface.

Table 1-1 Summary of recent work on particle adsorption kinetics onto fluid-fluid interfaces.

Particle	Desorption Energy (k_BT)	Type of interface	Early ΔE (k_BT)	Late ΔE (k_BT)	Ref
EC	10^4	Air-water	5.9[a]	10[d]	Bizmark[88]
PEG-Iron oxide	10^3	Water-decane	5.6-10.6[a]		Nelson[93]
Silica	45	Water-decane	8[b]	N/A	Dugyala[89]
Poly(lactic-co-glycolic acid)	10^4	Air-water Water-octane	5[b]	N/A	Gyulai[90]
TOPO-CdSe	3.3-13	Water-toluene	1.5[c]	6[d]	Kutuzov[83]
alkanethiol-capped gold	kT	Water-hexane	0.3-7.7[c]	4.6-11[d]	Ferdous[81]
alkanethiol-capped gold	kT	Water-hexane Water-nonane	Same magnitude	2-8[d]	Ferdous[82]
Graphene oxide	N/A	Water-toluene	N/A	2-5[d]	Fang[80]
Poly(NiPAAm) based microgel	Irreversible	Water-heptane	N/A	N/A	Li[85]

[a]The energy barriers were calculated from Equation 1.25 and 1.26.

[b]The energy barriers were calculated from Equation 1.12 and 1.13.

[c]The energy barriers were calculated from Equation 1.5 and 1.12.

[d]The energy barriers were calculated from Equation 1.9 and 1.12.

1.5 Microstickies measurement and agglomeration

The economic benefit of deinked pulp (DIP) over virgin pulp has increased the use of deinked pulp in manufacturing of printing and writing papers. Due to adhesives and binders used in coatings, labels and envelopes, the number of stickies in recycled fiber has increased steadily. Stickies originate from pressure sensitive adhesives, hot melts, toner, waxes, coating and binders that are used in labels, tapes, envelopes, stamps, paperboards for a variety of functions in binding, sealing, coating and printing. There is a wide variety of chemical compounds used in the formulation of PSAs, hot melts, waxes and binders. The most commonly elastomers used in PSAs are polyacrylate, styrene butadiene rubber (SBR), styrene isoprene styrene (SIS), styrene acrylate, polyvinyl acetate/acrylate (PVAc/ACRY) copolymers along with tackifiers such as rosin. Ethylene vinyl acetate (EVA) and copolymers, poly vinyl acetate (PVAc), polyethylene, polyisoprene, long chain hydrocarbons, tackifiers are major ingredients of hot melts, waxes and binders[94-95]. Except for tackifiers and certain waxes, all mentioned molecules belong to the class of synthetic polymers which are often detected in the deposits found in forming fabrics, center rolls, press section, dryers and calendar stacks.

The agglomerated stickies could lead to both paper quality losses and process failures[96]. For example, stickies could deposit onto the fibers and decrease the physical strength of paper products[97-98]. Besides, the stickies could attach to the press cans and dryer calendars and induce web breaks during papermaking processes[96]. Due to the close of water in paper mills, the build-up of stickies in recycled white water deteriorates the situation.

1.5.1 Microstickies measurement

Stickies are generally classified as either macrostickies or microstickies based on their sizes. Macrostickies refer to tacky particles retained on a laboratory screen of 100 μm or 150 μm opening. On the other hand, microstickies or colloidal stickies are hydrophobic particles that are dispersed throughout the pulp. It is well known that microstickies tend to agglomerate and deposit on the paper machine after changes in the environment, including pH, temperature and polyelectrolyte concentration.

Microstickies measurement methods are not well established. Most evaluation methods of microstickies can be divided into two categories, indirect measurements and direct measurements[99]. Indirect methods focus on measuring the total amount of microstickies in the system. These indirect methods include the thermogravimetric method[100], IPST method (total organic carbon content)[101], chemical oxygen demand[102-103], solvent extraction methods followed by FTIR[95], high pressure liquid chromatography[104], size exclusion columns[104], evaporating solvent light scattering detector[104], pyrolysis-gas chromatography-mass spectrometry method[105], turbidity difference method[106], and head-gas chromatography method[107]. Most of these methods could provide quantitative

evaluation on both microstickies amount and composition. However, these indirect methods are not based on the deposition phenomenon.

On the other hand, direct measurements mainly focus on the deposition tendency of microstickies. The surfaces used for deposition include LDPE[108-112], HDPE[109-111], machine wire[109-111, 113-114], polypropylene[115], polyamide[115], PET[115], etc. Image analysis combined with deposition could estimate the accumulation of deposits and the size of specks.

1.5.2 Microstickies agglomeration and removal

There are several methods in terms of paper mill stickies removal through chemical methods[116-121], physical methods[98, 122]. For chemical methods, there are two different mechanisms for stickies control, including adsorption removal[117] and chemical fixation[123]. Both talc and bentonite have plate structure with hydrophobic faces with hydrophilic edges which facilitates a strong interaction with hydrophobic stickies and results in stickies deposition onto their hydrophobic surfaces. On the other hand, cationic polymers including poly-diallyldimethylammonium chloride, poly-aluminum chloride and cationic starch remove stickies by fixing them onto fibers in order to remove stickies from the water system.

Secondly, physical methods include flotation[124], stickies agglomeration[122], heat dispersing[125]. Dissolved air flotation is a common used method to clean process water in papermill and it is an effective method when combined with flocculants and coagulants[123]. In addition, it has also been shown that physical agitations like

temperature elevation, shear force and bubbles could agglomerate microstickies and improve their removal efficiency through screening.

However, the current technologies are still unable to solve the problems. For example, the residual chemicals added into the paper mill could accumulate in the water and cause serious issues. In addition, the chemicals could also affect the forming and drying of paper products. Furthermore, in terms of the non-chemical methods, temperature elevation is energy intensive due to the high heat capacity of water. Finally, both shear force and bubbles could agglomerate microstickies in a fiber free system, but could not coagulate microstickies efficiently in the presence of fibers.

1.6 Thesis motivations and objectives

The fiber cleaning is the most important process for paper recycling and the industry is facing new challenges from hydrophilic inks and microstickies. Both of them cause fiber quality problems and paper machine runnability problems. The current research addresses the two problems separately with focus in deinking as shown in Figure 1-7. The objectives of research in deinking include

(a) Develop a quantitative method to categorize inks based on their behavior during pulping
(b) Improve the pulping process by adsorption deinking to reduce the residual ink amount on fiber
(c) Study advanced flotation methods to improve the ink particles removal from water and pulp slurry with low consistency

Besides deinking, the current research also investigates the microstickies problems by (a) detection the deposition of microstickies on fiber surfaces and (b) agglomeration of microstickies to improve the separation efficiency.

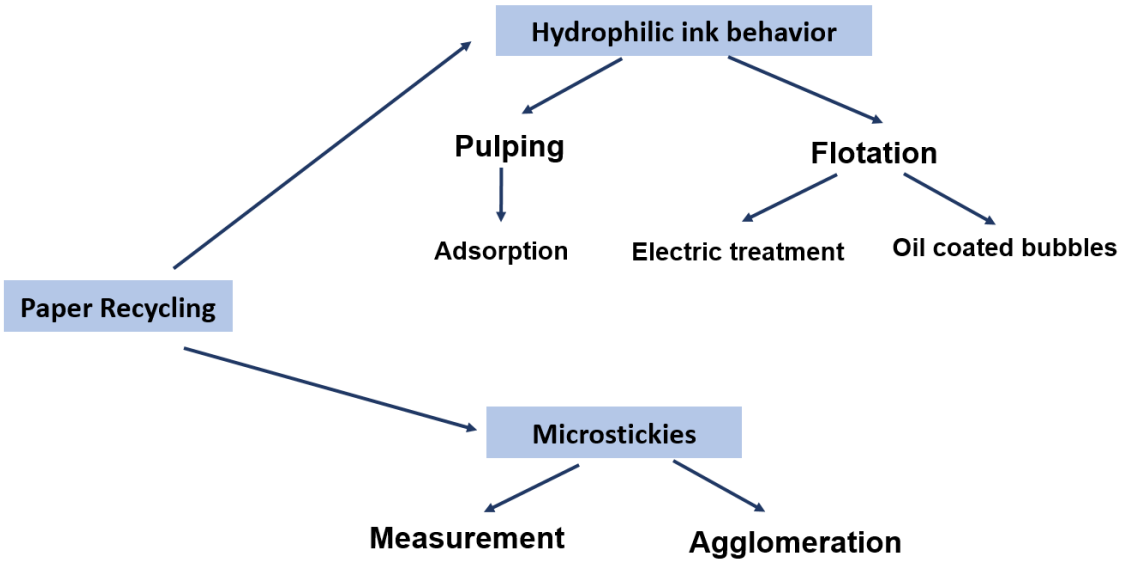

Figure 1-7 Summary of the research objectives in deinking and microstickies removal.

1.7 Thesis outline

Chapter 2 presents a novel method to distinguish bound ink, redeposited ink and free ink and studies the adsorption deinking by chitosan during pulping.

Chapter 3 studies the effect of electric treatment on hydrophilic ink flotation deinking and washing deinking.

Chapter 4 investigates the method to detect the difference in particle adsorption kinetics between oil-water interface and air-water interface, which is a fundamental evidence to

prove the benefit of oil-coated bubble flotation, and demonstrates the efficacy of oil-coated bubble flotation in hydrophilic ink deinking through a house-made flotation device.

Chapter 5 shows the deposition of microstickies on cellulose fibers and prepares a model cellulose surface to quantify the deposition amount under different agitation methods.

Chapter 6 explores the effect of chemicals on microstickies stability and the agglomeration of microstickies by external electric treatment.

Chapter 7 summarizes primary conclusions from the research projects and provides recommendations for future study.

1.8 References

[1] Dorris, G.; Ben, Y.; Richard, M., Overview of flotation deinking. *Progress in paper recycling* **2011,** *20* (1), 3-42.

[2] Agency, U. S. E. P., Advancing sustainable materials management: 2013 fact sheet. 2015.

[3] Carre, B.; Magnin, L. In *Digital prints: a survey of the various deinkability behaviours*, Pulp and Paper Technical Association of Canada: 2004; pp 159-169.

[4] Fischer, A., Inkjet head towards ecological dead end. *Recycling Magazine* **2008,** (5), 8-15.

[5] Fischer, A.; Is, *What makes a digital print recyclable? Results of a European survey*. 2006; p 514-516.

[6] Hodgson, K. T., Deinking considerations with flexographic wastepaper. *Prog. Pap. Recycl.* **1996,** *5* (3), 71-74.

[7] Klass, C. P., Will ink jet papers become a deinking nightmare? *Paper360* **2009,** *4* (1), 10-13.

[8] Ben, Y.; Dorris, G., Is deinkability of inkjet prints an issue? *Tappi Journal* **2011,** *10* (10), 17-27.

[9] Dorris, G.; Ben, Y. In *Is there an easy solution to the deinking of water-based inks*, PTS-CTP Deinking Symposium, 1998; pp 1-10.

[10] Aksoy, H.; Yilmaz, S.; Celik, M.; Yuzbasioglu, D.; Unal, F., Genotoxicity study in lymphocytes of offset printing workers. *J. Appl. Toxicol.* **2006,** *26* (1), 10-15.

[11] Philippe, I. J. In *Effective flotation deinking of ONP with increasing levels of flexographic print*, TAPPI Pulping Conference, TAPPI Press: 1996; pp 805-810.

[12] Yarnell, A., Rethinking Deinking. *Chem. Eng. News* **2011,** *89* (31), 42-44.

[13] Sabin, P.; Benjelloun-Miayah, B.; Delmas, M., Offset printing inks based on rapeseed oil and sunflower oil. Part II: varnish and ink formulation. *Journal of the American Oil Chemists' Society* **1997,** *74* (10), 1227-1233.

[14] Husovska, V. Investigation of recycled paper deinking mechanisms. West Michigan University, 2013.

[15] Fernandez, E. O.; Hodgson, K. T., Stabilization mechanisms of water-based newsprint inks. *Journal of pulp and paper science* **1996,** *22* (11), J452-J456.

[16] Carre, B.; Magnin, L.; Galland, G. In *Printing processes and deinkability*, IPW. International paperworld, 2004; pp 41-45.

[17] Oittinen, P.; Saarelma, H., Electronic Printing. In *Papermaking Science and Technology, Book 7: Recycled Fiber and Deinking*, Ltd., F., Ed. Helsinki, 2000; pp 173-191.

[18] Carre, B.; Magnin, L.; Galland, G.; Vernac, Y., Deinking difficulties related to ink formulation, printing process, and type of paper. *Tappi Journal* **2000,** *83* (6), 60.

[19] Dumea, N.; Lado, Z.; Poppel, E., Differences in the recycling behaviour of paper printed by various techniques. *Cellulose Chemistry & Technology* **2009,** *43* (1), 57-64.

[20] Faul, A.; Oberndorfer, J., The challenge to deink inkjet prints together with recovered paper from households. In *TAPPI PEERS Conference*, TAPPI: Norfolk, VA, 2010.

[21] Kemppainen, K.; Körkkö, M.; Niinimäki, J., Fractional pulping of toner and pigment-based inkjet ink printed papers-ink and dirt behavior. *BioResources* **2011,** *6* (3), 2977-2989.

[22] Ben, Y.; Dorris, G., Irreversible ink redeposition during repulping. Part II: ONP/OMG furnishes. *Journal of pulp and paper science* **2000,** *26* (8), 289-293.

[23] Ben, Y.; Pelton, R.; Dorris, G., Retention and dislodgement of flexographic ink in a fibrous mat during thickening and displacement washing. *Journal of pulp and paper science* **1996,** *22* (11), J411-J419.

[24] Dorris, G.; Nguyen, N., Flotation of model inks. II: Flexo ink dispersions without fibres. *Journal of pulp and paper science* **1995,** *21* (2), J55-J62.

[25] Galland, G.; Carre, B.; Rousset, X.; Vernac, Y. In *Deinking difficulties related to waterbased ink printed papers analysis of redeposition phenomena*, TAPPI Recycling Symposium, TAPPI PRESS: 2000; pp 503-516.

[26] Galland, G.; Vernac, Y.; Carré, B.; Rousset, X. In *Effect of pulping conditions on ink redeposition and ink removal when recycling waterbased ink printed papers*, Proc Pulping Conf. Atlanta GA, TAPPI press, 2001.

[27] Ben, Y.; Dagenais, M.; Dorris, G., Irreversible ink redeposition during repulping. Part I: Model deinking systems. *Journal of pulp and paper science* **2000,** *26* (3), 83-89.

[28] Bennington, C. P.; Wang, M.-H., A kinetic model of ink detachment in the repulper. *Journal of pulp and paper science* **2001,** *27* (10), 347-352.

[29] Fabry, B.; Carré, B.; Cremon, P. In *Pulping optimisation: Effect of pulping parameters on defibering, ink detachment and ink removal*, Conf. Proc. of 6th Research forum on recycling, 2001; pp 37-44.

[30] Miller, N., Sustainable Digital Print Solutions: Deinkable Inks, Papers, and Optimized Deinking Processes. *Proceedings PaperCon* **2009,** *9*.

[31] Bhattacharyya, M. K.; Ng, H. T.; Mittelstadt, L. S.; Hanson, E. G., Deinking of digital prints: effect of near-neutral deinking chemistry on deinkability. *Journal of Imaging Science and Technology* **2012,** *56* (6), 60503-1-60503-5.

[32] Galland, G.; Vernac, Y.; Carre, B., The advantages of combining neutral and alkaline deinking, Part I: Comparison of deinking of offset and flexo printed paper. *Pulp & Paper Canada* **1997,** *98* (6), 46-49.

[33] Korkko, M.; Bussini, D.; Laitinen, O.; Elegir, G.; Niinimaki, J., True-neutral fractional deinking for flexographic and offset newsprints. *Appita Journal: Journal of the Technical Association of the Australian and New Zealand Pulp and Paper Industry* **2012,** *65* (1), 71.

[34] Morrow, H.; Horacek, B.; Hale, K.; Rosencrance, S., True-neutral deinking. *Paper Age* **2005,** *121*, 34-35.

[35] Das, A.; Paul, T.; Halder, S. K.; Jana, A.; Maity, C.; Mohapatra, P. K. D.; Pati, B. R.; Mondal, K. C., Production of cellulolytic enzymes by Aspergillus fumigatus ABK9 in wheat bran-rice straw mixed substrate and use of cocktail enzymes for deinking of waste office paper pulp. *Bioresource technology* **2013,** *128*, 290-296.

[36] Heise, O. U.; Unwin, J. P.; Klungness, J. H.; Fineran, W. G.; Sykes, M.; Abubakr, S., Industrial scaleup of enzyme-enhanced deinking of nonimpact printed toners. *Tappi Journal* **1996,** *79* (3), 207-212.

[37] Lee, C. K.; Ibrahim, D.; Omar, I. C., Enzymatic deinking of various types of waste paper: Efficiency and characteristics. *Process Biochemistry* **2013,** *48* (2), 299-305.

[38] Nyman, K.; Hakala, T., Decolorization of inkjet ink and deinking of inkjet-printed paper with laccase-mediator system. *BioResources* **2011,** *6* (2), 1336-1350.

[39] Ravi, K.; Schrinner, T.; Grossmann, H.; Ray, A.; Tandon, R., Improving adsorption deinking by identifying the optimum balance between polymer beads and deinking chemistry. *BioResources* **2016,** *11* (1), 1664-1671.

[40] Petzold, G.; Schwarz, S., Investigation of an improved deinking process of waste paper–The influence of surface tension and charge in suspension on ink removal. *Colloids and Surfaces A: Physicochemical and Engineering Aspects* **2015,** *480*, 398-404.

[41] Handke, T.; Großmann, H. Verfahren zum Recycling von Altpapier Method for recycling waste paper. DE102012204203 B4, 2014.

[42] Schwarz, S.; Petzold, G.; Oelmann, M. Cleaning particles from waste paper recycling process, involves introducing particle having impurities on its surface to water, and adding surfactant material before, simultaneously or after introducing step and then realizing energy input. DE102012208219 A1, 2013.

[43] Handke, T.; Schrinner, T.; Grossmann, H., Adsorptionsdeinking Ein neues Konzept zur Druckfarbenentfernung. *Wochenbl.für Pap.(WfP)* **2011**, 1-6.

[44] Wasmund, B.; Pelton, R., Model deinking studies: carbon black removal by oil-coated plastic pellets. *Tappi journal* **1994,** *77* (7), 152-156.

[45] Kemppainen, K.; Körkkö, M.; Haapala, A.; Illikainen, M.; Niinimäki, J. In *Benefits of Fractionation during pulping in Deinking*, TAPPI Peers Conference and 9th Research Forum on Recycling, Norfolk, Virginia, USA, 2010.

[46] Hsieh, J. S., Deinking of inkjet digital nonimpact printing. *Tappi Journal* **2012,** *11* (9), 9-15.

[47] Josephson, W. E.; Krishnagopalan, G. A., Deinking of furnishes containing flexographically printed old newsprint. *Appita Journal: Journal of the Technical Association of the Australian and New Zealand Pulp and Paper Industry* **2005,** *58* (6), 470.

[48] Bobu, E.; Ciolacu, F., Evaluation of neutral deinking methods in processing different printed papers. *Cellulose Chemistry and Technology* **2008,** *42* (7-8), 403-412.

[49] Ng, H. T.; Bhattacharyya, M. K.; Mittelstadt, L. S.; Hanson, E. G. In *Deinking of HP Digital Commercial Prints: Effect of Chemicals and Their Loadings on Deinkability*, NIP & Digital Fabrication Conference, Society for Imaging Science and Technology: 2009; pp 173-176.

[50] Bajpai, P., Application of enzymes in the pulp and paper industry. *Biotechnol. Prog.* **1999,** *15*, 147-157.

[51] Jeffries, T. W.; Klungness, J. H.; Sykes, M. S.; Rutledge-Cropsey, K. R., Comparison of enzyme-enhanced with conventional deinking of xerographic and laser-printed paper. *Tappi J.* **1994,** *77*, 173-9.

[52] Jeffries, T. W.; Patel, R. N.; Sykes, M. S.; Klungness, J., Enzymic solutions to enhance bonding, bleaching and contaminant removal. *Mater. Res. Soc. Symp. Proc.* **1992,** *266*, 277-87.

[53] Muvundamina, M.; Liu, J., Role of polymers in deinking mixed paper. *Tappi journal* **1997,** *80* (11), 172-178.

[54] Dai, Z.; Fornasiero, D.; Ralston, J., Particle–bubble attachment in mineral flotation. *J. Colloid Interface Sci.* **1999,** *217* (1), 70-76.

[55] Dai, Z.; Fornasiero, D.; Ralston, J., Particle–bubble collision models—a review. *Adv. Colloid Interface Sci.* **2000,** *85* (2), 231-256.

[56] Albijanic, B.; Ozdemir, O.; Nguyen, A. V.; Bradshaw, D., A review of induction and attachment times of wetting thin films between air bubbles and particles and its relevance in the separation of particles by flotation. *Adv. Colloid Interface Sci.* **2010,** *159* (1), 1-21.

[57] Kent, W.; Ralston, J., Polymer-stabilized emulsions and fine-particle recovery, II. The chalcopyrite-quartz system. *International journal of mineral processing* **1985,** *14* (3), 217-232.

[58] Ralston, J.; Kent, W.; Newcombe, G., Polymer-stabilized emulsions and fine-particle recovery, I. The calcite-quartz system. *International journal of mineral processing* **1984,** *13* (3), 167-186.

[59] Kusaka, E.; Kamata, Y.; Fukunaka, Y.; Nakahiro, Y., The role of hydrolyzed metal cations in the liquid-liquid extraction of ultrafine silica with dodecyl sulfate. *Minerals engineering* **1997,** *10* (2), 155-162.

[60] Kusaka, E.; Nakahiro, Y.; Wakamatsu, T., The role of zeta potentials of oil droplets and quartz particles during collectorless liquid-liquid extraction. *International journal of mineral processing* **1994,** *41* (3-4), 257-269.

[61] Liu, J.; Mak, T.; Zhou, Z.; Xu, Z., Fundamental study of reactive oily-bubble flotation. *Minerals engineering* **2002,** *15* (9), 667-676.

[62] Tarkan, H.; Bayliss, D.; Finch, J., Investigation on foaming properties of some organics for oily bubble bitumen flotation. *International Journal of Mineral Processing* **2009,** *90* (1), 90-96.

[63] Tarkan, H.; Finch, J., Air-assisted solvent extraction: towards a novel extraction process. *Minerals engineering* **2005,** *18* (1), 83-88.

[64] Tarkan, H.; Finch, J., Foaming properties of solvents for use in air-assisted solvent extraction. *Colloids and Surfaces A: Physicochemical and Engineering Aspects* **2005,** *264* (1), 126-132.

[65] Su, L.; Xu, Z.; Masliyah, J., Role of oily bubbles in enhancing bitumen flotation. *Minerals Engineering* **2006,** *19* (6), 641-650.

[66] Zhou, F.; Wang, L.; Xu, Z.; Liu, Q.; Chi, R., Reactive oily bubble technology for flotation of apatite, dolomite and quartz. *International Journal of Mineral Processing* **2015,** *134*, 74-81.

[67] Zhou, F.; Wang, L.; Xu, Z.; Liu, Q.; Deng, M.; Chi, R., Application of reactive oily bubbles to bastnaesite flotation. *Minerals Engineering* **2014,** *64*, 139-145.

[68] Zhou, F.; Wang, L.; Xu, Z.; Ruan, Y.; Zhang, Z.; Chi, R., Role of reactive oily bubble in apatite flotation. *Colloids and Surfaces A: Physicochemical and Engineering Aspects* **2017,** *513*, 11-19.

[69] Gomez, C.; Acuna, C.; Finch, J.; Pelton, R., Aerosol-enhanced flotation deinking of recycled paper: Silicone oil offers an effective way of forming a layer on the bubble surface. *Pulp & Paper Canada* **2001,** *102* (10), 28-30.

[70] Chang, C.-H.; Franses, E. I., Adsorption dynamics of surfactants at the air/water interface: a critical review of mathematical models, data, and mechanisms. *Colloids and Surfaces A: Physicochemical and Engineering Aspects* **1995,** *100*, 1-45.

[71] Eastoe, J.; Dalton, J., Dynamic surface tension and adsorption mechanisms of surfactants at the air–water interface. *Adv. Colloid Interface Sci.* **2000,** *85* (2), 103-144.

[72] Ward, A.; Tordai, L., Time‐dependence of boundary tensions of solutions I. The role of diffusion in time‐effects. *The Journal of Chemical Physics* **1946,** *14* (7), 453-461.

[73] Fainerman, V.; Makievski, A.; Miller, R., The analysis of dynamic surface tension of sodium alkyl sulphate solutions, based on asymptotic equations of adsorption kinetic theory. *Colloids and Surfaces A: Physicochemical and Engineering Aspects* **1994,** *87* (1), 61-75.

[74] Liggieri, L.; Ravera, F.; Passerone, A., A diffusion-based approach to mixed adsorption kinetics. *Colloids and surfaces A: physicochemical and engineering aspects* **1996,** *114*, 351-359.

[75] Chaverot, P.; Cagna, A.; Glita, S.; Rondelez, F., Interfacial tension of bitumen− water interfaces. Part 1: Influence of endogenous surfactants at acidic pH. *Energy Fuels* **2007,** *22* (2), 790-798.

[76] Eastoe, J.; Dalton, J. S.; Rogueda, P. G.; Crooks, E. R.; Pitt, A. R.; Simister, E. A., Dynamic surface tensions of nonionic surfactant solutions. *J. Colloid Interface Sci.* **1997,** *188* (2), 423-430.

[77] Eastoe, J.; Dalton, J. S.; Rogueda, P. G.; Griffiths, P. C., Evidence for Activation− Diffusion Controlled Dynamic Surface Tension with a Nonionic Surfactant. *Langmuir* **1998,** *14* (5), 979-981.

[78] Pei, X.; You, Y.; Zhao, J.; Deng, Y.; Li, E.; Li, Z., Adsorption and aggregation of 2-hydroxyl-propanediyl-α, ω-bis (dimethyldodecyl ammonium bromide) in aqueous solution: effect of intermolecular hydrogen-bonding. *J. Colloid Interface Sci.* **2010,** *351* (2), 457-465.

[79] Casandra, A.; Ismadji, S.; Noskov, B. A.; Liggieri, L.; Lin, S.-Y., A study on the method of short-time approximation–Criteria for applicability. *International Journal of Heat and Mass Transfer* **2015,** *90*, 752-760.

[80] Fang, S.; Chen, T.; Chen, B.; Xiong, Y.; Zhu, Y.; Duan, M., Graphene oxide at oil-water interfaces: Adsorption, assembly & demulsification. *Colloids and Surfaces A: Physicochemical and Engineering Aspects* **2016,** *511*, 47-54.

[81] Ferdous, S.; Ioannidis, M. A.; Henneke, D., Adsorption kinetics of alkanethiol-capped gold nanoparticles at the hexane–water interface. *Journal of Nanoparticle Research* **2011,** *13* (12), 6579-6589.

[82] Ferdous, S.; Ioannidis, M. A.; Henneke, D. E., Effects of temperature, pH, and ionic strength on the adsorption of nanoparticles at liquid–liquid interfaces. *Journal of Nanoparticle Research* **2012,** *14* (5), 850.

[83] Kutuzov, S.; He, J.; Tangirala, R.; Emrick, T.; Russell, T.; Böker, A., On the kinetics of nanoparticle self-assembly at liquid/liquid interfaces. *Physical Chemistry Chemical Physics* **2007,** *9* (48), 6351-6358.

[84] Rane, J. P.; Harbottle, D.; Pauchard, V.; Couzis, A.; Banerjee, S., Adsorption kinetics of asphaltenes at the oil–water interface and nanoaggregation in the bulk. *Langmuir* **2012,** *28* (26), 9986-9995.

[85] Li, Z.; Geisel, K.; Richtering, W.; Ngai, T., Poly (N-isopropylacrylamide) microgels at the oil–water interface: adsorption kinetics. *Soft Matter* **2013,** *9* (41), 9939-9946.

[86] Li, Z.; Harbottle, D.; Pensini, E.; Ngai, T.; Richtering, W.; Xu, Z., Fundamental study of emulsions stabilized by soft and rigid particles. *Langmuir* **2015,** *31* (23), 6282-6288.

[87] Wu, Y.; Wiese, S.; Balaceanu, A.; Richtering, W.; Pich, A., Behavior of temperature-responsive copolymer microgels at the oil/water interface. *Langmuir* **2014,** *30* (26), 7660-7669.

[88] Bizmark, N.; Ioannidis, M. A.; Henneke, D. E., Irreversible adsorption-driven assembly of nanoparticles at fluid interfaces revealed by a dynamic surface tension probe. *Langmuir* **2014,** *30* (3), 710-717.

[89] Dugyala, V. R.; Muthukuru, J. S.; Mani, E.; Basavaraj, M. G., Role of electrostatic interactions in the adsorption kinetics of nanoparticles at fluid-fluid interfaces. *Physical Chemistry Chemical Physics* **2016,** *18* (7), 5499-5508.

[90] Gyulai, G.; Kiss, É., Interaction of poly (lactic-co-glycolic acid) nanoparticles at fluid interfaces. *Journal of Colloid and Interface Science* **2017,** *500*, 9-19.

[91] Adamczyk, Z., Kinetics of diffusion-controlled adsorption of colloid particles and proteins. *J. Colloid Interface Sci.* **2000,** *229* (2), 477-489.

[92] Bizmark, N.; Ioannidis, M. A., Effects of ionic strength on the colloidal stability and interfacial assembly of hydrophobic ethyl cellulose nanoparticles. *Langmuir* **2015,** *31* (34), 9282-9289.

[93] Nelson, A.; Wang, D.; Koynov, K.; Isa, L., A multiscale approach to the adsorption of core–shell nanoparticles at fluid interfaces. *Soft matter* **2015,** *11* (1), 118-129.

[94] Hsu, N. N.; Schroeck, J. J.; Errigo, L., Identification of the origins of stickies in deinked pulp. *Tappi journal (USA)* **1997**.

[95] Johansson, H.; Wikman, B.; Lindstrom, E.; Osterberg, F., Detection and evaluation of micro-stickies. *Progress in paper recycling* **2003,** *12* (2), 4-12.

[96] Blanco Suárez, Á.; Miranda Carreño, R.; Negro Álvarez, C. M.; García Suárez, C.; García-Prol, M.; Sánchez, Á., Full characterization of stickies in a newsprint mill: the need for a complementary approach. *Tappi Journal* **2007,** *6* (1), 19-25.

[97] Francis, D.; Ouchi, M., Effect of dissolved and colloidal solids on newsprint properties. *Journal of Pulp and Paper Science* **2001,** *27* (9), 289-295.

[98] Du, X.; Hsieh, J. S., Analytical measurement of microstickies on fibers by model surfaces. *Nordic Pulp & Paper Research Journal* **2014,** *29* (2), 232-239.

[99] Goto, S.; Tsuji, H.; Iimori, T. In *A new method for measuring deposition of microstickies using QCM-D technique*, TAPPI 8 th Research Forum on Recycling, 2007; pp 23-26.

[100] Castro, C.; Dorris, G. M.; Brouillette, F.; Daneault, C., Thermogravimetric determination of synthetic polymers in recycled pulp systems and deposits. *Journal of Pulp and Paper Science* **2003,** *29* (5), 167-172.

[101] Haynes, R., Measurement of micro stickies formation. *Progress in Paper Recycling* **2003,** *12* (2), 19-26.

[102] Doshi, M. R.; Blanco, A.; Negro, C.; Dorris, G. M.; Castro, C. C.; Hamaan, A.; Haynes, R. D.; Houtman, C.; Scallon, K.; Putz, H. J.; Johansson, H.; Venditti, R. A., Comparison of microstickies measurement methods Part I: Sample preparation and measurement methods. *Progress in Paper Recycling* **2003,** *12* (4), 35-42.

[103] Doshi, M. R.; Blanco, A.; Negro, C.; Monte, C.; Dorris, G. M.; Castro, C. C.; Hamann, A.; Haynes, R. D.; Houtman, C.; Scallon, K., Comparison of microstickies measurement methods. Part II, Results and discussion. *Progress in Paper Recycling* **2003,** *13* (1), 44-53.

[104] Sarja, T.; MacNeil, D.; Künzel, U. In *Addressing the nature of stickies in deinked pulp*, Proc. 2006 TAPPI Engineering, Pulping and Environmental Conference, 2006; pp 5-8.

[105] Wang, Z.-W.; Li, B.; Wu, S.-B.; Lu, P., Physicochemical properties analysis and size distribution research of microstickies in whitewater. *BioResources* **2012,** *7* (4), 5794-5808.

[106] Sarja, T.; Zabihian, M.; Kourunen, P.; Niinimäki, J., New method for measuring potential secondary stickies in deinked pulp filtrates. *Water Sci. Technol.* **2004,** *50* (3), 207-215.

[107] Chai, X.; Samp, J.; Yang, Q.; Song, H.; Zhu, J.; Zhu, J.; Vahey, D. W.; Scott, C. T.; Myers, G. C.; Zhu, J., Determination of microstickies in recycled whitewater by headspace gas chromatography. *Progress in paper recycling* **2007,** *16* (3), 12.

[108] Elsby, L. In *Experiences from tissue and board production using stickies additives*, Pulping Conference, 1986; pp 187-191.

[109] Doshi, M.; Dyer, J.; Aziz, S.; Jackson, K.; Abubakr, S., Quantification of micro stickies. *Paper Recycling Challenge-Process Control&Measurement* **1997**, 119-122.

[110] Doshi, M.; DyerJ, A., Optimization of a stickies deposits testing procedure. *ProgPaperRecycling* **1998,** *8* (1), 65-68.

[111] Dyer, J.; Doshi, M., Micro stickies quantification. *Paper Recycling Challenge Ⅳ* **1999**, 101-102.

[112] Turrado, S.; Gonzalez, T.; Vazquez, C.; Saucedo, C.; Perez, R., Contaminant (stickies) content procedure. *Progress in Paper Recycling* **1999,** *8*, 80-82.

[113] Cathie, K.; Haydock, R.; Dias, I., Understanding the fundamental factors influencing stickies formation and deposition. *Pulp & Paper-Canada* **1992,** *93* (12), 157-159.

[114] Venditti, R.; Chang, H.; Jameel, H., Overview of stickies research at North Carolina State University. *PaperAge* **1999,** *115* (11), 18-20.

[115] Krauthauf, T.; Putz, H. J. In *Forced adsorption contact-a new way of stciky evaluation in recycled pulps*, TAPPI Papermakers Conference, Atlanta, Georgia, Atlanta, Georgia, 1999; pp 661-668.

[116] Brouillette, F.; Chabot, B.; Daneault, C. In *Comparison of the modes of action of stickies control chemicals in ONP/OMG deinked pulp*, 59th Appita Annual Conference and Exhibition: Incorporating the 13th ISWFPC (International Symposium on Wood, Fibre and Pulping Chemistry), Auckland, New Zealand, 16-19 May 2005: Proceedings, Appita Inc.: 2005; p 45.

[117] Hubbe, M. A.; Rojas, O. J.; Venditti, R. A., Control of tacky deposits on paper machines-A review. *Nordic Pulp and Paper Research Journal* **2006,** *21* (2), 154.

[118] Krentz, D. O.; Lohmann, C.; Schwarz, S.; Bratskaya, S.; Liebert, T.; Laube, J.; Heinze, T.; Kulicke, W. M., Properties and flocculation efficiency of highly cationized starch derivatives. *Starch - Stärke* **2006,** *58* (3 - 4), 161-169.

[119] Petzold, G.; Schönberger, L.; Genest, S.; Schwarz, S., Interaction of cationic starch and dissolved colloidal substances from paper recycling, characterized by dynamic surface measurements. *Colloids and Surfaces A: Physicochemical and Engineering Aspects* **2012,** *413*, 162-168.

[120] Wang, L.; Zhou, L.; Chen, F., Performance of fixing agents in controlling micro-stickies of recycled newspaper pulp. *China Pulp & Paper* **2006,** *25* (7), 1-4.

[121] Banerjee, S.; Le, T.; Haynes, R. D.; Bradbury, J. E., Solubilizing and detackifying stickies with β-cyclodextrin. *BioResources* **2012,** *7* (2), 1533-1539.

[122] Ben, Y.; Ricard, M.; Dorris, G., Quantifying microstickies via a new agglomeration technique. *Tappi Journal* **2014,** *13* (9), 27-38.

[123] Miao, Q.; Huang, L.; Chen, L., Advances in the control of dissolved and colloidal substances present in papermaking processes: A brief review. *BioResources* **2012,** *8* (1), 1431-1455.

[124] Ben, Y.; Dorris, G.; Hill, G.; Allen, J., Contaminant removal from deinking process water, Part I: Mill benchmarking: DAF units are very efficient in removing large suspended solids. *Pulp & Paper Canada* **2003,** *104* (1), 42-48.

[125] Gao, Y.; Qin, M.; Yu, H.; Zhang, F., Effect of heat-dispersing on stickies and their removal in post-flotation. *BioResources* **2012,** *7* (1), 1324-1336.

CHAPTER 2. HYDROPHILIC INK BEHAVIOR DURING PULPING AND ITS IMPLICATION IN ADSORPTION DEINKING

2.1 Introduction

Although an extensive amount of effort has been spent developing new technologies to improve the deinking efficiency of hydrophilic inkjet ink, very few of them focused on understanding the ink behavior during pulping and papermaking. For example, INGEDE Method 11 was developed to evaluate the deinkability of traditional offset ink. However, the pulping chemistry and pulping conditions may not be applicable to hydrophilic inkjet ink. In addition, it has been well-known that the irreversible redeposition of ink into fiber lumen is a major concern for hydrophilic inkjet ink[1-2]. But a method to distinguish between redeposited ink and bound ink is still missing. So it is difficult to pinpoint the contribution of bound ink and redeposited ink to the overall residual ink on fiber. Compared with flotation deinking, this new deinking method could dramatically reduce the water consumption by 90% and energy consumption by 20%[3-4]. It is still questionable whether adsorption deinking could solve the problem of hydrophilic inkjet ink.

The aim of the present work is hence to understand the ink behaviors during paper recycling and investigate the efficacy of adsorption deinking in hydrophilic inkjet ink removal. At first, the effects of pulping chemicals in INGEDE Method 11 to hydrophilic inkjet ink were investigated using inkjet printed newspaper. Then a method to distinguish between bound ink and redeposited ink was developed to understand the contribution of bound ink and

redeposited ink individually to the residual ink concentration on fiber products. Based on this new method, the effect of pulping consistency on bound and redeposited ink was studied. Finally, the efficacy of inkjet adsorption deinking by chitosan was studied in this research. To the authors' knowledge, this is the first report on inkjet adsorption deinking. Thus, the current research only focuses on concept validation and the adsorption isotherm, kinetics and adsorbent selection were also investigated.

2.2 Materials and Methods

2.2.1 Materials

All the deinking chemicals, including NaOH (AR), $CaCl_2$ (AR), Na_2SiO_3 (AR), and H_2O_2 (AR), were obtained from VWR International. Oleic acid used in deinking experiments was 80% (w/w). Chitosan was purchased from Fisher Scientific (Acros Organics) with molecular weight in the range of 600,000-800,000 and deacetylation degree between 75% and 85%. Talc and lignosulfonic acid sodium salt (lignosulfonate) were purchased from Sigma-Aldrich. Cationic-polyacrylamide (cPAM) with high molecular weight and low charge density (Nalco® 74508) was purchased from Nalco as retention aid agent. The printing substrate, blank newsprint was purchased from Uline and the product code is S-19325. The basis weight is 30lbs. and the ISO brightness is 58%. A commercial pigment-based inkjet ink (HP 60, LD Products, Long Beach, CA) was purchased to prepare model inkjet printed newspaper.

2.2.2 Methods

2.2.2.1 Preparation of model inkjet printed newspaper

A black and white image of the INGEDE gray deinking test page[5] was chosen to ensure the reproducibility of printed newspaper samples. The model newspaper was printed by a commercial pigment-based inkjet ink HP 60 on one side of blank newspaper with an inkjet printer (Deskjet 1000, HP, Palo Alto, CA).

2.2.2.2 Standard deinking procedure INGEDE Method 11

International Association of the Deinking Industry (INGEDE) Method 11[6] was used for the deinking method in many of the following experiments. INGEDE Method 11 is a laboratory scale deinking procedure that was developed to approximate the deinking performance of a given sample for industrial deinking operations. The printed samples in lab were shredded to the size of 2cm * 2cm. After that, the small pieces of samples were immersed to deinking solution with sodium hydroxide (0.6%), sodium silicate (1.8%), oleic acid (0.8%) and water with hardness of 128 mg Ca^{2+}/L, and shredded under mechanical force for 20 min. The pulp was then stored at 40°C for 1 hour to allow for increased ink detachment, and floated in a 5L flotation cell by a Denver flotation device to remove the inks for 10 min. All deinking samples followed the INGEDE Method 11 procedure unless specified otherwise.

2.2.2.3 Evaluation of pulping chemicals for deinking of hydrophilic inks

A factorial design of experiments was performed with the absence of the deinking chemicals (“0”) or normal loading of deinking chemicals (“1”), as shown in Table 2-1. All the other experiment conditions followed INGEDE Method 11. The effects of each chemical and the synergistic effects called “interaction” between each of the chemicals

were studied by comparing the %ISO Brightness and effective residual ink concentration (ERIC) of paper pad samples from different conditions following the Yates algorithm.

Table 2-1 Factorial design of experiments to study the effect of pulping chemicals to deinking performance.

	Sodium hydroxide	Sodium silicate	Oleic acid	Calcium ions
1	1	0	0	0
2	1	1	0	0
3	1	0	1	0
4	1	0	0	1
5	1	1	1	0
6	1	1	0	1
7	1	0	1	1
8	1	1	1	1
9	0	0	0	0
10	0	1	0	0
11	0	1	1	0
12	0	1	0	1
13	0	1	1	1
14	0	0	1	0
15	0	0	1	1
16	0	0	0	1

2.2.2.4 Lignosulfonate stabilization to prevent ink redeposition during pulping

The effect of lignosulfonate to prevent redeposition of hydrophilic ink was evaluated using a variation of Method 11. In the modified method, unprinted newsprint was used instead of hydrophilic ink printed newsprint with all deinking chemicals and 3 mass% lignosulfonate on fiber, and ink was added to the pulp slurry after 2 min of the pulping stage. The pulping stage lasted for another 20 min and pulp samples were collected to make paper pads for ERIC measurement. The effect of lignosulfonate on ink redeposition prevention was studied by comparing the ERIC of samples with and without lignosulfonate. The mass of ink added was approximately the same amount of ink that was printed on newspaper, which was determined by finding the average mass of ink per mass of paper for the hydrophilic ink printed newsprint. The average mass of ink per mass of paper was determined by weighing 100 pieces of paper before and after printing. Three runs of each trial were performed for each experiment.

2.2.2.5 Hyperwash of deinking pulp

Hyperwashing was performed after the pulping or flotation step described in any deinking procedure. The pulp slurry was diluted to 0.02% consistency during hyperwash and then screened through a 100-micron screen (McMaster-Carr, Atlanta, GA). The screened pulp was used to make paper pad samples for effective residual ink concentration (ERIC) and ISO% Brightness measurement following INGEDE Method 1. Hyperwash could remove all the inks in liquid phase to avoid ink redeposition during pad formation.

2.2.2.6 Evaluation of hydrophilic inks behavior during pulping

The hydrophilic ink behavior was determined using three independent modifications to the Method 11 deinking procedure. The effective residual ink concentration (ERIC) of each

modification was measured. These three modifications were lignosulfonate & hyperwashing, INGEDE Method 11 & hyperwashing, and INGEDE Method 11 pulping & flocculants.

For lignosulfonate & hyperwashing, 3% lignosulfonate was added to the pulp at the beginning of pulping to prevent the ink redeposition during pulping, and the pulp was hyperwashed following the procedure described before. In the next modification INGEME Method 11 & hyperwash, hyperwashing was performed on the pulp at the completion of the standard Method 11 deinking procedure. Hyperwash could remove all the inks in liquid phase to avoid ink redeposition during pad formation. At last, the INGEDE Method 11 pulping & flocculants only followed the pulping portion of the Method 11 procedure and 2 grams of cationic polymer, Nalco® 74508 was dosed to retain the entire sample of ink on fiber. The cationic flocculent is necessary because a portion of the negatively charged ink particles will be removed in the liquid phase during the sample formation without the flocculent. The pulp didn't go through flotation.

2.2.2.7 Evaluation of pulping consistency on bound and redeposited inks

The effect of pulping consistency on bound and redeposited inks was studied following the procedures of lignosulfonate & hyperwashing and Method 11 described in the last section, with three different consistency level, 5% 10% and 15%. The total redeposited ink was defined as the combination of the ink redeposited during pulping and the ink redeposited during paper formation.

2.2.2.8 Adsorbents selection

Two adsorbents, chitosan and talc, were selected to determine the adsorption capacity of hydrophilic inks. 0.5 g/L original ink suspension (HP 60) suspension was prepared and 1 grams of the adsorbent material was added to 1 liter ink suspension. The concentration of ink remaining in solution was measured by UV/Vis spectroscopy (Spectronic 601, Milton Roy, Ivyland, PA) at 300nm after mixing overnight.

Chitosan showed a much higher adsorption capacity than talc and the adsorption kinetics of chitosan was studied further. The same 0.5 g/L original ink suspension was prepared with 1 grams of chitosan added to 1 liter ink suspension. 3 mL ink suspension sample was taken from the system and filtered through a 1 micron filter paper. The filtrate was analyzed by UV-vis spectroscopy to calculate the ink particle concentration. The size of ink is 60nm based on dynamic light scattering measurement by Malvern Zetasizer Nano ZS90 so inks were retained in the filtrate.

To study the adsorption isotherm of hydrophilic ink onto chitosan, the chitosan concentration was 0.275 g/L, and the initial ink concentration varied from 0.35 g/L to 0.5 g/L. Then, the suspension was mixed for 24 hours and filtered through a 1 micron filter paper. The ink concentration of filtrate was measured by UV-vis spectrometer. Similarly, for the adsorption isotherm of hydrophilic ink onto cellulose fiber, a pulp was prepared from unprinted newsprint at a consistency of 0.5%, and an ink suspension was made with 1% (w/w) ink. Then, various ratios of these suspensions were mixed ranging from 100-200 grams of pulp suspension and 15-200 grams of ink suspension. The samples were mixed for 24 hours, and the ink concentration was then measured by UV-Vis spectrometry through supernatant after centrifuging samples for 2 hours at 2000 RPM.

The adsorption capacity was calculated by Equation 2.1

$$q = \frac{(C_i - C_e)V}{m} \quad \textbf{(2.1)}$$

Where C_i is the initial ink concentration, C_e is the ink concentration during equilibrium, V is the volume of ink solution and m is the mass of absorbent.

2.2.2.9 Adsorption deinking procedure

Deinkability tests were carried out with 100% hydrophilic pigmented inkjet printed newsprint prepared from the printing procedure described previously. For the chitosan adsorption deinking experiments, 20% chitosan by fiber mass was added with the hydrophilic inkjet printed paper during the pulping step following the same procedure as Method 11. However, after pulping, the chitosan was separated from the pulp and no flotation was performed. The ISO% Brightness and Effective Residual Ink Concentration (ERIC) were measured and compared with the value of samples from standard Method 11.

2.2.3 Characterization

Pulp samples were taken after pulping as well as after flotation. An undeinked paper pad was made from the pulp taken after pulping, and deinked paper pad were made from pulp samples after either adsorption deinking, flotation or hyperwash. The paper pads were made according to INGEDE Method 1. Brightness and effective residual ink concentration (ERIC) were measured for each of these samples using a Technidyne ColorTouch ISO (Technidyne; New Albany, IN, USA).

2.3 Results and Discussion

2.3.1 Evaluation of pulping chemicals for deinking of hydrophilic inks

A standard deinking method called INGEDME Method 11 was developed to emulate industrial deinking systems for laboratory scale deinking and the chemicals in INGEDME Method 11 have been optimized for the deinking of hydrophobic inks. The deinking chemicals in Method 11 include oleic acid, sodium silicate, hydrogen peroxide, sodium hydroxide, and calcium chloride. Sodium hydroxide could swell the paper fibers and improve the ink detachment in an alkaline condition. Additionally, sodium silicate acts as a dispersant, which improves detachment of the ink from the paper fiber and prevents ink redeposition[7]. Finally, oleic acid complexes with calcium ions and acts as a coagulant to agglomerate ink particles to around 10 microns which is more suitable for separation by flotation. However, the hydrophilic inkjet inks in our study are very different from traditional hydrophobic inks. For example, the size of hydrophilic ink is only 60 nm and the zeta-potential is -35 mV. It is unclear if the functions of deinking chemicals carry over for hydrophilic inks.

All the chemicals used for INGEDE Method 11 except hydrogen peroxide were evaluated. Hydrogen peroxide was excluded from this analysis because this study focused on the removal of ink through flotation instead of bleaching effect. Figure 2-1 and Figure 2-2 shows that sodium hydroxide, oleic acid, and sodium silicate have a positive effect on deinking of hydrophilic inks during pulping, i.e. high value of ISO% Brightness and low value of ERIC, while calcium chloride has a negative effect. There are three implications from the results. First, it has previously been shown that calcium chloride causes deposition

of hydrophilic flexographic inks during the formation of paper, so this is consistent with results above[8]. Second, the sodium hydroxide seems to have a beneficial effect on deinking in this study. Previous researches on neutral deinking have shown some conflicting result[9-19]. A well accepted theory is that ink would be more dispersed under higher pH, leading to deposition into the fiber lumen. On the other hand, neutral condition would reduce the electrostatic repulsion between ink particles, and between ink particles and fibers. Thus, the redeposition seems most to be at the fiber surfaces[9]. At last, sodium silicate causes dispersion, which has previously been shown to improve detachment of hydrophilic ink during pulping[20-21].

Next, the interaction between the deinking chemicals can be seen from Figure 2-1 and Figure 2-2. Interaction represents the synergistic effect between different factors, which was calculated by Yates algorithm. For hydrophobic inks, the interaction between oleic acid and calcium is thought to act as a collector for flotation. But this secondary interaction is not observed for hydrophilic inks. Instead, a tertiary effect appeared between sodium hydroxide, oleic acid and calcium ions, which suggests that the synergistic effect of oleic acid and calcium ions is dominant under high pH levels. As discussed earlier, ink particles could agglomerate under neutral conditions, which makes effect of the oleic/calcium collector less significant.

Based on the study, more research work is needed to have a better understanding on pulping chemicals. In addition, the chemical dose will carry over to all the downstream operations including flotation, washing, etc., which further complicates the situation. Thus, the same pulping chemicals were applied and followed in the other sections of the paper.

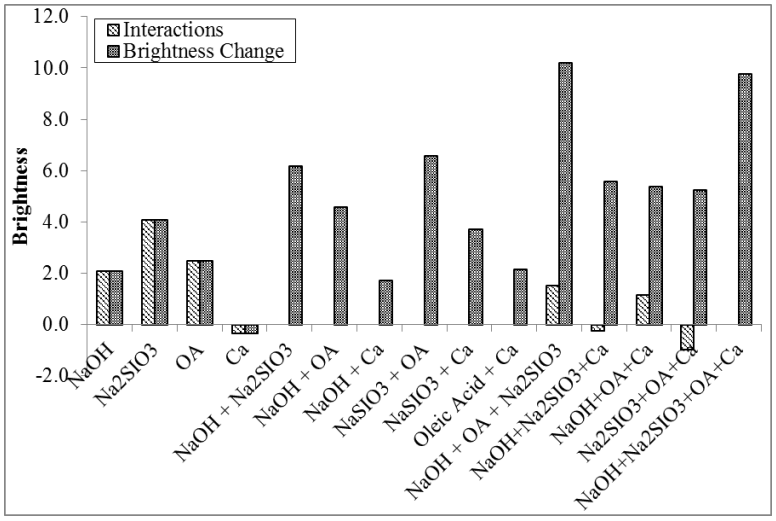

Figure 2-1 Effect of INGEDE Method 11 deinking chemicals and interactions between each of the deinking chemicals on ISO% Brightness of newsprint printed with pigmented inkjet ink.

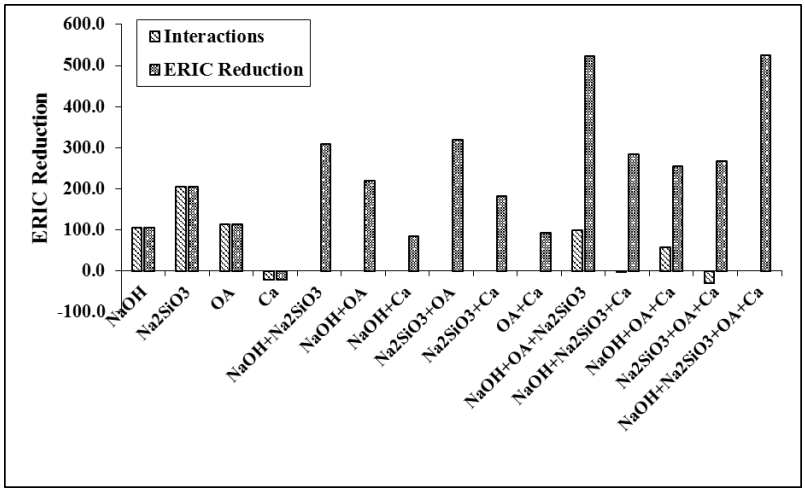

Figure 2-2 Effect of INGEDE Method 11 deinking chemicals and interactions between each of the deinking chemicals on ERIC of newsprint printed with pigmented inkjet ink.

2.3.2 Lignosulfonate stabilization to prevent ink redeposition

Previous research has shown that lignosulfonate is an effective stabilizer for nanoparticles, polymers and dyes due to both electrostatic repulsive forces and steric repulsive forces[22-

25]. In addition, lignosulfonate could also adsorb to paper fibers through hydrophobic interactions[26-27]. Thus, it is possible that lignosulfonate also prevents redeposition of hydrophilic ink. The influence of lignosulfonate on the redeposition of hydrophilic pigmented inkjet ink onto unprinted newsprint was evaluated by dosing ink with/without lignosulfonate into unprinted clean pulp slurry during pulping. The amount of ink required was determined using the average mass of inkjet ink per mass of paper fiber. On average, there are 0.0031g inkjet ink printed on one piece of newsprint with average weight of 2.928 g. Figure 2-3 shows the ERIC value of pulp slurry under different conditions and the ERIC of pulp slurry with lignosulfonate and ink was far smaller than that without lignosulfonate. In addition, the ERIC of pulp slurry with lignosulfonate and ink was very close to that of unprinted clean paper fiber without ink. Thus, lignosulfonate has been proved to prevent the majority of the redeposition of hydrophilic inks during pulping.

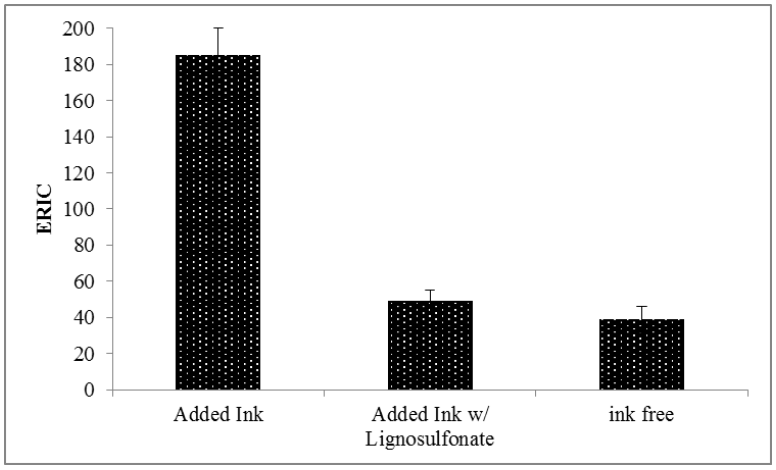

Figure 2-3 Evaluation of proportion of ink redeposited during paper recycling with and without lignosulfonate using a variation of INGEDE Method 11.

2.3.3 Ink behavior during pulping operation

There are still some gaps in the understanding of the behavior of hydrophilic inks during deinking operations. It is always assumed that hydrophilic inks are quickly dispersed during pulping and then redeposit onto fiber surfaces[1]. However, a method to distinguish between bound ink and redeposited ink is still missing. As a result, a thorough investigation of the behavior of hydrophilic ink during paper recycling is not possible. In this section, the fate of hydrophilic inks was investigated based on a new method.

Table 2-2 Deinking methods for determination of behavior of hydrophilic inks during paper recycling operations.

	Bound Ink	Redeposited Ink (Pulping)	Redeposited Ink (Paper Formation)	Separated Ink (Flotation & Filtrate)
Lignosulfonate & Hyperwashing	X			
Method 11 & Hyperwashing	X	X		
Method 11	X	X	X	
Method 11 & Flocculent	X	X	X	X

Since lignosulfonate has been shown to prevent ink redeposition successfully, a set of experiments were designed to find the proportion of the hydrophilic ink that is bound along with the proportion of ink that is redeposited either during the pulping operations or during papermaking operations. For the purposes of this experiments, the ink is defined as "bound", redeposited (during pulping or during formation), and free ink, and each of these proportions were evaluated using a series of modifications to INGEDE Method 11. These

values can be estimated based on the deinking performance of each of the deinking methods in the series, which included lignosulfonate & hyperwashing, INGEDE Method 11 & hyperwashing, standard INGEDE Method 11, and INGEDE Method 11 pulping & flocculants. Each method distinguishes a specific type of ink as shown in Table 2-2.

Lignosulfonate & hyperwashing shows the total of ink that is bound during typical pulping operations since redeposition during pulping and pad formation are inhibited by lignosulfonate and hyperwash, respectively. INGEDE Method 11 & hyperwashing shows the amount of ink that is bound and redeposited during pulping during typical pulping operations because hyperwash could wash away all the residual inks in water phase after pulping. Standard Method 11 shows the amount of ink that is bound and redeposited during pulping and pad formation. Finally, INGEDE Method 11 pulping & flocculants is able to show the total amount of ink present on the paper because all the inks redeposit onto the fiber with flocculants.

The results of these pulping methods are shown in Figure 2-4, and the amount of ink that is bound, redeposited during pulping, redeposited during paper formation, and free inks were estimated by comparing all of these methods, which is summarized in Table 2-3. There are three significant aspects of this data. First, the proportion of bound ink was 16%, which is contrary to previous theories that assumed fast and completely dispersion of hydrophilic ink during pulping. Thus, pulping with higher consistency or longer time, while avoiding redeposition, is a key to reduce the bound ink on fiber. Second, the severe redeposition of inkjet ink occurs both in pulping and in pad formation. This result is consistent with a previous research about hydrophilic flexographic ink[8]. In addition, the reason for ink redeposition during pad formation is the high concentration of ink in water

phase. So a method to remove ink during pulping could prevent ink redeposition during pulping and paper formation. Finally, the proportion of hydrophilic ink that is redeposited was about twice as much as the bound ink. Thus, the major concern for improving the deinkability of hydrophilic inks is to prevent redeposition of the inks. Another interesting note is that the estimation of redeposition of ink during pulping is consistent when comparing the redeposition of ink from Figure 2-3 and Figure 2-4.

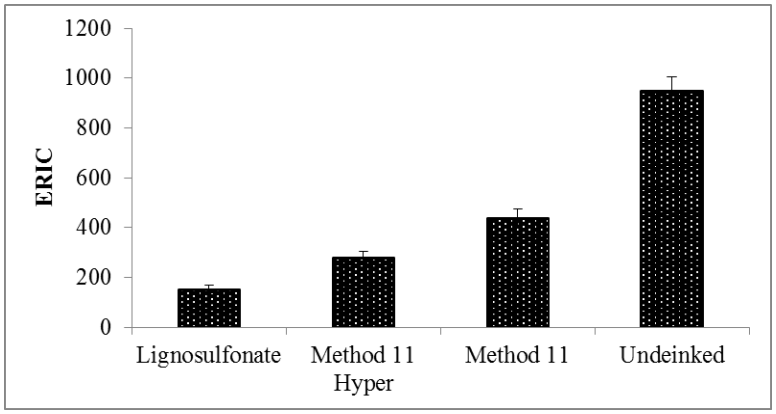

Figure 2-4 ERIC measurements for various adaptations of INGEDE Method 11 for determination of the fate of pigmented inkjet ink during paper recycling.

Table 2-3 Estimated mass percent of pigmented inkjet ink that is bound and redeposited during pulping or pad formation determined from Figure 2-4.

	Bound Ink	Redeposited (pulping)	Redeposited (pad formation)	Separated Ink (Flotation & Filtrate)
Mass% Ink	15.8	13.7	17.9	52.6

2.3.4 Evaluation of pulping consistency on bound and redeposited ink

After performing this analysis, it is necessary to understand the proportion of bound ink and redeposited ink on the fiber under different pulping consistencies in order to reduce

the residual ink on fiber surfaces. Generally speaking, increasing pulping consistency has a similar effect with increasing pulping time[1-2, 9-10, 19]. Longer pulping time induces ink fragmentation and provides more time for ink redeposition. Similarly, ink fragmentation and redeposition is also controlled by friction level, which is the result of pulping consistency[10]. However, a certain level of pulping is also essential to detach ink from fiber surface and get acceptable defibering of the raw material. The trade-off between the two phenomena is the key for inkjet deinking. Furthermore, from application perspective, it is far more beneficial to pulping at higher consistency, than pulping for longer time. So effect of pulping consistency on bound and redeposited ink was studied by following the method in the last section.

Lignosulfonate & hyperwashing and Standard Method 11 from last section was performed to measure the “bound” and “redeposited ink” and the pulping consistency was changed to 5% and 10%. As can be seen from Figure 2-5, the proportion of redeposited ink decreased as the consistency decreased which can be explained by lower ink concentration in the water phase, and weaker fiber-fiber friction under low consistency. In addition, when looking at the portion of bound ink, the bound ink decreased as the consistency increased from 5-15%. Thus, the optimal pulping method for hydrophilic ink should be able to inhibit redeposition without sacrificing pulping time/consistency to ensure the detachment of inks from fiber surfaces.

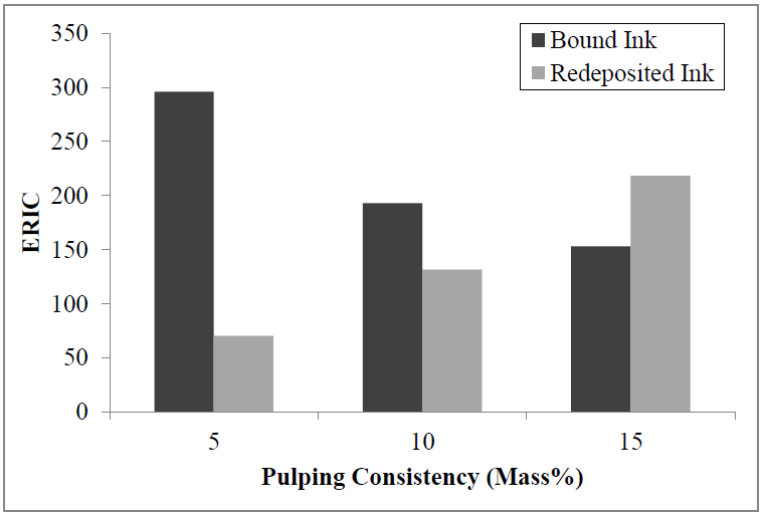

Figure 2-5 Bound vs. redeposited inks under different pulping consistencies.

2.3.5 Adsorption deinking

Based on the ink behavior analysis, research was focused on the prevention of inkjet ink redeposition. Kemppainen[2] proved the importance of removing the detached inks as soon as they have been detached in order to prevent redeposition. Adsorption deinking is an ideal option since pulping and deinking happens simultaneously. Besides that, adsorption deinking has other advantages, including energy and water saving[3-4, 28], potential to remove mixed inks with different adsorbents, and adsorbent regeneration with surfactant solutions[29].

The removal of ink using adsorption deinking depends strongly on the adsorbent that is used. Two different adsorbents, talc and chitosan were chosen because of their ability to form hydrogen bonds with hydrophilic ink particles, and the adsorption capacity was determined in an ink/water suspension without the presence of cellulose fibers. As shown in Figure 2-6, talc adsorbed 30% ink particles from aqueous suspension and chitosan reduced the concentration of ink by over 90%. Chitosan has been widely used for dye

removal and heavy metal removal. The adsorption property attributes to the amino groups through electrostatic attraction, and hydroxyl groups through hydrogen bonding[30]. Since the ink particles have a pKa value of 4 and they are negatively charged in water, both electrostatic attraction force and hydrogen bonding exist between chitosan and ink. However, talc consists of two types of surface area, namely uncharged hydrophobic planes and negatively charged hydrophilic edges[31]. Thus, overall adsorption is driven by hydrophobic interaction[32] and physical entrapment because the electrostatic repulsion force prevents the adsorption of ink onto edges. This could also be the reason why talc is not as effective as chitosan for ink adsorption. So chitosan was selected as the deinking adsorbents to study in this section.

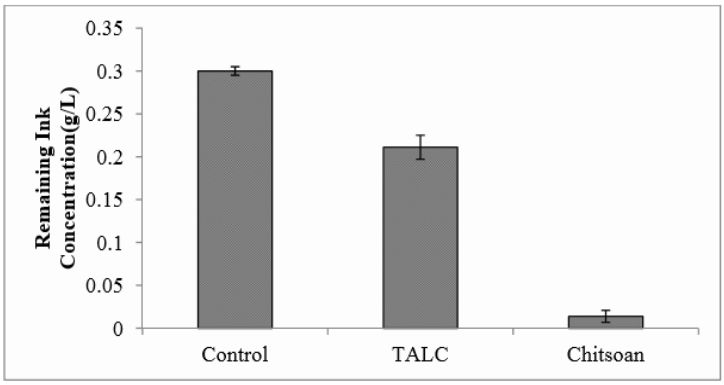

Figure 2-6 Adsorption performance of Talc and Chitosan without the presence of fibers.

The adsorption isotherms and kinetics of chitosan were further studied. As described previously chitosan can remove 90% of ink particles from solution. However, the adsorption kinetics from Figure 2-7 showed that the ink removal was only about 50% for pigmented inks during the 20min time frame of deinking, which suggests that an adsorbent with faster kinetics could improve the adsorption deinking efficiency. Additionally, it can

be concluded from Figure 2-8 that the adsorption isotherm followed Langmuir model with maximum adsorption capacity of chitosan and cellulose fiber was 1.7 g ink/g chitosan and 0.8 g ink/g fiber, respectively. The adsorption capacity of chitosan is significantly greater than that of cellulose fiber, which is a fundamental basis to ensure that chitosan could compete over cellulose fibers for ink adsorption.

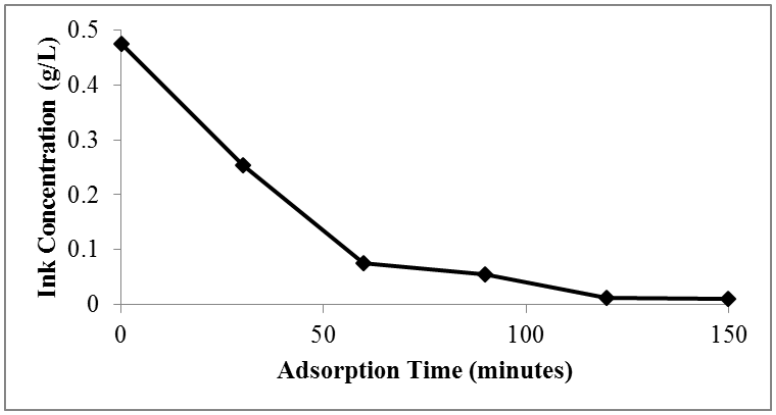

Figure 2-7 Time dependent adsorption of pigmented inkjet ink using chitosan.

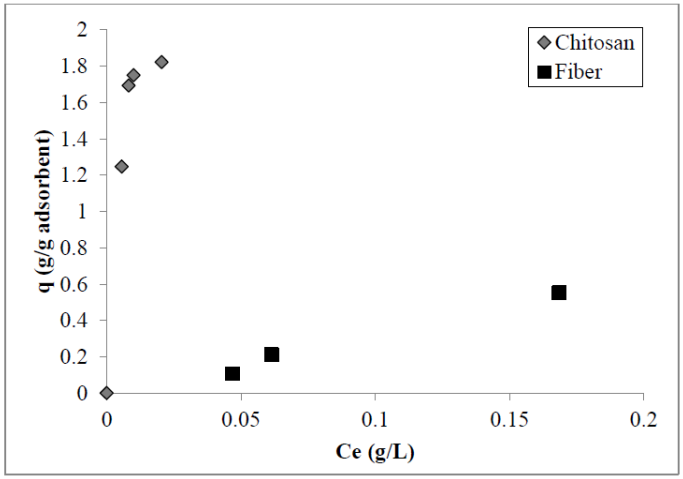

Figure 2-8 Equilibrium adsorption isotherm of inkjet ink onto chitosan and fiber.

Although chitosan removes ink particles from aqueous suspensions, it is still unknown whether the same performance can be observed during pulping with the presence of fibers.

Thus, it is necessary to test chitosan adsorption deinking for deinking printed paper. For newsprint recycling purposes, the ISO Brightness should reach 58% with ERIC lower than 200 ppm. In this study, the undeinked samples have 44% ISO Brightness with 900 ppm ERIC.

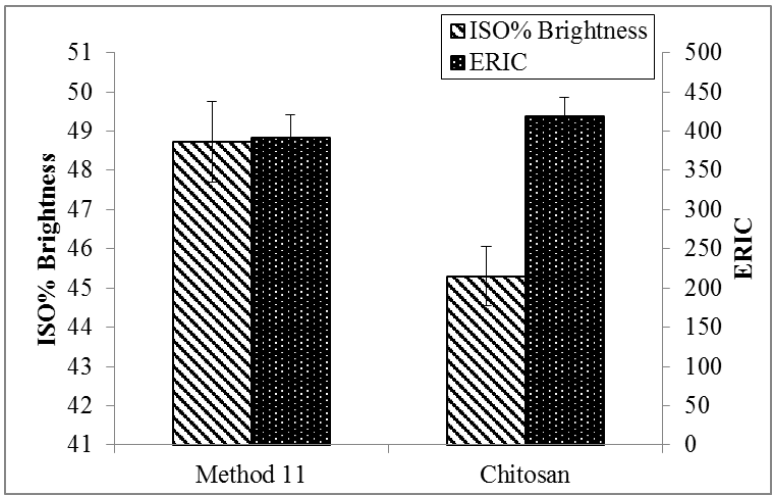

Figure 2-9 Impact of chitosan adsorption deinking on the ISO% Brightness and ERIC of pigmented-based inks pulped at 15% consistency.

As can be seen in Figure 2-9, standard INGEDE Method 11 improved the ISO Brightness to 49% and reduced ERIC to 450 ppm. However, the ISO brightness for the pulp deinked with chitosan was only 45% which was much darker than the standard method. This suggests that the attraction interaction between the detached ink and the chitosan is not strong enough for adsorption. A possible reason is that the majority of the water in the system is bound to the fiber surfaces at 15% consistency and this consistency is too high to have good mixing between chitosan and fiber. As a result, the attachment of ink to the chitosan surface is prevented. Because of this, 10% consistency was chosen to facilitate the transfer of ink particles into the liquid phase and enhance the mixing between chitosan and fiber, which will more closely approximate the removal of ink from an ink/water solution.

At 10% consistency, the adsorption deinking had a much higher efficacy as shown in Figure 2-10. Compared with INGEDE Method 11, the adsorption deinking improved the ISO Brightness by 5 more points, while reducing ERIC by additional 70 ppm, besides 90% reduction in water consumption and 20% reduction in energy consumption.

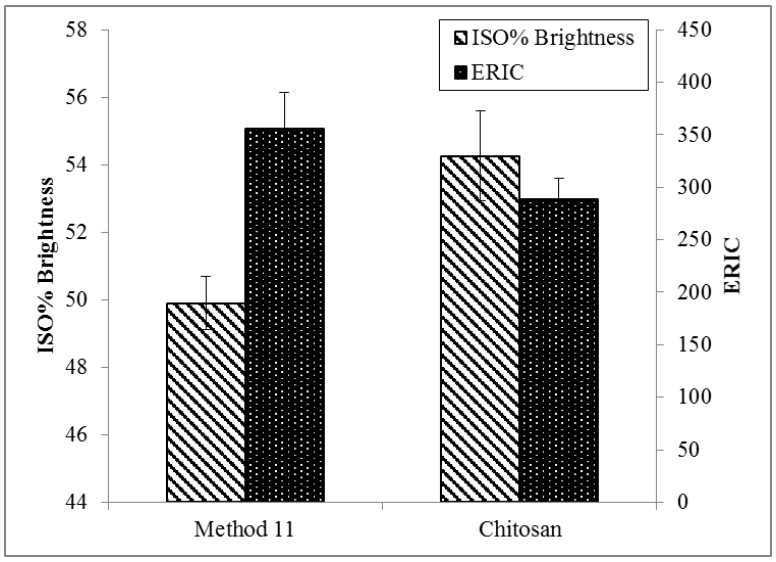

Figure 2-10 Impact of chitosan adsorption deinking on the ISO% Brightness and ERIC of pigmented-based inks pulped at 10% consistency.

2.4 Conclusions

The effects of pulping chemistry and consistency to inkjet deinking were studied and the ink behavior during pulping and papermaking was also investigated. According to the ERIC value of different scenarios, about 50% of inks could be removed through flotation, while 32% would redeposit onto the fiber and the rest 18% are bound inks. Thus, adsorption deinking that could prevent ink redeposition is of great importance to inkjet deinking. Chitosan was selected as an adsorbent to show that about 50% of pigmented-based inkjet inks can be effectively adsorbed in the time frame of pulping due to the hydrogen bonding potential of chitosan. It was also shown that chitosan could improve ISO Brightness by 5

points during pulping of 100% inkjet printed newsprint when the consistency is adjusted to 10%. For future study, it is important to focus the development of an adsorbent with faster kinetics and greater capacity, and adsorbents for mixed waste paper.

2.5 References

[1] Ben, Y.; Dorris, G., Is deinkability of inkjet prints an issue? *Tappi Journal* **2011,** *10* (10), 17-27.

[2] Kemppainen, K.; Körkkö, M.; Niinimäki, J., Fractional pulping of toner and pigment-based inkjet ink printed papers-ink and dirt behavior. *BioResources* **2011,** *6* (3), 2977-2989.

[3] Handke, T.; Schrinner, T.; Grossmann, H., Adsorptionsdeinking Ein neues Konzept zur Druckfarbenentfernung. *Wochenbl.für Pap.(WfP)* **2011**, 1-6.

[4] Handke, T.; Großmann, H. Verfahren zum Recycling von Altpapier Method for recycling waste paper. DE102012204203 B4, 2014.

[5] INGEDE (International Association of the Deinking Industry) Deinking page http://www.ingede.com/digital/test-ingede-gray-letter.pdf.

[6] INGEDE Method 11: Assessment of Print Product Recyclability-Deinking Test.

[7] Dorris, G.; Ben, Y.; Richard, M., Overview of flotation deinking. *Progress in paper recycling* **2011,** *20* (1), 3-42.

[8] Ben, Y.; Pelton, R.; Dorris, G., Retention and dislodgement of flexographic ink in a fibrous mat during thickening and displacement washing. *Journal of pulp and paper science* **1996,** *22* (11), J411-J419.

[9] Galland, G.; Carre, B.; Rousset, X.; Vernac, Y. In *Deinking difficulties related to waterbased ink printed papers analysis of redeposition phenomena*, TAPPI Recycling Symposium, TAPPI PRESS: 2000; pp 503-516.

[10] Galland, G.; Vernac, Y.; Carré, B.; Rousset, X. In *Effect of pulping conditions on ink redeposition and ink removal when recycling waterbased ink printed papers*, Proc Pulping Conf. Atlanta GA, TAPPI press, 2001.

[11] Bhattacharyya, M. K.; Ng, H. T.; Mittelstadt, L. S.; Hanson, E. G., Deinking of digital prints: effect of near-neutral deinking chemistry on deinkability. *Journal of Imaging Science and Technology* **2012,** *56* (6), 60503-1-60503-5.

[12] Morrow, H.; Horacek, B.; Hale, K.; Rosencrance, S., True-neutral deinking. *Paper Age* **2005,** *121*, 34-35.

[13] Korkko, M.; Bussini, D.; Laitinen, O.; Elegir, G.; Niinimaki, J., True-neutral fractional deinking for flexographic and offset newsprints. *Appita Journal: Journal of the Technical Association of the Australian and New Zealand Pulp and Paper Industry* **2012,** *65* (1), 71.

[14] Galland, G.; Vernac, Y.; Carre, B., The advantages of combining neutral and alkaline deinking, Part I: Comparison of deinking of offset and flexo printed paper. *Pulp & Paper Canada* **1997,** *98* (6), 46-49.

[15] Ng, H. T.; Bhattacharyya, M. K.; Mittelstadt, L. S.; Hanson, E. G. In *Deinking of HP Digital Commercial Prints: Effect of Chemicals and Their Loadings on Deinkability*, NIP & Digital Fabrication Conference, Society for Imaging Science and Technology: 2009; pp 173-176.

[16] Ciampa, S., *The effects of repulping variables on deinking of flexographic inks*. 1995.

[17] Nesbit, S. E. Flexographic ink behaviour during newspaper repulping. University of British Columbia, 1999.

[18] Ng, H.; Bhattacharyya, M.; Mittelstadt, L.; Hanson, E. In *Deinking and recycling HP digital inks: From lab scale to pilot scale*, TAPPI Peers Conference and 9th Research Forum on Recycling, 2010.

[19] Gao, Y.; Yuan, X.; Gao, L.; Li, J., Study on neutral chemical deinking of laser printed papers. *Tappi Journal* **2016,** *15* (1), 49-57.

[20] Ben, Y.; Dorris, G., Irreversible ink redeposition during repulping. Part II: ONP/OMG furnishes. *Journal of pulp and paper science* **2000,** *26* (8), 289-293.

[21] Ali, T.; McLellan, F.; Adiwinata, J.; May, M.; Evans, T., Functional and performance characteristics of soluble silicates in deinking. Part I: Alkaline deinking of newsprint/magazine. *Journal of pulp and paper science* **1994,** *20* (1), J3.

[22] Du, X. T.; Hsieh, J. S., Microstickies agglomeration by electric field. *Water Sci. Technol.* **2016,** *73* (12), 2841-2848.

[23] Li, Z.; Pang, Y.; Ge, Y.; Qiu, X., Evaluation of steric repulsive force in the aqueous dispersion system of dimethomorph powder with lignosulfonates via X-ray photoelectron spectroscopy. *The Journal of Physical Chemistry C* **2011,** *115* (50), 24865-24870.

[24] Lou, H.; Zhu, D.; Yuan, L.; Qiu, X.; Lin, X.; Yang, D.; Li, Y., Fabrication of high-concentration aqueous graphene suspensions dispersed by sodium lignosulfonate and its mechanism. *The Journal of Physical Chemistry C* **2015,** *119* (40), 23221-23230.

[25] Milczarek, G.; Rebis, T.; Fabianska, J., One-step synthesis of lignosulfonate-stabilized silver nanoparticles. *Colloids and Surfaces B: Biointerfaces* **2013,** *105*, 335-341.

[26] Eriksson, T.; Börjesson, J.; Tjerneld, F., Mechanism of surfactant effect in enzymatic hydrolysis of lignocellulose. *Enzyme Microb. Technol.* **2002,** *31* (3), 353-364.

[27] Li, H.; Fu, S.; Peng, L.; Zhan, H., Surface modification of cellulose fibers with layer-by-layer self-assembly of lignosulfonate and polyelectrolyte: effects on fibers wetting properties and paper strength. *Cellulose* **2012,** *19* (2), 533-546.

[28] Petzold, G.; Schwarz, S., Investigation of an improved deinking process of waste paper–The influence of surface tension and charge in suspension on ink removal. *Colloids and Surfaces A: Physicochemical and Engineering Aspects* **2015,** *480*, 398-404.

[29] Schwarz, S.; Petzold, G.; Oelmann, M. Cleaning particles from waste paper recycling process, involves introducing particle having impurities on its surface to water, and adding surfactant material before, simultaneously or after introducing step and then realizing energy input. DE102012208219 A1, 2013.

[30] Vakili, M.; Rafatullah, M.; Salamatinia, B.; Abdullah, A. Z.; Ibrahim, M. H.; Tan, K. B.; Gholami, Z.; Amouzgar, P., Application of chitosan and its derivatives as adsorbents for dye removal from water and wastewater: A review. *Carbohydrate polymers* **2014,** *113*, 115-130.

[31] Liu, J.; Vandenberghe, J.; Masliyah, J.; Xu, Z.; Yordan, J., Fundamental study on talc–ink adhesion for talc-assisted flotation deinking of wastepaper. *Minerals engineering* **2007,** *20* (6), 566-573.

[32] Khraisheh, M.; Holland, C.; Creany, C.; Harris, P.; Parolis, L., Effect of molecular weight and concentration on the adsorption of CMC onto talc at different ionic strengths. *International Journal of Mineral Processing* **2005,** *75* (3), 197-206.

CHAPTER 3. ELECTROFLOTATION AND ELECTRIC TREATMENT ASSISTED FLOTATION

3.1 Introduction

Electric treatment has been applied in wastewater treatment[1-4], sludge dewatering[5-9], algae harvesting[10-12], mineral recovery[13-14] and particles agglomeration[15-18] through three different mechanisms, including electrocoagulation, electroflotation and electrophoresis. Both electrocoagulation and electrophoresis could agglomerate particles in water, while electroflotation generates fine bubbles with greater surface area. As a result, bubbles are more likely to catch larger particles in water and float to the water surface. Based on this theory, the current work focuses on the impact of electric treatment on hydrophilic inks agglomeration and on deinking efficiency. The effects of anode material and electric treatment time on deinking performance were also investigated to understand the electric treatment mechanism and optimize the electric treatment process. Finally, a combined treatment was established to recycle hydrophilic ink printed paper.

3.2 Experimental procedure

3.2.1 Materials

Deionized (DI) water from an ion-exchange system with a resistivity of greater than 18 MΩ cm^{-1} was used in all described experiments. All the deinking chemicals, including NaOH (AR), $CaCl_2$ (AR), Na_2SiO_3 (AR), and H_2O_2 (AR), were obtained from VWR International. Oleic acid used in deinking experiments was 80% (w/w). The printing substrate, blank newsprint was purchased from Uline and the product code is S-19325. The

basis weight is 30lbs. and the ISO brightness is 58%. A commercial pigment-based hydrophilic inkjet ink (HP 60, LD Products, Long Beach, CA) was purchased to prepare model hydrophilic ink printed newspaper. Stainless steel and graphite electrode were purchased from McMaster-Carr.

3.2.2 Methods

3.2.2.1 Electric treatment of ink suspension in DI water

0.5 mL ink was dispersed in 1L DI water to prepare 0.5g/L ink suspension. The suspension was treatment with 3.6kV and 200mA with stainless steel or graphite as anode, and stainless steel container as cathode for 30min. The container has 13 cm in length and width, with 19cm in height. The lower end of anode was 3cm below the surface of water.

3.2.2.2 Preparation of model hydrophilic ink printed newspaper

A commercial pigment-based hydrophilic inkjet ink (HP 60, LD Products, Long Beach, CA), was used to print a black and white image of the INGEDE gray deinking test page[19] on one side of blank newspaper (30 lbs. newsprint sheets, Uline, Pleasant Prairies, WI) using an inkjet printer (Deskjet 1000, HP, Palo Alto, CA). The INGEDE deinking test page was chosen to ensure the reproducibility of printed newspaper samples.

3.2.2.3 Standard deinking procedure INGEDE Method 11

International Association of the Deinking Industry (INGEDE) Method 11[20] was used for the deinking method in many of the following experiments. INGEDE Method 11 is a laboratory scale deinking procedure that was developed to approximate the deinking

performance of a given sample for industrial deinking operations. The printed samples in lab were shredded to the size of 2cm * 2cm. After that, the small pieces of samples were immersed to deinking solution with sodium hydroxide (0.6%), sodium silicate (1.8%), oleic acid (0.8%) and water with hardness of 128 mg Ca^{2+}/L and pulped with mechanical force for 20min. The pulp was stored at 40°C for 1 hour to allow for increased ink detachment, and floated in a 5L flotation cell by a Denver flotation device to remove the inks. All deinking samples followed the INGEDE Method 11 procedure unless specified otherwise.

3.2.2.4 Electric treatment and flotation simultaneously

The flotation procedure is the same with INGEDE Method 11, except that DI water was applied to dilute the pulp slurry after pulping. Either stainless steel or graphite electrode was applied as the anode, and the stainless-steel flotation cell was connected to the cathode. The treatment voltage is 1kV and current is 250mA. The treatment was conducted with flotation simultaneously for 10min as in Figure 3-1(a).

3.2.2.5 Electric treatment of pulp slurry

Pulp slurry was diluted to 1% solid by water with hardness of 128 mg Ca^{2+}/L and treated with electric charge by 0.5h, 1h, or 2h, with 0.06kV and 400mA as shown in Figure 3-2(b). The pulp slurry was agitated by an impeller with 500 rpm.

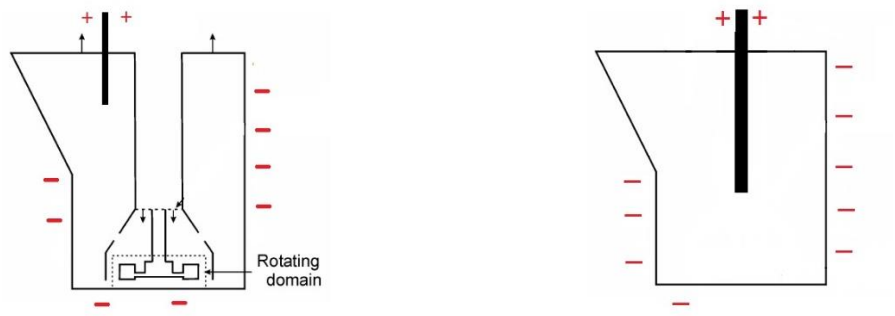

Figure 3-1 Apparatus for electric treatment (left a) with flotation (right b) alone.

3.2.2.6 Hyperwashing of deinking pulp

Hyperwashing can be performed after the pulping or flotation step described in any deinking procedure. In order to hyperwash the pulp, it was diluted to 0.02% consistency. The paper fibers were then screened out of solution using a 100-micron screen (McMaster-Carr, Atlanta, GA). The pulp was then used to make filter pad samples for effective residual ink concentration (ERIC), ISO% Brightness. Hyperwash could remove all the inks in liquid phase to avoid ink redeposition during pad formation.

3.2.3 Characterization

3.2.3.1 Particle size and zeta-potential of hydrophilic ink

The particle size and zeta-potential of hydrophilic ink was analyzed using a zetasizer (Malvern Zetasizer Nano ZS90, Malvern Instrument Co. Ltd., UK). The particle size was measured 10 times with 50 scans each cycle. The zeta-potential was measured in DI water, 50mM NaCl and 100mM NaCl solutions. with ink concentration of 0.2g/L. The pH of the suspension was then adjusted to several values by adding HCl or NaOH solution.

3.2.3.2 Chemical structure of hydrophilic ink

Silicon wafers were spin-coated with ink suspension prior to XPS measurement. XPS analysis was performed with Thermo K-Alpha XPS. The XPS spectra of the cellulose films were obtained using a monochromatic Al Ka X-ray source (1486.6 eV) at a voltage of 15 kV and a current of 10 mA. The vacuum level of the analyzing chamber was maintained below 5E-7 Pa during the measurements. The pass energy and step width during the survey scan were set at 200 eV and 1 eV, respectively. In the element narrow scan mode, these scan parameters were set at 50 and 0.1 eV, respectively. The binding energies for all spectra were determined with respect to the C 1s reference signal (unoxidized C–C band) at 285.0 eV.

3.2.3.3 Fiber sample preparation and measurement

Pulp samples were taken after pulping, after electric treatment, after flotation and after washing. An undeinked filter pad was made from the pulp taken after pulping, and deinked filter pad were made from pulp samples after either electric treatment, flotation or hyperwash. The filter pads were made according to INGEDE Method 1. Brightness and effective residual ink concentration (ERIC) were measured for each of these samples using a Technidyne ColorTouch ISO (Technidyne; New Albany, IN, USA).

3.3 Results and Discussion

3.3.1 Hydrophilic ink property and the effect of electric treatment on ink size

Before studying deinking process of ink printed paper, it is necessary to have a basic understanding of the ink structure and property. Based on dynamic light scattering and

zeta-potential measurement shown in Figure 3-2, the size of ink is 60 nm and ink particles are highly negatively charged with isoelectric point of pH=4. The ink particles also show electric double layer screening effect when additional electrolytes were introduced. In addition, XPS spectrum in Figure 3-3 shows that ink only contains carbon and oxygen that oxygen element renders carbon black hydrophilic. As described previously in the paper, the submicron size, high surface charge density and hydrophilic surface are the major reasons why hydrophilic ink is not compatible with flotation deinking. Thus, the hydrophilic ink in our study is a good representative for inks that caused problems in paper mill.

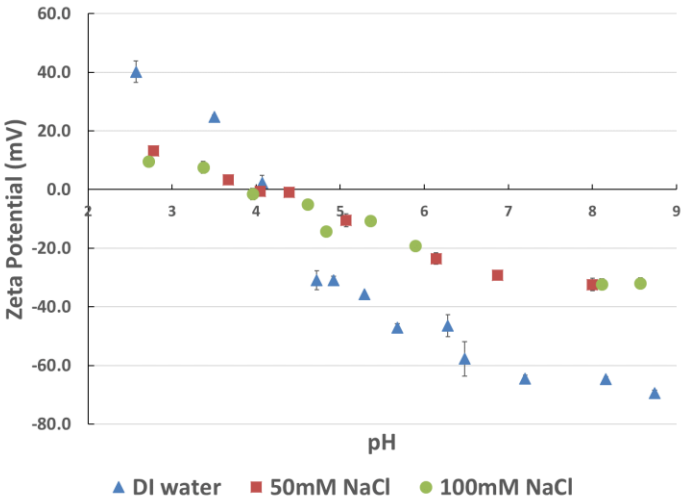

Figure 3-2 Zeta-potential of ink particles (0.2g/L) in water under different pH and ionic strength.

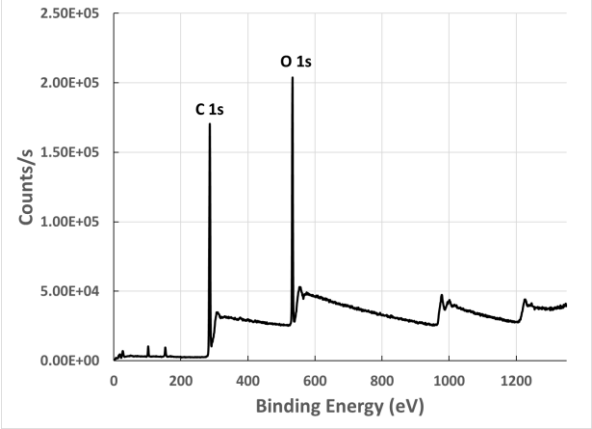

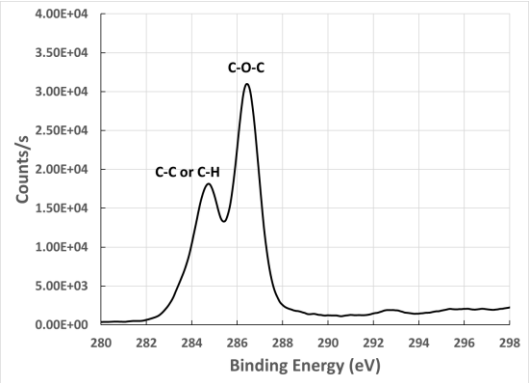

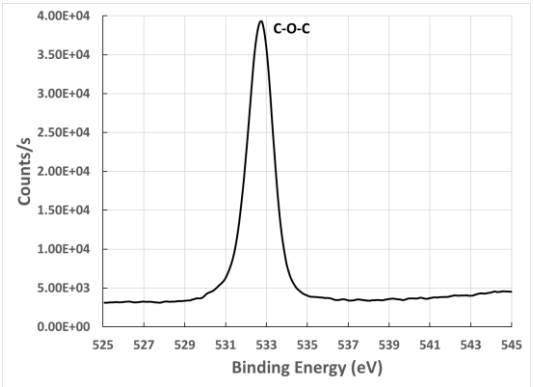

Figure 3-3 XPS spectrum of inks (a) survey (b) carbon (c) oxygen.

The electric treatment has multiple effects simultaneously, including electroflotation, electrocoagulation and electrophoresis. Graphite anode is very stable while stainless steel electrode releases metal ions, causing electrocoagulation. Electrocoagulation could be very beneficial for hydrophilic ink removal because it can agglomerate ink particles. In order to verify this hypothesis, ink particles were dispersed in DI water to suppress current density and inhibit electroflotation effect. The ink particle after electric treatment is shown in Figure 3-4. Both graphite and stainless steel electrode agglomerated ink particles to 400nm and 700nm, respectively. The agglomeration with graphite electrode is mainly driven by electrophoresis. Since the ink particles are highly charged in water, they have a tendency

to migrate under electric field and increase the local particle concentration[15, 21-23]. As a result, particles are more likely to collide in high concentration region, increasing particle size. However, stainless steel further increased particles to 700nm because the process is driven by both electrophoresis and electrocoagulation. Besides electrophoresis, the metal ions from stainless steel anode increase ionic strength and screen the electrostatic repulsion between particles and agglomerate ink particles.

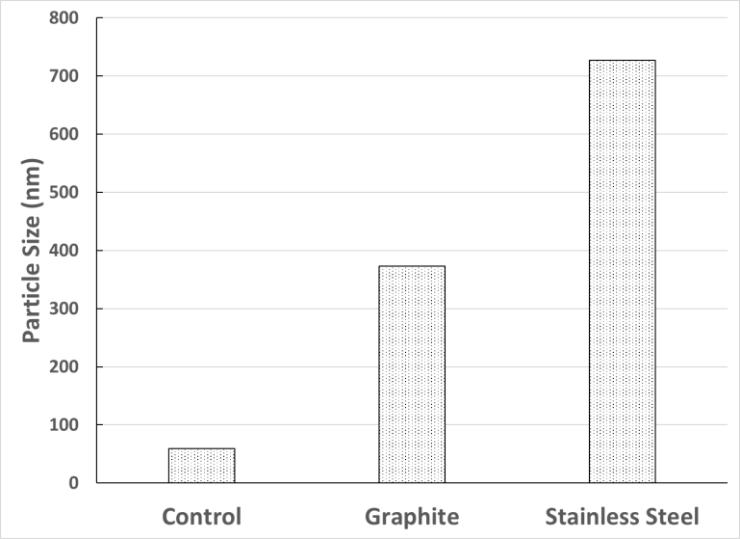

Figure 3-4 Effect of electric treatment on ink size without the presence of fiber.

3.3.2 The effect of electric treatment on flotation deinking

Although ink particles increased dramatically after electric treatment, it is still a question whether ink can be removed by electric treatment assisted flotation. However, the effect of electric treatment on cellulose fiber had to be investigated because the change in fiber color would interfere with the effective residual ink concentration (ERIC) measurement. The influence of flotation, and flotation with electric treatment simultaneously to fiber ISO% brightness and ERIC was studied as shown in Figure 3-5. Since there were no ink particles

on fiber, the ISO% Brightness was around 60 and ERIC was lower than 30ppm. And there was no significant difference between the samples with and without electric treatment.

Since electric treatment doesn't change fiber brightness, the electric treatment assisted flotation was studied. Standard sheet samples were printed in order to make reproducible samples. The INGEDE Method 11, an optimized standardized method for offset deinking was followed to deink hydrophilic ink printed paper. The ISO% Brightness and ERIC of fiber pads after pulping, flotation and flotation with electric treatment are shown in Figure 3-6. Traditional flotation only removed very small amount of inks that ERIC dropped 20 ppm. This phenomenon is consistent with the ink property in the first section. However, electric treatment with flotation simultaneously both decreased ERIC and increased the ISO% Brightness. The ISO% brightness was increased by almost 2 points and ERIC was reduced by another 70 ppm when the pulp was electrically treated with graphite as anode. The reduction in ERIC can be explained by electroflotation and electrophoresis mechanism. It has been shown that electrophoresis increases size of ink particles and electroflotation generates bubbles with fine size through water electrolysis which increases the surface area of air bubbles greatly. This combinational effect accounts for the reduction in ERIC because air bubbles are more likely to catch ink particles with greater size.

When the anode material is stainless steel, the ERIC reduction was similar to graphite while the improvement in ISO% Brightness was only 0.5 point. Stainless steel electrode can increase ink particle size even more with electrocoagulation, which should have further improved flotation efficiency compared with graphite. However, this was not observed from the experiment results so a series of experiment with electric treatment alone was conducted to understand the mechanism.

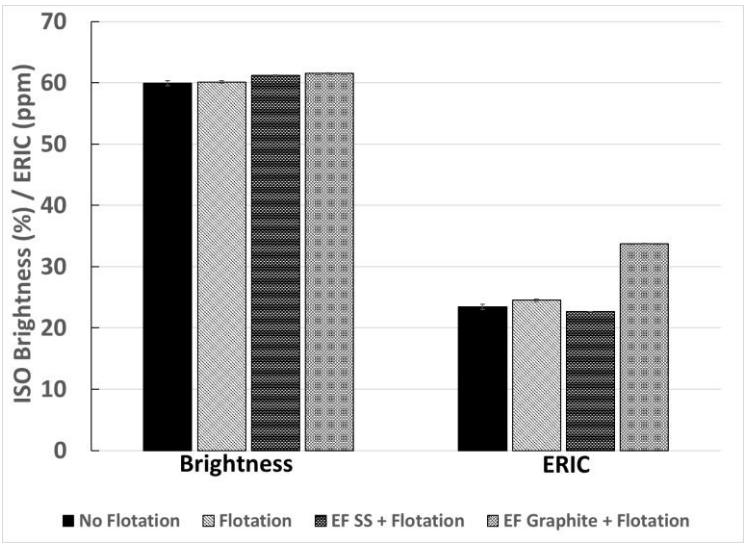

Figure 3-5 Effect of flotation and electric treatment assisted flotation on ISO% Brightness and ERIC of unprinted fiber.

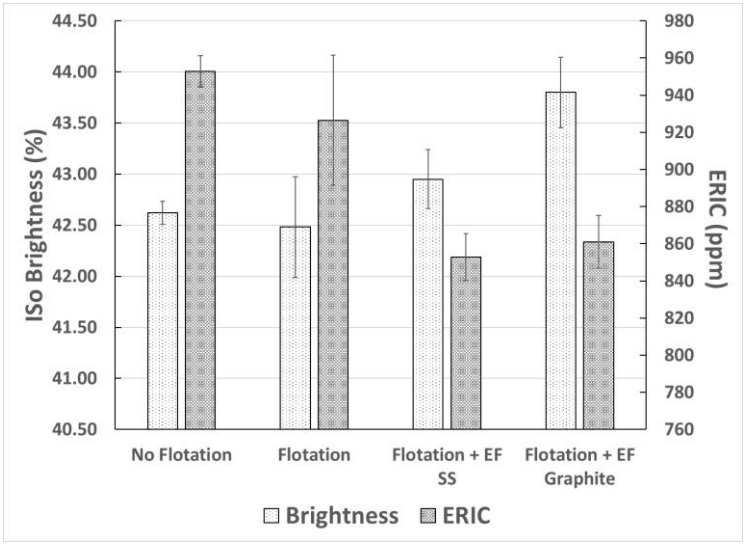

Figure 3-6 Effect of flotation and electric treatment assisted flotation on ISO% Brightness and ERIC of printed fiber.

3.3.3 The effect of electric treatment on ink removal

The pulp was diluted to 1% consistency and electrically treated by graphite or stainless steel anode for 0.5h, 1h and 2h under 0.06kV and 400mA. A thin layer of ink particles was observed on the water surface through electroflotation and skimmed off. The yield can

reach 99% because the electroflotation has a very high selectivity and only ink particles are floated to water surface. As a result, ERIC went down after electric treatment from 950ppm to 850ppm in the case of stainless steel, and to 700ppm when graphite is anode. And graphite electrode always showed a better removal performance compared with stainless steel electrode in all the three different lengths of treatment time based on Figure 3-7. There are two possible reasons for this phenomenon. The first one is the redeposition of ink during electric treatment. As discussed previously, metal ions from electric treatment reduce the electrostatic repulsion through charge screening effect. Thus not only the particle-particle repulsion, but also the particle-fiber repulsion is reduced, leading to the redeposition of ink particles onto fiber surface. The other reason is the ink entrapment in fiber network during sample preparation. Since the ink particle size is greatly increased after treatment, they are easier to be entrapped into fiber network, resulting in a higher residual ink value.

In order to understand which of the two is the major driver, the pulp was hyperwashed after electric treatment before sample preparation. Hyperwashing removes ink particles in the water phase, preventing ink entrapment during sample preparation[24]. If redeposition is the major reason for high ERIC value, pulp samples treated by stainless steel anode should have a higher ERIC compared with graphite after hyperwashing. However, if entrapment is the major driver, ERIC values of graphite treated samples and stainless steel treated samples should be very close because entrapment is prevented through hyperwashing. As shown in Figure 3-8, samples with electric treatment by stainless steel electrode showed a much higher ERIC value than graphite electrode even after hyperwashing. This proves that ink redeposition during electric treatment is the reason for high ERIC value in samples

with stainless steel anode. This mechanism also explains why stainless steel has a similar flotation efficiency with graphite when electric treatment was conducted simultaneously with flotation in the previous section. Although ink particle sizes are greater with stainless steel anode, they also redeposit onto fiber during the flotation process. Thus the benefits from larger ink particle size cancel out with the ink redeposition, and therefore additional benefits were not observed.

Another interesting phenomenon from Figure 3-7 is the change in ERIC value with different lengths of electric treatment time. With graphite anode, the residual ERIC value dropped steadily with an increase in treatment time through electroflotation and electrophoresis, while the ERIC value first increased and then decreased with treatment time if stainless steel anode was chosen. This observation can also be explained by the counter effect between electroflotation and ink redeposition. Both of the two effects benefit from longer treatment time. However, the redeposition process is less sensitive to a high ionic strength that the energy barrier by electrostatic repulsion force cannot be reduced furthermore if the ionic strength is already very high. On the other hand, the electroflotation effect benefits from longer treatment time continuously, and this explains why ERIC first increased and then decreased with treatment time when stainless steel is anode.

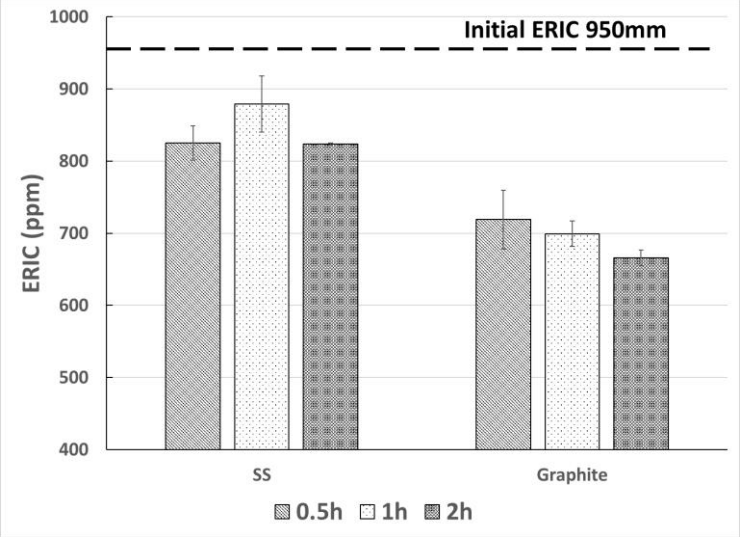

Figure 3-7 Effect of electric treatment on ERIC of printed fiber with different electrodes and lengths of treatment time.

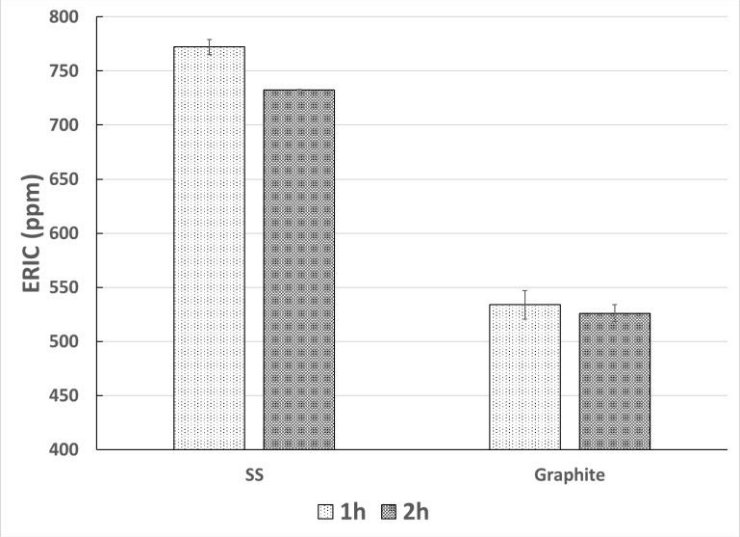

Figure 3-8 Effect of electric treatment on ERIC of printed fiber with different electrodes and lengths of treatment time followed by hyperwashing.

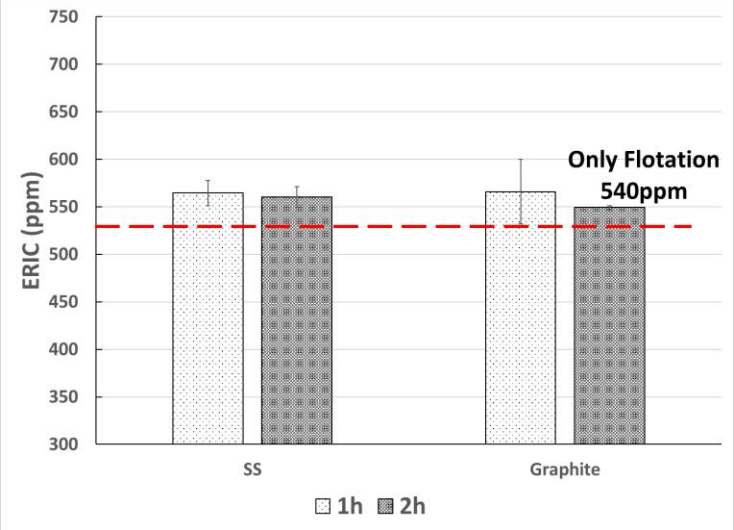

Figure 3-9 Effect of electric treatment on ERIC of printed fiber with different electrodes and lengths of treatment time followed by flotation.

In the previous section, electric treatment was conducted simultaneously with flotation. And with the understanding developed earlier in this section about electric treatment alone and electric treatment followed by hyperwashing, it is interesting to study the flotation efficiency after electric pretreatment. Figure 3-9 shows that any differences in ERIC developed in electric pretreatment (Figure 3-7) disappeared after flotation that ERIC went down to 550ppm in all conditions. However, the yield of flotation differed dramatically that the yield of stainless steel treated sample was 80% while that of graphite was 97%, which was consistent with observation during flotation that stainless steel treated samples always had a thicker foam layer. It has been proved that salts are able to improve foam stability and removal of particles due to weaker electrostatic repulsion force[25-27]. Thus, the metal ions from stainless steel contributes to a stable foam and higher yield loss. Although the fiber qualify was the same after flotation, graphite anode is still a better option due to its high yield. However, the control experiment with only flotation reduced the ERIC to 540ppm which is the same level of ERIC from electric pretreatment followed by

flotation. Thus, any advantages obtained from electric pretreatment diminishes after flotation.

3.3.4 The effect of electric treatment on ink removal followed by flotation and hyperwashing

In paper mills, fibers are extensively hyperwashed after flotation to remove fine particles. Thus, pulp fibers were treated with flotation and hyperwash after electric pretreatment to mimic the real recycling process. As shown in Figure 3-10, the fiber ERIC value further dropped to 400ppm from 550ppm (Figure 3-9) when graphite was chosen, which is very close to 250ppm recycling requirement. Thus, a combined electric pretreatment, flotation and hyperwash process is a promising recycling method for hydrophilic inks. Another important observation is the samples with stainless steel treatment for 2 hr. The ERIC values were the same (550ppm) before and after hyperwashing as in Figure 3-9 and Figure 3-10, which further proves the redeposition mechanism of stainless steel electrode. Although stainless steel electrode is a widely applied anode in wastewater treatment[13, 28-29], graphite is a better material as an anode in deinking application due to the detrimental ink redeposition effect from metal ion induced electrocoagulation. At last, the non-sacrificial nature of graphite also ensures a longer application life time.

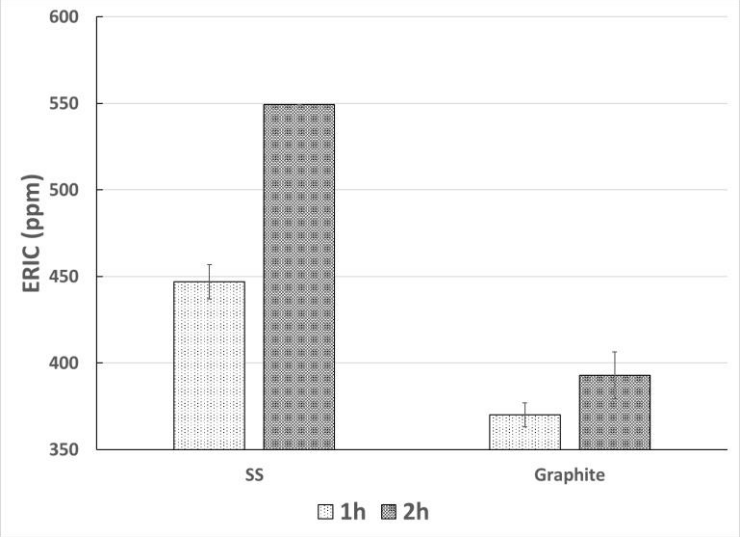

Figure 3-10 Effect of electric treatment on ERIC of printed fiber with different electrodes and lengths of treatment time after flotation and hyperwashing.

3.4 Conclusions

Electric treatment was selected to improve the recycle of hydrophilic ink printed paper. The electric treatment agglomerated ink particles from 60nm to 700nm. In addition, electric treatment assisted flotation reduced ERIC by additional 70ppm compared with traditional flotation. Furthermore, pulp samples were treated with electric treatment alone, electric treatment followed by hyperwashing, and electric treatment followed by flotation to understand the separation mechanism and optimize the process. Both electroflotation and electrophoresis mechanisms improves separation efficiency with less than 1% yield loss while electrocoagulation led to ink redeposition onto fiber. Thus graphite is a better material candidate as anode compared with stainless steel. Graphite also showed a 17% higher yield in flotation with electric pretreatment and longer application life time. However, special attention has to be given to flotation because benefits from electric pretreatment disappears after traditional flotation in this study. Finally, a combined process

similar to paper mill recycling process was created and the ERIC value decreased to less than 400ppm from original 950ppm. Electric treatment based on graphite showed great separation efficiency and high yield, and it is a promising technology to solve separation problems caused by sub-micron hydrophilic particles with high negative surface charge.

3.5 References

[1] Ashrafi, O.; Yerushalmi, L.; Haghighat, F., Wastewater treatment in the pulp-and-paper industry: A review of treatment processes and the associated greenhouse gas emission. *J. Environ. Manage.* **2015,** *158*, 146-157.

[2] Mahesh, S.; Garg, K. K.; Srivastava, V. C.; Mishra, I. M.; Prasad, B.; Mall, I. D., Continuous electrocoagulation treatment of pulp and paper mill wastewater: operating cost and sludge study. *RSC Advances* **2016,** *6* (20), 16223-16233.

[3] Mu, W.; Ben, H.; Du, X.; Zhang, X.; Hu, F.; Liu, W.; Ragauskas, A. J.; Deng, Y., Noble metal catalyzed aqueous phase hydrogenation and hydrodeoxygenation of lignin-derived pyrolysis oil and related model compounds. *Bioresource technology* **2014,** *173*, 6-10.

[4] Soloman, P.; Basha, C. A.; Velan, M.; Balasubramanian, N.; Marimuthu, P., Augmentation of biodegradability of pulp and paper industry wastewater by electrochemical pre-treatment and optimization by RSM. *Separation and Purification Technology* **2009,** *69* (1), 109-117.

[5] Citeau, M.; Larue, O.; Vorobiev, E., Influence of salt, pH and polyelectrolyte on the pressure electro-dewatering of sewage sludge. *Water research* **2011,** *45* (6), 2167-2180.

[6] Mahmoud, A.; Olivier, J.; Vaxelaire, J.; Hoadley, A. F., Electrical field: A historical review of its application and contributions in wastewater sludge dewatering. *Water research* **2010,** *44* (8), 2381-2407.

[7] Mahmoud, A.; Olivier, J.; Vaxelaire, J.; Hoadley, A. F., Electro-dewatering of wastewater sludge: influence of the operating conditions and their interactions effects. *Water research* **2011,** *45* (9), 2795-2810.

[8] Olivier, J.; Conrardy, J.-B.; Mahmoud, A.; Vaxelaire, J., Electro-dewatering of wastewater sludge: An investigation of the relationship between filtrate flow rate and electric current. *Water research* **2015,** *82*, 66-77.

[9] Rahmani, A. R.; Nematollahi, D.; Godini, K.; Azarian, G., Continuous thickening of activated sludge by electro-flotation. *Separation and Purification Technology* **2013,** *107*, 166-171.

[10] Gao, S.; Yang, J.; Tian, J.; Ma, F.; Tu, G.; Du, M., Electro-coagulation–flotation process for algae removal. *J. Hazard. Mater.* **2010,** *177* (1), 336-343.

[11] Mascia, M.; Vacca, A.; Palmas, S., Electrochemical treatment as a pre-oxidative step for algae removal using Chlorella vulgaris as a model organism and BDD anodes. *Chemical engineering journal* **2013,** *219*, 512-519.

[12] Zhang, D.; Yu, Y.; Li, C.; Chai, C.; Liu, L.; Liu, J.; Feng, Y., Factors affecting microalgae harvesting efficiencies using electrocoagulation-flotation for lipid extraction. *RSC Advances* **2015,** *5* (8), 5795-5800.

[13] Casqueira, R.; Torem, M.; Kohler, H., The removal of zinc from liquid streams by electroflotation. *Minerals engineering* **2006,** *19* (13), 1388-1392.

[14] Sarkar, M. S. K. A.; Donne, S. W.; Evans, G. M., Utilization of hydrogen in electroflotation of silica. *Advanced Powder Technology* **2011,** *22* (4), 482-492.

[15] Du, X. T.; Hsieh, J. S., Microstickies agglomeration by electric field. *Water Sci. Technol.* **2016,** *73* (12), 2841-2848.

[16] Hsieh, J. S., Deinking of inkjet digital nonimpact printing. *Tappi Journal* **2012,** *11* (9), 9-15.

[17] Shemi, A.; Hsieh, J.; Lee, D., Clarification of flexographic wastewater by electrocoagulation and electroflotation. *Appita Journal: Journal of the Technical Association of the Australian and New Zealand Pulp and Paper Industry* **2014,** *67* (3), 212.

[18] Shemi, A.; Hsieh, J. S., Electroflotation combined with flotation deinking of flexographic newsprint. *Ind. Eng. Chem. Res.* **2010,** *49* (5), 2380-2387.

[19] INGEDE (International Association of the Deinking Industry) Deinking page http://www.ingede.com/digital/test-ingede-gray-letter.pdf.

[20] INGEDE Method 11: Assessment of Print Product Recyclability-Deinking Test.

[21] Wakamatsu, T., Method and apparatus for characterization of electric field-induced aggregation in pre-crystalline protein solutions. *Rev. Sci. Instrum.* **2015,** *86* (1), 015112.

[22] Wu, L.; Zhao, W.; Yang, R.; Yan, W.; Sun, Q., Aggregation of egg white proteins with pulsed electric fields and thermal processes. *J. Sci. Food Agric.* **2016**.

[23] Zhou, W.; Shi, J.; Lv, L.; Chen, L.; Chen, Y., A mechanistic investigation of morphology evolution in P3HT–PCBM films induced by liquid crystalline molecules under external electric field. *Phys. Chem. Chem. Phys.* **2015,** *17* (1), 387-397.

[24] Ben, Y.; Dorris, G., Is deinkability of inkjet prints an issue? *Tappi Journal* **2011,** *10* (10), 17-27.

[25] Bournival, G.; Ata, S.; Jameson, G., The influence of submicron particles and salt on the recovery of coarse particles. *Minerals Engineering* **2014,** *69*, 146-153.

[26] Duan, X.; Hou, J.; Cheng, T.; Li, S.; Ma, Y., Evaluation of oil-tolerant foam for enhanced oil recovery: Laboratory study of a system of oil-tolerant foaming agents. *Journal of Petroleum Science and Engineering* **2014,** *122*, 428-438.

[27] Firouzi, M.; Howes, T.; Nguyen, A. V., A quantitative review of the transition salt concentration for inhibiting bubble coalescence. *Adv. Colloid Interface Sci.* **2015,** *222*, 305-318.

[28] Mansoorian, H. J.; Mahvi, A. H.; Jafari, A. J., Removal of lead and zinc from battery industry wastewater using electrocoagulation process: Influence of direct and alternating current by using iron and stainless steel rod electrodes. *Separation and Purification Technology* **2014,** *135*, 165-175.

[29] SenthilKumar, P.; Umaiyambika, N.; Gayathri, R., Dye removal from aqueous solution by electrocoagulation process using stainless steel electrodes. *Environmental Engineering & Management Journal (EEMJ)* **2010,** *9* (8).

CHAPTER 4. PROBING BARRIERS TO PARTICLE ADSORPTION AT FLUID-FLUID INTERFACES

4.1 Introduction

Solid particles can adsorb spontaneously onto fluid-fluid interfaces and act as stabilizers. A series of functional materials have been developed including, Pickering emulsions[1-3], Pickering foams[4-6], bijels[7-9], oil foams[10-11] and dry oil powders[12], and these materials have been studied in a variety of applications like oil recovery[13], drug delivery[14-15], catalysis[16], nanoporous membranes[17] and cosmetics[18]. A detailed introduction to the thermodynamics and kinetics of particles adsorption to fluid-fluid interfaces has been summarized in Chapter 1.4.2 and a comparison between different kinetics models can be found in Appendix C.

In this chapter, we study and compare the kinetics of particles adsorption at air-water and oil-water interfaces through the established method as in Equation 1.12 and Equation 1.13. The effective diffusion coefficient can be obtained by the initial slope of dynamic interfacial tension, and the energy barrier is calculated by comparing effective diffusion coefficient and Stokes-Einstein diffusion coefficient. We specifically focus on the early-stage kinetics because this is the time regime when particle-interface interactions dominate the adsorption kinetics, which is consistent with flotation separation theory. From the difference in kinetics between air-water and oil-water interfaces, we show that particles adsorb to oil-water interfaces faster than air-water interfaces, which can be rationalized by attractive van der Waals interactions between particles and oil-water interfaces, and

repulsive van der Waals interactions between particles and air-water interfaces. Finally, we prove the efficacy of oil-coated bubble flotation in hydrophilic ink deinking.

4.2 Experimental procedure

4.2.1 Materials

Silicone oil with a viscosity of 10 cSt and a density of 0.93 g/mL was purchased from Sigma-Aldrich with product code 378321. Deuterium oxide was also obtained from Sigma-Aldrich with produce code. A commercial pigment-based hydrophilic inkjet ink (HP 60, LD Products, Long Beach, CA) was purchased to prepare model hydrophilic ink suspension. This hydrophilic ink has been proven to be incompatible with traditional flotation[19]. Ethyl cellulose (EC) particles were synthesized by following the previously reported method[20-21]. 1 wt% of EC (Sigma-Aldrich, product code: 247499-100G) was dissolved in acetone by stirring at 1100 rpm under 45℃. An equal volume of ultrapure DI water (18.2 MΩ•cm) was then quickly poured into the prepared EC solution under stirring and the solution turned turbid because of EC nanoparticle precipitation. The suspension was then stirred under 45℃ until all acetone was evaporated. The obtained EC suspension was washed by acid precipitation, centrifugation, supernatant replacement by DI water and sonication for five cycles to make sure the surface-active impurities from EC and acetone were removed from the particle suspension. The EC suspension with different particle concentrations were prepared by diluting the stock suspension with DI water and deuterium oxide to ensure the ratio of DI water and deuterium oxide in final EC suspension is 1:1. The addition of deuterium oxide could improve the accuracy of interfacial tension measurement by increasing the density difference between the two phases[22].

4.2.2 Methods and Characterizations

4.2.2.1 Particle size and zeta-potential

Particle hydrodynamic radius and zeta-potential of EC particles in water was measured by dynamic and electrophoretic light scattering using a Malvern Zetasizer Nano ZS90.

4.2.2.2 Measurement of surface tensions and interfacial tensions

The dynamic surface and interfacial tension was measured via axisymmetric drop shape analysis of pendant drops with a Ramé-hart goniometer (model-250). An inverted pendant drop of oil or an air bubble immersed in the aqueous phase was created by a syringe pump with a steel needle and the volume of the oil drop and air bubble was controlled by the pump. This setup is identical to the flotation operation where air bubbles (dispersed phase) are blown into particle suspension (continuous phase). A high-speed CCD camera was programmed to capture the variation of oil drop/bubble shape with time and the interfacial/surface tension was calculated by analyzing the contour shape resulting from the balance of gravitational forces and tension forces. All experiments were performed at room temperature of 21℃. The dynamic surface/interfacial tension was measured for two different initial EC concentrations (0.05 and 0.08 wt%) and three NaCl concentrations (0.2mM, 10mM and 20mM). The EC particle concentrations were chosen to make sure the bulk concentration can be treated as a constant during the measurement[20]. At least five identical measurements were repeated for each condition.

4.2.2.3 Contact angle

Glass slides pretreated with Piranha solution were coated by 4% EC-ethanol solution with spin coating (1500rpm, 30s). The measurements were carried out in a quartz cell filled with water with an inverted setup because silicone oil is lighter than water. The prepared substrate was submerged in the cell and suspended by a holder with the coated surface facing downwards. A drop of silicone was squeezed out from a U-shaped needle.

4.2.2.4 Flotation deinking

Flotation deinking was performed to show the advantage of oil-coated bubbles over air bubble. A flotation cell was designed and made in house with an oil chamber on the bottom and the sample chamber on top separated by a fritted disk. Silicone oil was chosen because it has a positive spreading coefficient and can fully engulf air bubbles. 100µL ink suspension was diluted by 400mL DI water and the NaCl concentration was 100mL to screen any electrostatic repulsion. The flotation was carried out for 3 min with an air flow rate of 5000 cm^{-3}/min.

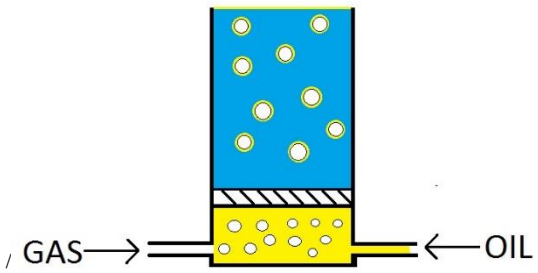

Figure 4-1 Schematic diagram of a flotation cell made in house.

4.3 Results and Discussion

4.3.1 The effect of EC particle concentrations and salt concentrations on adsorption kinetics

EC suspension with average radii of 130nm was prepared with the previously described method and the effect of two different EC concentration (0.05% and 0.08%) with three salt concentrations (0.2mM, 10mM and 20mM) on adsorption kinetics were studied by dynamic interfacial tensiometry as shown in Figure 4-2 and Figure 4-3. There was no significant change in interfacial tension from control experiments with particle-free supernatants of centrifuged particle dispersions, which proves the absence of surface-active impurities in the system. All the dynamic interfacial tension curves showed a similar trend that there was a significant decrease at initial time regime, followed by a sluggish change indicating that the system approaches steady-state. At early stage, the surface coverage of the interface is very low. Thus, the energy barrier for particle adsorption only originates from particle-interface interactions. As the surface coverage increases, the adsorbed particles create an additional energy barrier by (1) interfacial area blocking and (2) DLVO forces between adsorbed particles and the particles near the interface. The energy barrier at late stage is around 17kT (Appendix A Table A-1) and the possibility that particles can overcome a 17kT energy barrier from only thermal fluctuation with energy level of kT is very low. This explains why the change in interfacial tension at late stage is very small.

Previous study by Bizmark showed that EC suspensions with a concentration greater than 0.04% can prevent significant reduction in bulk concentration during the course of measurement and reach surface tension of 38.9 ± 0.6 mN/m at steady state[20]. The steady-state dynamic surface tension from the current research in Figure 4-2 was 39.1 ± 0.8 mN/m and in good agreement with data reported by Bizmark. The desorption energy ΔG =

4.65×10^5 kT based on Equation 1.1 given EC contact angle $\theta = 73°$[23]. In addition, the maximum packing density Θ_{max} can also be predicted from Equation 1.24 developed in a recently publication[23]. The predicted value $\Theta_{max} = 0.92$, shows close agreement with the assumption of hexagonal close packing density of 0.91. Similarly, the steady-state interfacial tension for silicone oil-water interface from Figure 4-3 was 14.2 ± 0.7 mN/m, which is equivalent to maximum packing density of 0.85 given EC contact angle $\theta = 84°$ at silicone oil-water interface. The desorption energy ΔG of EC at oil-water interface is 4.40×10^5 kT and EC shows a strongly irreversible adsorption at both oil-water and air-water interfaces because the desorption energy is much greater than thermal fluctuation. It can also be concluded from the desorption energy that one single EC particle shows a similar thermodynamic benefit at air-water and oil-water interfaces. Thus, any differences in the reduction rates of interfacial tension are caused by adsorption kinetics.

The effect of EC concentration on dynamic interfacial tension can be observed from Figure 4-2 and Figure 4-3 that higher EC concentration resulted in faster particle adsorption. This can be explained by greater driving force for diffusion resulting from higher particle concentration, especially from bulk to sublayer where the mass transfer is diffusion controlled. However, it is difficult to conclude any significant effect of salt concentration on dynamic interfacial tension.

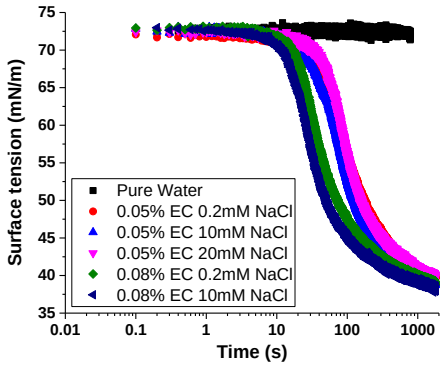

Figure 4-2 The dynamic surface tension of air-EC suspension as a function of EC concentration and NaCl concentration.

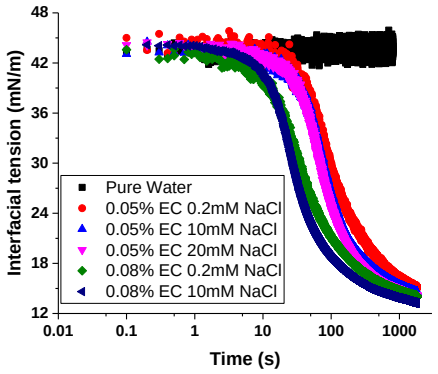

Figure 4-3 The dynamic interfacial tension of silicone oil-EC suspension as a function of EC concentration and NaCl concentration.

4.3.2 Modelling of EC particle adsorption

The initial stage analysis was performed by fitting dynamic interfacial tension to Equation 1.13. For air-water interface, we define the "initial stage" as the time period when surface tension drops 2mN/m from the starting value. For silicone oil-water interface, the same method was applied with 3mN/m as the critical value. The fitted plots for air-water

dynamic surface tension and silicone oil-water dynamic interfacial tension are shown in Figure 4-4 and Figure 4-5, respectively and summarized in Table 4-1. In order to identify whether there is a significant difference in early-stage adsorption kinetics between different conditions, the results were analyzed by t-test in Appendix B and the same conclusion is obtained for air-water interface and oil-water interface. With 95% confidence, one finds difference in the early-stage slope between different EC concentrations (0.05% vs 0.08%), and between different NaCl concentrations when they are in the lower end (0.2mM vs 10mM). However, the difference is not observed between different NaCl concentrations in the higher end (10mM vs 20mM). The Debye length of particles with 10mM NaCl concentration are 50% greater than that of the same particles with 20mM NaCl concentration, yet no significant difference in adsorption kinetics were observed. Thus 10mM can be taken as a salt concentration when electrostatic interactions have minimal effect on adsorption energy barrier. The dynamic interfacial tension of EC suspensions with salt concentrations greater than 20mM cannot be measured due to the agglomeration of particles[24]. The current findings are contradictory with a previous publication by Bizmark, who showed that the adsorption kinetics was not influenced by salt concentration as long as it is smaller than the critical coagulation concentration[24]. This inconsistency is caused by different modelling methods for particle adsorption kinetics, and discussed in Appendix C.

Additionally, early-stage interfacial tension shows a faster decrease at the oil-water interface than at the air-water interface, indicating a lower energy barrier given their comparable desorption energy.

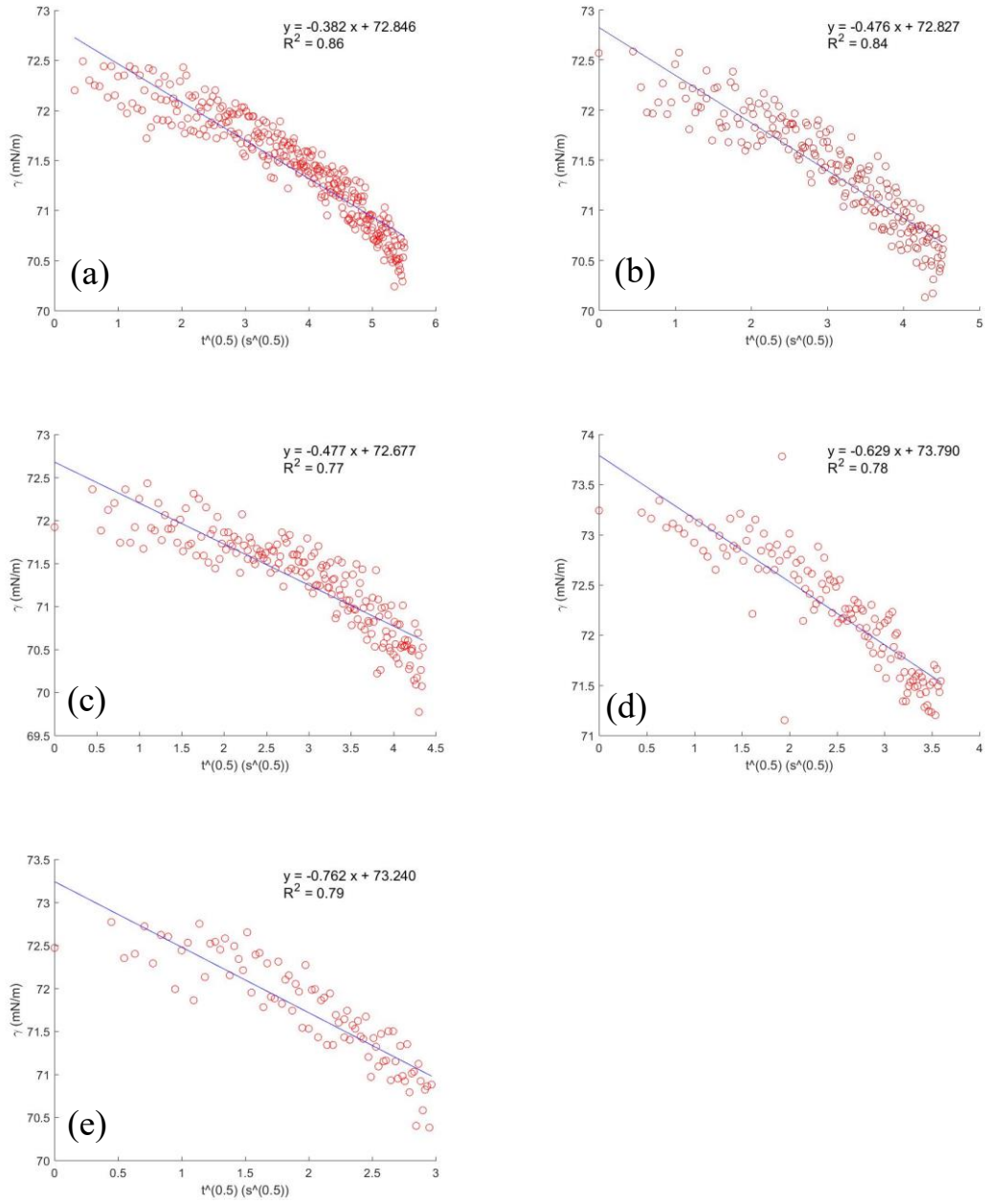

Figure 4-4 Plots of early stage dynamic surface tension data (a) 0.05% EC 0.2mM NaCl (b) 0.05% EC 10mM NaCl (c) 0.05% EC 20mM NaCl (d) 0.08% EC 0.2mM NaCl (e) 0.08% EC 10mM NaCl. Solid blue lines are linear regression with parameters indicated in each panel.

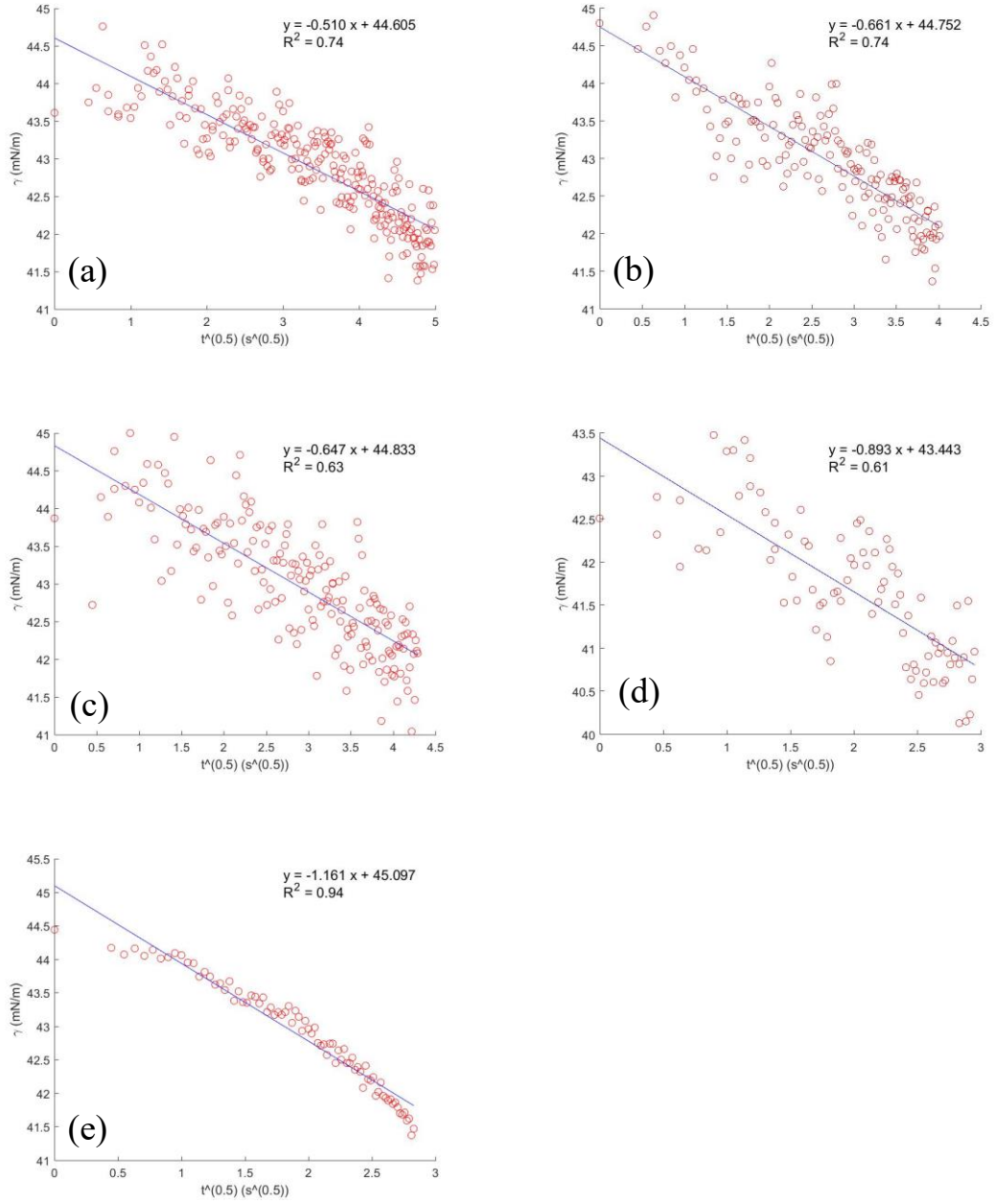

Figure 4-5 Plots of early stage dynamic interfacial tension data (a) 0.05% EC 0.2mM NaCl (b) 0.05% EC 10mM NaCl (c) 0.05% EC 20mM NaCl (d) 0.08% EC 0.2mM NaCl (e) 0.08% EC 10mM NaCl. Solid blue lines are linear regression with parameters indicated in each panel.

Table 4-1 Fitted slope and computed energy barrier from Equation 1.12 and Equation 1.13. The actual diffusion coefficient of EC particle is 1.7×10^{-12} m^2 s^{-1}.

Mass concentration (g/L)	Salt concentration (mM)	Type of interface	$\frac{d\gamma}{d\sqrt{t}}$ ($N\ m^{-1}\ s^{-0.5}$)	ΔE (kT)	ΔG (kT)
0.5	0.2	air-water	-3.69E-04 ± 1.91E-06	-2.02 ± 1.04E-02	4.65E+0.5
0.5	10		-4.77E-04 ± 1.40E-06	-2.54 ± 5.86E-03	
0.5	20		-4.81E-04 ± 8.54E-06	-2.55 ± 3.55E-02	
0.8	0.2		-6.25E-04 ± 5.07E-06	-2.14 ± 1.62E-02	
0.8	10		-7.68E-04 ± 7.19E-06	-2.55 ± 1.87E-02	
0.5	0.2	oil-water	-5.46E-04 ± 3.71E-06	-2.92 ± 1.36E-02	4.40E+0.5
0.5	10		-6.66E-04 ± 7.23E-06	-3.32 ± 2.17E-02	
0.5	20		-6.46E-04 ± 3.01E-06	-3.26 ± 9.33E-03	
0.8	0.2		-9.23E-04 ± 1.82E-05	-3.02 ± 3.95E-02	
0.8	10		-1.15E-03 ± 2.47E-05	-3.47± 4.29E-02	

4.3.3 Energy barrier analysis based on the early stage modelling

Equation 1.12 and Equation 1.13 describe the relationship between the change in interfacial tension and parameters that affects the kinetics and thermodynamics of the adsorption process. The bulk concentration c_{eq}, the Stokes-Einstein diffusion coefficient and the energy barrier determine the kinetics, *i.e.* the time consumption when a particle diffuses to the sublayer, overcomes the energy barrier, and adsorbs on the interfaces. On the other hand, the desorption energy ΔG shows the thermodynamics of the process, *i.e.* the magnitude in interfacial tension change when one particle adsorbs on the interfaces.

The energy barriers for particle adsorption on interfaces were calculated based on Equation 1.12 and Equation 1.13, and summarized in Table 4-1. It is surprising that the particle adsorption energy barriers were negative, indicating the absence of energy barrier. However, this is contradictory with the experiment results that salt concentration shows a significant impact on adsorption kinetics, demonstrating the presence of energy barrier originated from electrostatic interactions. Thus, the negative energy barrier results from the uncertainties in desorption energy.

It has been proved that the contact angles of particles at interfaces are not identical even if they adsorb to interface from the same particle suspension[25-26]. Thus, there is a discrepancy in contact angle measured from macroscopic film and the contact angle of a single particle at interface. Thus, it is possible that the contact angle of particles that adsorb on interfaces at early stage is greater than the bulk average because their wettability is more favourable in reducing interfacial tension. Similarly, it is also well-known that dynamic light scattering overestimates the particle size, and early adsorbed particles are expected to be smaller than the bulk average because of lower energy barrier. As a result, it is necessary to calibrate the desorption energy term to account for the uncertainties from contact angle and particle size.

It has been shown by t-test that 10mM NaCl can eliminate the effect of electrostatic interactions through screening effect. Thus, the effect of electrostatic interactions on energy barrier was analyzed by comparing the energy barrier at 0.2mM NaCl and 10mM NaCl, and the desorption energy was calibrated to obtain zero energy barrier when NaCl concentration is 10mM as shown in Table 4-2. The energy barriers induced by electrostatic

interactions are in the order of 0.4-0.5kT, and the magnitude of energy barrier is independent of type of interfaces.

This observation is consistent with theoretical prediction. Electrostatic interactions have two components, electric double layer component between the charged particles and the charged interfaces, and image force component between the charged particles and its image charges in the other medium which is air or oil in our case. For the electric double layer component, it has been shown that the hydroxide ions adsorb strongly on air-water interfaces and oil-water interfaces. As a result, the zeta-potentials of air bubble and silicone oil droplet in water are very similar and so do the electric double layer interactions[27]. For image force, the magnitude of the image charge is dependent on the relative permittivity of different mediums and the charge of original particles, as shown in Equation 4.1[28]. In our case, the relative permittivity of air or oil is much smaller than that of water, leading to a comparable image charge in air and in oil. Thus, the image force components are also very similar for air-water system and oil-water system, and this explains the consistency between theories and our experimental results from dynamics interfacial tension analysis.

$$q_{image} = q_{particle} \frac{\varepsilon_{water} - \varepsilon_{air/oil}}{\varepsilon_{water} + \varepsilon_{air/oil}} \quad \textbf{(4.1)}$$

Table 4-2 Adjusted energy barrier by changing desorption energy to achieve barrierless adsorption at 10mM.

Mass concentration (g/L)	Salt concentration (mM)	Type of interface	ΔE (kT)(Adjusted)	ΔG (kT) (Adjusted)
0.5	0.2	air-water	5.16E-01 ± 1.04E-02	1.66E+06
0.5	10	air-water	0	1.66E+06
0.8	0.2	air-water	4.13E-01 ± 1.62E-02	1.67E+06
0.8	10	air-water	0	1.67E+06
0.5	0.2	oil-water	3.97E-01 ± 1.36E-02	2.31E+06
0.5	10	oil-water	0	2.31E+06
0.8	0.2	oil-water	4.45E-01 ± 3.95E-02	2.50E+06
0.8	10	oil-water	0	2.50E+06

Assuming the early stage energy barrier is induced by only electrostatic and van der Waals interactions, the differences in van der Waals induced energy barrier between interfaces were calculated by directly comparing the energy barrier in Table 4-1 from different interfaces because the electrostatic interactions have a similar effect on particle adsorption at air-water and oil-water interfaces. Table 4-3 shows the difference in van der Waals induced early energy barrier and the positive value indicates that the energy barrier that a particle has to overcome to reach oil-water interface is lower than the energy barrier for air-water interface. More importantly, the van der Waals force is attractive for particle adsorption to oil-water interface, but repulsive when particles approaching air-water interface as shown in Table 4-4. This observation provides a significant implication to flotation separation of hydrophilic particles that air bubbles coated by a thin layer of oil

show a lower energy barrier for particles to attach due to positive van der Waals interactions.

Table 4-3 Differences in van der Waals induced energy barrier between air-water and oil-water interfaces.

Mass concentration (g/L)	Salt concentration (mM)	$\Delta E_{air} - \Delta E_{oil}$ (kT)
0.5	0.2	8.95E-1 ± 1.71E-02
0.5	10	7.77E-1 ± 2.25E-02
0.5	20	7.01E-1 ± 3.67E-02
0.8	0.2	8.92E-1 ± 4.27E-02
0.8	10	9.23E-1 ± 4.68E-02

Table 4-4 Hamaker constants for Materials 1,2 across Medium 3.

Material 1	Material 2	Medium 3	Hamaker constant (kT)
EC	EC	Vacuum	1.4E+01[29]
Water	Water	Vacuum	9.0E+00
Silicone oil	Silicone oil	Vacuum	1.1E+01[30]
EC	Air	Water	-2.0E+00
EC	Silicone oil	Water	4.0E-01

4.3.4 Oil-coated bubble flotation deinking

Most of the current efforts in improving flotation separation efficiency focused on surface modification of particles in water[31-33]. However, different surface modifiers are necessary to change the surface property of each particle category, which is difficult to be applied in an industrial setup. The particle adsorption kinetics study in previous sections provides an alternative method to improve flotation efficiency by coating air bubbles with an oil layer.

Flotation deinking was performed to show the efficacy of oil-coated bubble flotation in hydrophilic inks removal. Figure 4-6 shows the ink suspension with and without flotation treatment. The accept from air bubble flotation did not show any improvement compared with the ink suspension without treatment, indicating the incompatibility between air bubble flotation and hydrophilic inks. However, the accept from oil-coated bubble had a much lower turbidity than untreated sample and improvement in water quality demonstrates the success of oil-coated bubble flotation in hydrophilic particles removal.

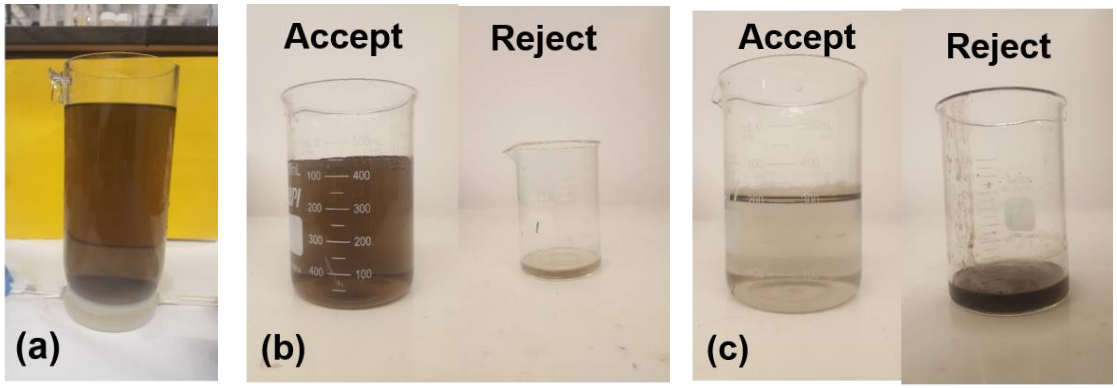

Figure 4-6 Ink suspension (a) before flotation, and accept/reject after (b) air bubble flotation (c) oil-coated bubble flotation.

4.4 Conclusions

The particle adsorption kinetics on fluid-fluid interfaces were studied by dynamic interfacial tension measurement, and the early stage energy barriers were analyzed by kinetics models to understand the effect of interface type on energy barrier. The electrostatic interactions have a similar impact on air-water and oil-water interfaces, and the difference in energy barrier is in all likelihood caused by van der Waals interactions. The oil-water interface allows faster adsorption rates and lower energy barriers for all particle and salt concentrations studied in this chapter, and the difference originates from the attractive van der Waals interactions. While the van der Waals interactions are repulsive in the case of particle adsorption on air-water interface. The difference in van der Waals interactions of these two cases are detected and quantified by dynamic interfacial tension measurement. The insights from this chapter are essential to improve the separation efficiency of hydrophilic particles from water, like mineral recovery and paper deinking process.

4.5 References

[1] Jiang, Y.; Liu, X.; Chen, Y.; Zhou, L.; He, Y.; Ma, L.; Gao, J., Pickering emulsion stabilized by lipase-containing periodic mesoporous organosilica particles: A robust biocatalyst system for biodiesel production. *Bioresource technology* **2014,** *153*, 278-283.

[2] Tang, J.; Lee, M. F. X.; Zhang, W.; Zhao, B.; Berry, R. M.; Tam, K. C., Dual responsive pickering emulsion stabilized by poly [2-(dimethylamino) ethyl methacrylate] grafted cellulose nanocrystals. *Biomacromolecules* **2014,** *15* (8), 3052-3060.

[3] Zhou, J.; Qiao, X.; Binks, B. P.; Sun, K.; Bai, M.; Li, Y.; Liu, Y., Magnetic Pickering emulsions stabilized by Fe3O4 nanoparticles. *Langmuir* **2011,** *27* (7), 3308-3316.

[4] Binks, B. P.; Murakami, R., Phase inversion of particle-stabilized materials from foams to dry water. *Nature materials* **2006,** *5* (11), 865-869.

[5] Jin, H.; Zhou, W.; Cao, J.; Stoyanov, S. D.; Blijdenstein, T. B.; de Groot, P. W.; Arnaudov, L. N.; Pelan, E. G., Super stable foams stabilized by colloidal ethyl cellulose particles. *Soft Matter* **2012,** *8* (7), 2194-2205.

[6] Stocco, A.; Rio, E.; Binks, B. P.; Langevin, D., Aqueous foams stabilized solely by particles. *Soft Matter* **2011,** *7* (4), 1260-1267.

[7] Haase, M. F.; Stebe, K. J.; Lee, D., Continuous Fabrication of Hierarchical and Asymmetric Bijel Microparticles, Fibers, and Membranes by Solvent Transfer‐Induced Phase Separation (STRIPS). *Advanced Materials* **2015,** *27* (44), 7065-7071.

[8] Lee, M. N.; Thijssen, J. H.; Witt, J. A.; Clegg, P. S.; Mohraz, A., Making a robust interfacial scaffold: bijel rheology and its link to processability. *Advanced Functional Materials* **2013,** *23* (4), 417-423.

[9] Witt, J. A.; Mumm, D. R.; Mohraz, A., Bijel reinforcement by droplet bridging: a route to bicontinuous materials with large domains. *Soft Matter* **2013,** *9* (29), 6773-6780.

[10] Binks, B. P.; Rocher, A.; Kirkland, M., Oil foams stabilised solely by particles. *Soft Matter* **2011,** *7* (5), 1800-1808.

[11] Binks, B. P.; Sekine, T.; Tyowua, A. T., Dry oil powders and oil foams stabilised by fluorinated clay platelet particles. *Soft Matter* **2014,** *10* (4), 578-589.

[12] Binks, B. P.; Johnston, S. K.; Sekine, T.; Tyowua, A. T., Particles at oil–air surfaces: powdered oil, liquid oil marbles, and oil foam. *ACS applied materials & interfaces* **2015,** *7* (26), 14328-14337.

[13] Zhang, T.; Davidson, D.; Bryant, S. L.; Huh, C. In *Nanoparticle-stabilized emulsions for applications in enhanced oil recovery*, SPE improved oil recovery symposium, Society of Petroleum Engineers: 2010.

[14] Chevalier, Y.; Bolzinger, M.-A., Emulsions stabilized with solid nanoparticles: Pickering emulsions. *Colloids and Surfaces A: Physicochemical and Engineering Aspects* **2013,** *439*, 23-34.

[15] Marku, D.; Wahlgren, M.; Rayner, M.; Sjöö, M.; Timgren, A., Characterization of starch Pickering emulsions for potential applications in topical formulations. *International journal of pharmaceutics* **2012,** *428* (1), 1-7.

[16] Crossley, S.; Faria, J.; Shen, M.; Resasco, D. E., Solid nanoparticles that catalyze biofuel upgrade reactions at the water/oil interface. *Science* **2010,** *327* (5961), 68-72.

[17] Böker, A.; He, J.; Emrick, T.; Russell, T. P., Self-assembly of nanoparticles at interfaces. *Soft matter* **2007,** *3* (10), 1231-1248.

[18] Frelichowska, J.; Bolzinger, M.-A.; Pelletier, J.; Valour, J.-P.; Chevalier, Y., Topical delivery of lipophilic drugs from o/w Pickering emulsions. *Int. J. Pharm.* **2009,** *371* (1), 56-63.

[19] Du, X. T.; Lee, D. T.; Hsieh, J. S., Inkjet ink behaviors and its implication in adsorption deinking. *Separation Science and Technology* **2016,** *51* (18), 2857-2867.

[20] Bizmark, N.; Ioannidis, M. A.; Henneke, D. E., Irreversible adsorption-driven assembly of nanoparticles at fluid interfaces revealed by a dynamic surface tension probe. *Langmuir* **2014,** *30* (3), 710-717.

[21] Zhang, Y.; Shitta, A.; Meredith, J. C.; Behrens, S. H., Bubble Meets Droplet: Particle‐Assisted Reconfiguration of Wetting Morphologies in Colloidal Multiphase Systems. *small* **2016,** *12* (24), 3309-3319.

[22] Berry, J. D.; Neeson, M. J.; Dagastine, R. R.; Chan, D. Y.; Tabor, R. F., Measurement of surface and interfacial tension using pendant drop tensiometry. *Journal of colloid and interface science* **2015,** *454*, 226-237.

[23] Zhang, Y.; Wang, S.; Zhou, J.; Zhao, R.; Benz, G.; Tcheimou, S.; Meredith, J. C.; Behrens, S. H., Interfacial Activity of Nonamphiphilic Particles in Fluid–Fluid Interfaces. *Langmuir* **2017,** *33* (18), 4511-4519.

[24] Bizmark, N.; Ioannidis, M. A., Effects of ionic strength on the colloidal stability and interfacial assembly of hydrophobic ethyl cellulose nanoparticles. *Langmuir* **2015,** *31* (34), 9282-9289.

[25] Isa, L.; Lucas, F.; Wepf, R.; Reimhult, E., Measuring single-nanoparticle wetting properties by freeze-fracture shadow-casting cryo-scanning electron microscopy. *Nature communications* **2011,** *2*, 438.

[26] Snoeyink, C.; Barman, S.; Christopher, G. F., Contact angle distribution of particles at fluid interfaces. *Langmuir* **2015,** *31* (3), 891-897.

[27] Creux, P.; Lachaise, J.; Graciaa, A.; Beattie, J. K.; Djerdjev, A. M., Strong specific hydroxide ion binding at the pristine oil/water and air/water interfaces. *The Journal of Physical Chemistry B* **2009,** *113* (43), 14146-14150.

[28] Wang, H.; Singh, V.; Behrens, S. H., Image charge effects on the formation of Pickering emulsions. *The journal of physical chemistry letters* **2012,** *3* (20), 2986-2990.

[29] Bergström, L.; Stemme, S.; Dahlfors, T.; Arwin, H.; Ödberg, L., Spectroscopic ellipsometry characterisation and estimation of the Hamaker constant of cellulose. *Cellulose* **1999,** *6* (1), 1-13.

[30] Drummond, C. J.; Chan, D. Y., van der Waals interaction, surface free energies, and contact angles: dispersive polymers and liquids. *Langmuir* **1997,** *13* (14), 3890-3895.

[31] Beaussart, A.; Parkinson, L.; Mierczynska-Vasilev, A.; Beattie, D. A., Adsorption of modified dextrins on molybdenite: AFM imaging, contact angle, and flotation studies. *Journal of colloid and interface science* **2012,** *368* (1), 608-615.

[32] Laitinen, O.; Kemppainen, K.; Ämmälä, A.; Sirviö, J. A.; Liimatainen, H.; Niinimäki, J., Use of chemically modified nanocelluloses in flotation of hematite and quartz. *Industrial & Engineering Chemistry Research* **2014,** *53* (52), 20092-20098.

[33] Reddy, M. S.; Okuda, T.; Kurose, K.; Tsai, T.-Y.; Nakai, S.; Nishijima, W.; Okada, M., Surface ozonation of polyvinyl chloride for its separation from waste plastic mixture by froth floatation. *Journal of Material Cycles and Waste Management* **2010,** *12* (4), 326-331.

CHAPTER 5. ANALYTICAL METHODS OF MICROSTICKIES DEPOSITION BY MODEL SURFACES

5.1 Introduction

Most of the previous studies focused on deposition of stickies onto paper machine. And the detrimental effect of stickies on paper quality has been shown to increase the dirt count [1] and decrease the mechanical strength of paper (shown in this study). All the previous methods failed to provide an accurate measurement about the deposition of microstickies on fiber due to the difference in surface properties between fiber and paper machine. Thus, it is important to have a model surface with similar properties to cellulose fiber. In addition, image analysis could only evaluate the speck area and number of microstickies but cannot characterize the composition, which is also important to prevent deposition. Finally, all the previous measurement methods were based on commercial pulp or pulp from paper mills. Thus, the exact amount of microstickies in the system was unknown, and there is no way to evaluate different measurement methods. Therefore, some fundamental studies based on a model sticky system with known microstickies amount are necessary.

In this study, silicon wafers were coated with cellulose to mimic the property of cellulose fiber and were used as a model surface for microstickies deposition. Polyvinyl acetate was chosen as the model microstickies and the deposition process was conducted in water, PVAc two-component system and PVAc, fiber, water three-component system. Microstickies agglomeration and deposition was induced either by shear force or by aeration, avoiding any chemical change in the system. The surfaces were further analyzed

by XPS and water contact angle to characterize the chemical structure and functional groups of microstickies.

5.2 Materials and Methods

5.2.1 Materials

Deionized water from an ion-exchange system with a resistivity of 18 MΩ cm^{-1} was used in all described experiments. Micro-crystalline cellulose was obtained from Avicel PH-101 (Fluka Chemical Corporation). Polyvinyl acetate (PVAc) with average molecular weight of 100,000, methanol, 50% N-methylmorpholine-N-Oxide (NMMO) and Dimethyl Sulfoxide (DMSO) were purchased from Fisher Scientific. Polyvinylamine (PVAm) with average molecular weight of 340,000 was donated by BASF Corporation as Lupamin 9095 with 95% hydrolysis. Flexible high-density polyethylene (HDPE) was purchased from Henta Corporation. Silicon wafer was obtained from TEM Tailsil.

5.2.2 Methods

5.2.2.1 Preparation of cellulosic based model surfaces

Figure 5-1 illustrated the procedure for cellulosic model surface preparation. Silicon wafers with a top silicon oxide layer were used as the base substrate for the cellulose film. The silicon oxide top layer was obtained by oxidizing the wafer at ambient atmospheric pressure in Tystar Nitride Furnace at 1050°C for 30 min. It was then cut into smaller pieces with a diamond knife and washed with acetone, methanol, and isopropanol. The wafers were cleaned under UV-Ozone for 5 min and stored in a petri-dish.

Polyvinylamine was used as an anchoring polymer for the cellulose film on the silicon surface. To do this, the silicon surfaces were immersed in PVAm (0.1%) for 15 min followed by washing with DI water for 3 min and dried under 50°C for 30 min.

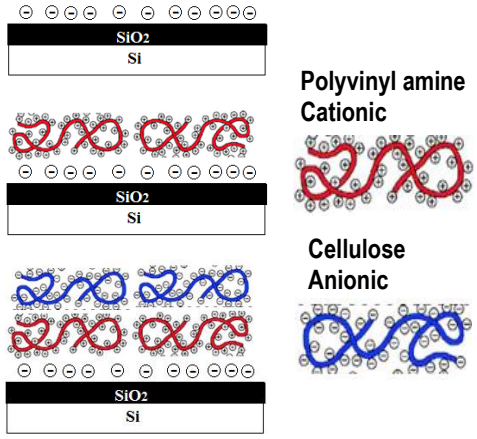

Figure 5-1 Preparation procedure of cellulosic model surface.

A cellulose solution was prepared by dissolving microcrystalline Avicel cellulose in 50%wt water/N-methylmorpholine-N Oxide (NMMO) at 105°C. The ratio of NMMO and water was controlled because cellulose is soluble in NMMO only in the dark area of phase diagram shown in Figure 5-2. Temperature and time should be carefully controlled to prevent cellulose degradation. Dimethyl Sulfoxide (DMSO) was added to adjust the concentration (0.5%) and viscosity of the cellulose suspension.

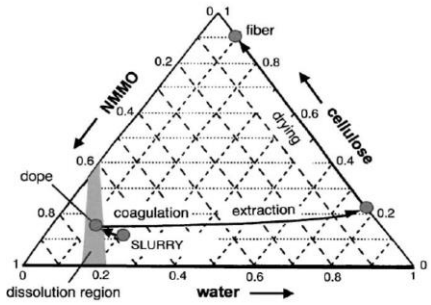

Figure 5-2 Ternary diagram of cellulose, water and NMMO.

The cellulose solution was then spin coated (SCS G3P8 Spin Coater) by depositing 600 µl of the prepared cellulose solution on the PVAm-modified substrates at 2500 rpm for 15 s. The cellulose-coated substrates were removed from the coater, immersed in water for 4 h and then dried under room temperature for 8 h[2].

5.2.2.2 Shear force and aeration induced agglomeration and deposition

Polyvinyl acetate was dissolved in methanol[3] with a mass fraction of 1% and 2%. Then, 50g of PVAc solution was injected into 300g water or 300 g pulp (0.5% consistency) to generate microstickies. Two different surfaces, HDPE and cellulose coated silicon wafer were chosen as the surfaces for deposition measurement. For shear force induced agglomeration, the surfaces were submerged in solution and rotated at 500 rpm for 15 mins.

For aeration induced agglomeration, the surfaces were submerged in the same solutions and aeration diffusers connected to an air pump were put into solution for 15 min to generate small air bubbles and induce agglomeration of microstickies. The surfaces were dried under 70°C for 2 hours and the weight of each surface was measured before and after deposition. The experimental setup was shown in Figure 5-3.

Figure 5-3 Experimental setup for (left) shear force and (right) aeration induced agglomeration and deposition.

5.2.2.3 Macrostickies classifier for stickies measurement (Pulmac method)

50g of the PVAc/methanol solution (1%) was injected into 300g of pulp slurry (0.5% consistency), and the two agglomeration methods described previously were utilized. After that, solutions before and after agglomeration were filtered using a Pulmac Master Screen with a slot size of 100μm. The rejects were collected on a filter paper and measured by INGEDE Method 4[4].

5.2.3 Characterization

5.2.3.1 Tensile strength measurement

Handsheets were prepared with the procedure of TAPPI T205 before and after deposition. The basis weight of the handsheet is 60 g/m^2. One handsheet was cut into three stripes with width of 1 inch. The tensile strength was measured by QC-1000 Tensile Tester and the tensile index was calculated by Equation 5.1

$$TensileIndex(\frac{N \times m}{g}) = \frac{TensileStrength.(N)/Width(m)}{Basisweight(g/m^2)} \quad \textbf{(5.1)}$$

5.2.3.2 X-Ray photoelectron spectroscopy

XPS analysis was performed with Thermo K-Alpha XPS. The XPS spectra of the cellulose films were obtained using a monochromatic Al Ka X-ray source (1486.6 eV) at a voltage of 15 kV and a current of 10 mA. The vacuum level of the analyzing chamber was maintained below 5E-7 Pa during the measurements. The pass energy and step width during the survey scan were set at 200 and 1 eV, respectively. In the element narrow scan mode, these scan parameters were set at 50 and 0.1 eV, respectively. The binding energies for all spectra were determined with respect to the C 1s reference signal (unoxidized C–C band) at 285.0 eV.

5.2.3.3 Water Contact Angle

The water contact angle was measured by Rame-hart Model 250 goniometer to characterize the hydrophobicity of the polymer-coated wafer. Prior to beginning the contact angle measurement, the software was calibrated, and the alignment of the stand was checked. Then, 8 to 10 drops of water were placed on different areas of the samples, and the contact angles were averaged. The drops were around 6 µl.

5.2.3.4 INGEDE Method 4

The filter paper prepared with the Pulmac Master Screen was dried and dyed by India ink. After that, the entire surface of filter paper was sprinkled with Duralum Special White 220 grit powder, placed in an oven and covered with a steel gravity press for 10 minutes. The

samples prepared by INGEDE Method 4 were scanned using Spec*Scan@2000 setting for Stickies INGEDE BLACK.

5.3 Results and Discussion

5.3.1 Chemical composition of cellulose coated wafer

Figure 5-4 profiles the XPS survey scan spectra of the silicon dioxide, PVAm coated and cellulose coated wafers. Si has the binding energy of 154 eV and oxygen has the binding energy of 532 eV. After coating with PVAm, a clear N1s peak was detected at ca. 400 eV, suggesting the success of cationic polymer coating. However, after coating with cellulose, the peaks of Si and N became very small, and the peaks of C and O were dominant in the spectrum. N and Si was not detected because the newly coated cellulose layer is thick enough to stop the penetration of X-ray into the PVAm and SiO_2 layers.

Table 5-1 summarizes the element composition of the wafer surfaces and the data further proves the success of every step during the coating procedure. For the wafer coated with cellulose, C% was even higher than O% because the C/O ratio in cellulose is 1.2.

The water contact angle was also measured after each coating step as shown in Figure 5-5. Initially, the silicon wafer was covered by hydroxyl groups formed by UVO and the water droplet was flat. However, after coated with PVAm, the surface became more hydrophobic, and the contact angle increased to about 60 degrees. This contact angle value is very similar to the results reported by other researchers[5]. Finally, the surface went back to hydrophilic again, and the contact angle was very small after coated with cellulose.

Table 5-1 Surface element composition of wafer.

	Si(%)	O(%)	C(%)	N(%)
SiO_2	36.49	63.51		
PVAm	26.7	47.16	17.76	8.37
Cellulose	8.49	44.23	47.29	

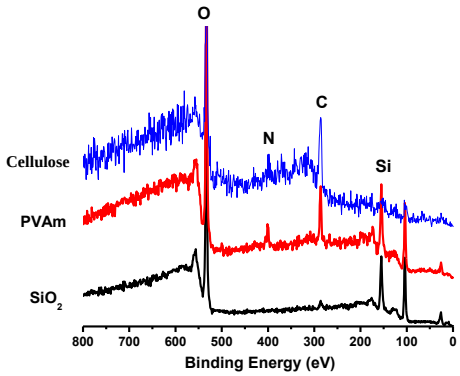

Figure 5-4 XPS survey spectrum of wafer.

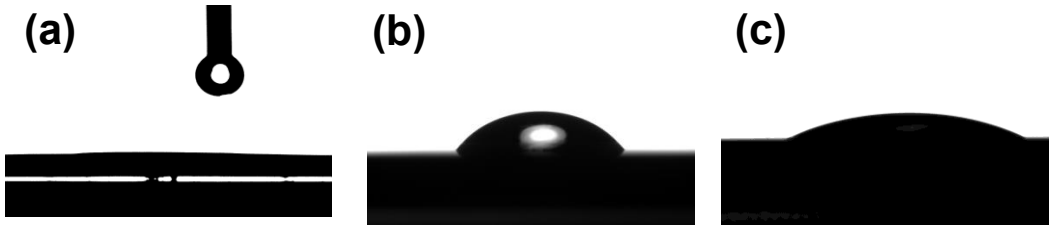

Figure 5-5 Water contact angle of (a) SiO_2 (b) PVAm 60º (c) cellulose coated wafer.

5.3.2 Deposition of microstickies on fibers and its influence on paper property

Before the measurement results, there are two issues to be clarified. First, the deposition of microstickies on fibers must be proven. In addition, the influence of deposition on fiber property should be studied.

It has been reported that stickies would associate with fibers or fines[6-8]. In this chapter, handsheets were made by microstickies/fiber suspension system and the cross-sections of handsheets were analyzed by XPS. Compared with handsheets made by pure cellulose, a new C=O peak appeared in the carbon-spectrum that proves the association between fibers and PVAc microstickies as in Figure 5-6.

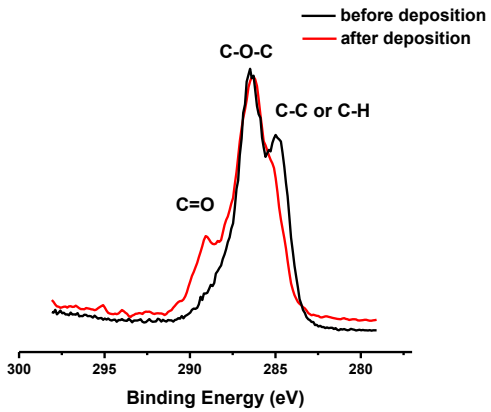

Figure 5-6 XPS carbon spectrum of handsheets before and after deposition experiments.

The physical strength of handsheets depends on the inter-fiber and intra-fiber bonding ability and bonding strength. It has been reported that organic materials, including lignosulfonate, lignin and defoamer would reduce the paper strength by 6% to 17%[9]. The deposition of organic materials on fiber destroys the hydrogen-bonding property between the fibers. Similar phenomenon was observed in Figure 5-7 that the tensile index of handsheets made after deposition experiments was 20% lower. Thus, it is necessary to develop a quantitative method to measure the deposition of microstickies on cellulosic fibers.

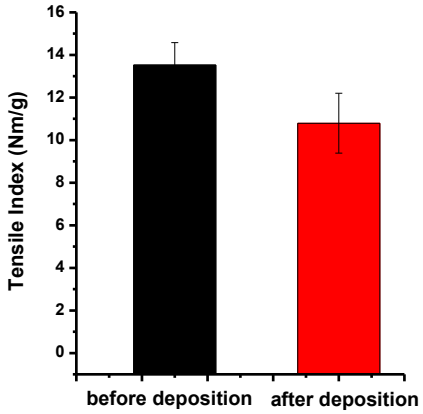

Figure 5-7 Tensile index of handsheets before and after deposition.

5.3.3 Deposition of microstickies on cellulose coated wafer

The microstickies suspension was prepared by injecting 1% or 2% PVAc/methanol solution into water or pulp suspension. Two different methods, shear force and aeration, were chosen to induce agglomeration of PVAc microstickies. Figure 5-8 shows the deposition results of PVAc onto cellulose coated wafers. In the PVAc/water system, the deposition amount was very large, and the deposition percentage was higher than 80% for both concentrations. However, in the PVAc/pulp system, the deposition amount was tiny, and the deposition percentage was less than 10%. The difference in the deposition amount is caused by the association between microstickies and fibers/fines with two mechanisms. First, the deposition of microstickies on fibers reduces the local concentration of PVAc and fewer PVAc particles are available to adsorb on model surfaces. In addition, the collision frequency between stickies and model surfaces is lower due to the inhibition of cellulose fines in water. Thus, the deposition amount is greatly reduced in pulp, and the results from shear force could not reveal the real deposition tendency of PVAc[7-8].

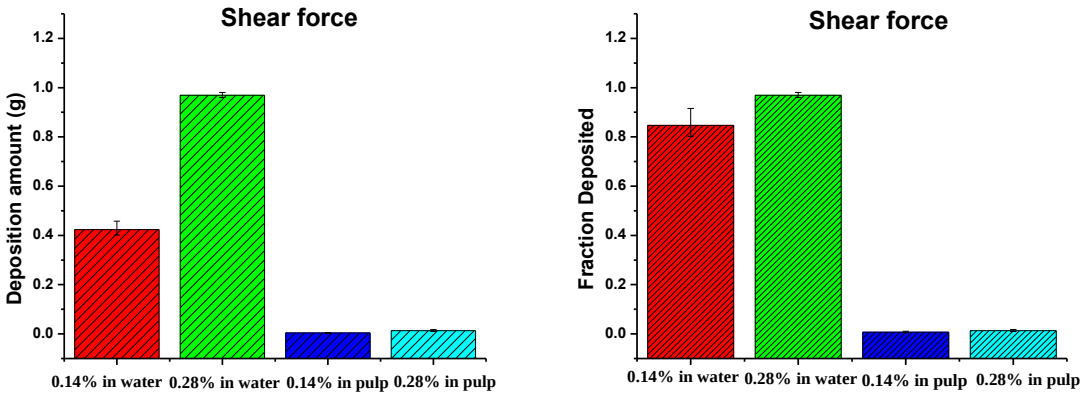

Figure 5-8 (left) Deposition amount and (right) deposition percentage of PVAc on wafer by shear force.

It has been reported that carbon dioxide bubbles generated from vacuum could also induce microstickies agglomeration[10]. However, this method was only applicable in acidic condition. Here, bubbles generated from aeration were used to induce agglomeration of PVAc microstickies. One main advantage is that the chemical environment is retained by avoiding any addition of chemicals.

In Figure 5-9, the deposition amount and percent of PVAc under aeration are shown, and comparisons between shear force and aeration are presented in Figure 5-10. The deposition amount of PVAc induced by aeration in pulp solution was far greater than that induced by shear force. Tiny bubbles generated by aeration with very large surface area selectively adsorb to hydrophobic PVAc microparticles and float onto the surface of the solution. This agglomeration process is less influenced by fiber in water because of the difference in hydrophobicity between fiber and PVAc. With the rising of bubbles, the bubble diameter increases and bubbles break up eventually. After that, all PVAc particles aggregate with each other and form larger particles.

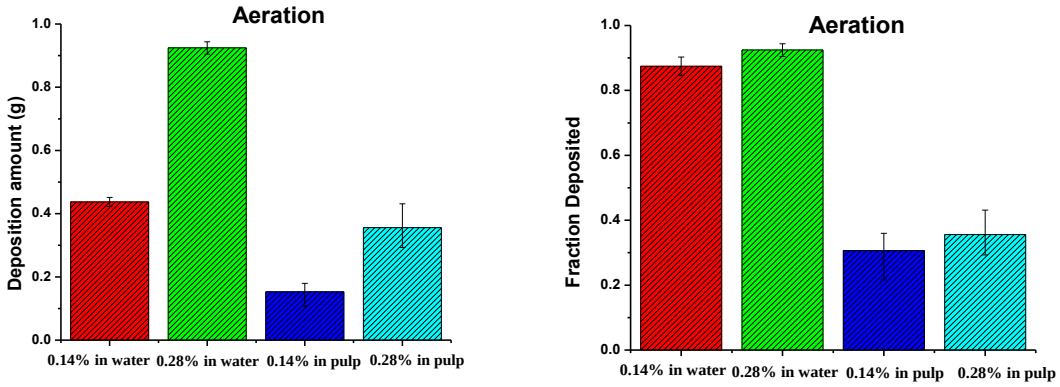

Figure 5-9 (left) Deposition amount and (right) deposition percentage of PVAc on wafer by aeration.

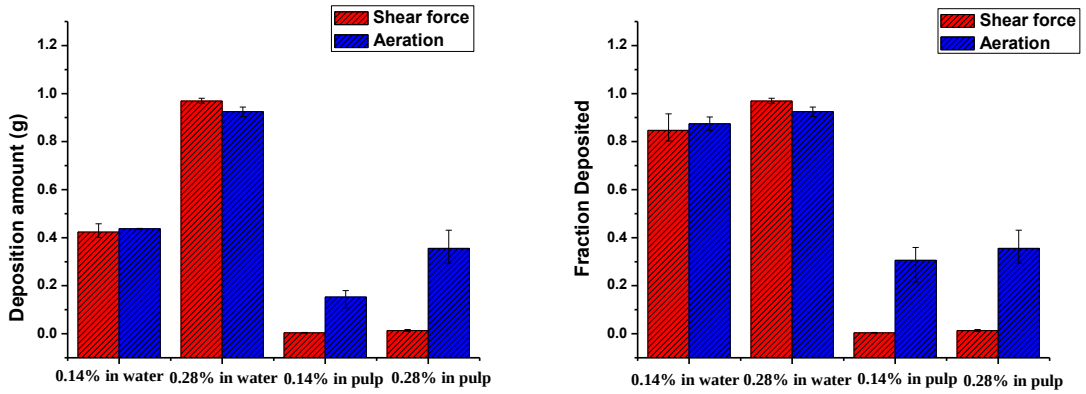

Figure 5-10 Comparison between shear force and aeration induced deposition.

Figure 5-11 and Figure 5-12 shows the XPS spectrums of the silicon wafer after the deposition experiment. The ratio of carbon and oxygen was summarized in Table 5-2. After deposition of microstickies, the surface element composition had a large increase in the percentage of carbon because of the deposition of PVAc, which has a high carbon/oxygen

ratio. In addition, in the carbon spectrum, C=O and C-O-C bonds were also observed, proving the deposition of PVAc on cellulosic model surfaces.

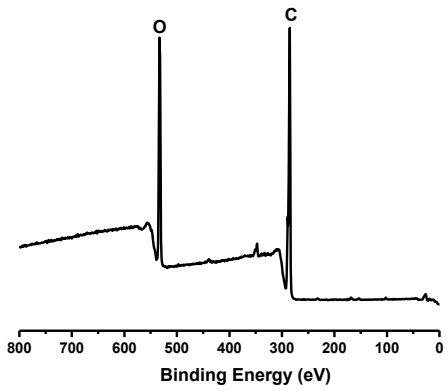

Figure 5-11 XPS survey spectrum of wafer after deposition experiments.

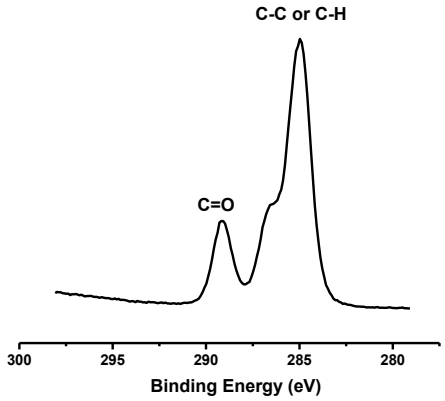

Figure 5-12 XPS carbon spectrum of wafer after deposition experiments.

Table 5-2 Surface element composition of wafers after deposition experiments.

	Si(%)	O(%)	C(%)	N(%)
SiO_2	36.49	63.51		
PVAm	26.7	47.16	17.76	8.37
Cellulose	8.49	44.23	47.29	
PVAc		25.36	74.64	

5.3.4 Deposition of microstickies on HDPE and comparison with cellulosic model surface

Doshi et al. used various surfaces for deposition measurement, including LDPE, HDPE, polyester, etc, and the most consistent results were obtained from HDPE[11]. The same deposition experiments were repeated with HDPE surfaces, and the trend of results was very similar to that of cellulose coated wafer. The average deposition amount of 1% PVAc in pulp was 3.15 mg, which is close to the result reported by Doshi[11]. However, it is impossible to evaluate the accuracy of this method because the total number of stickies was unknown in commercial pulp.

Figure 5-13 and Figure 5-14 shows the comparison between the deposition amount and percent on HDPE and the wafer under shear force and aeration. When the agglomeration was induced by shear force, the deposition amount on HDPE was very close to that on wafer. However, if it was induced by aeration, the deposition amount on HDPE surfaces was much greater.

In shear force induced deposition, the fibers and PVAc particles follows the motion of water and the forces exerted on particles includes interactions between particles,

interactions between particles and surface, and hydrodynamic force. Although the properties of HDPE and model surface are very different, the deposition amount on HDPE and model surface is very close under shear induced deposition, which proves that hydrodynamic force dominates the deposition process and the collision is random.

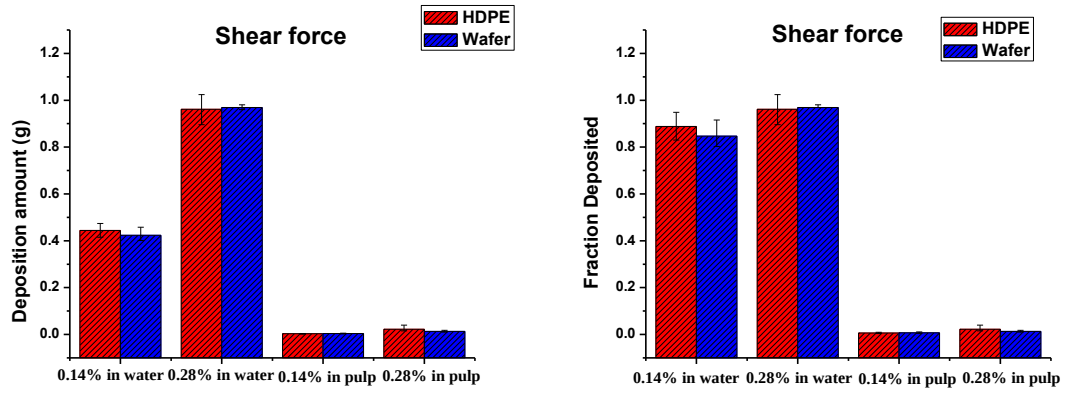

Figure 5-13 Comparison between cellulosic model surface and HDPE under shear force in terms of (left) deposition amount and (right) deposition percentage.

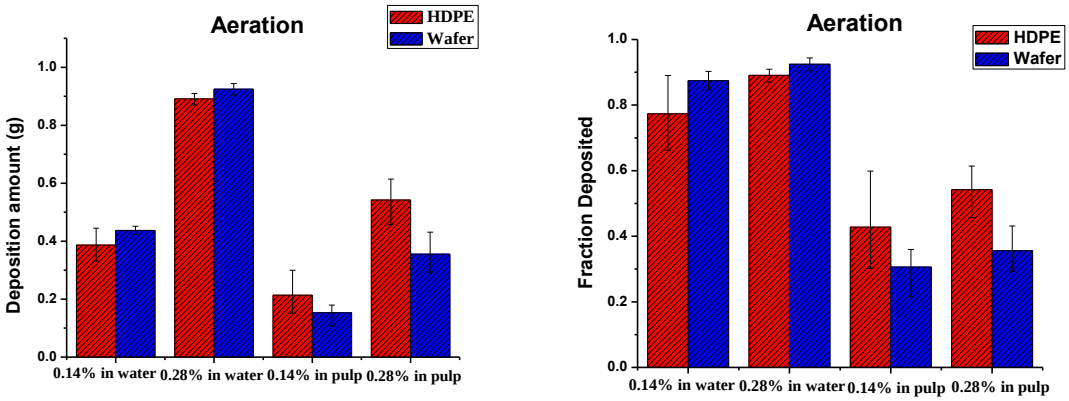

Figure 5-14 Comparison between cellulosic model surface and HDPE under aeration in terms of (left) deposition amount and (right) deposition percentage.

While for the aeration induced deposition, the bubbles selectively adsorb on the PVAc particles and the deposition of PVAc is dominated by the chemical interaction between the deposition surface and PVAc. From Figure 5-13 and Figure 5-14, it can be concluded that the difference between deposition on the HDPE and model surface was 35%.

5.3.5 Image analysis of microstickies

Figure 5-15 and Table 5-3 shows the image analysis results from INGEDE method 4. After shear force agitation, the particle size decreased a lot and the cumulative count increased, indicating the dispersion of particles. In addition, the cumulative area also became smaller because the sizes of particles were smaller than the detection limit of scanner. However, after aeration, both the size and cumulative area of stickies increased, resulting from the agglomeration of microstickies when they attached to gas bubbles. The size distribution shown in Figure 5-16 further proves the dispersion effect of shear force and agglomeration effect of aeration. The result from INGEDE method 4 shows the same trend with results from the deposition experiments.

In order to develop a new measurement method, it is necessary to compare the results with the current measurement methods. In this chapter, HDPE deposition and INGEDE Method 4 were chosen for comparison. INGEDE Method 4 measures the free stickies in water suspension. HDPE deposition measures the deposition amount on a hydrophobic surface and this new method measures the deposition amount on hydrophilic cellulose fiber. However, results from these three methods are not independent. For example, the deposition amount is relevant to the stickies size distribution and concentration in the

suspension. In INGEDE Method 4, the speck area from shear force is much smaller than that from aeration, which is consistent with the results that the deposition amount on cellulose model surfaces under shear force agitation was much smaller than that under aeration.

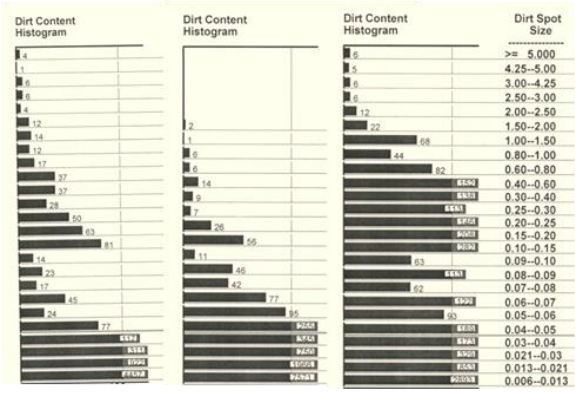

Figure 5-15 INGEDE Method 4 analysis (left) before agitation (middle) after shear force and (right) after aeration.

Table 5-3 Cumulative count and area from INGEDME Method 4.

	Cumulative count	Cumulative area (mm^2)
Before	6379	304.23
After shear	11285	194.68
After aeration	6180	2618.06

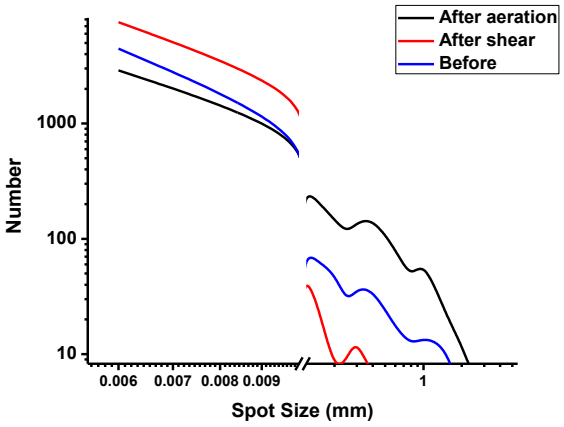

Figure 5-16 Spot Size distribution from INGEDE Method 4.

5.4 Conclusions

The deposition of microstickies on fiber reduces the physical strength of paper products and a model surface was prepared by coating silicon wafer with cellulose to mimic the property of paper fibers. A stickies model system was also set up by injecting PVAc/methanol solution into water or pulp. Two different agglomeration methods were selected to compare the measurement results between new and old measurement methods. For the shear force induced agglomeration, the deposition amount was not influenced by the chemical properties of surfaces because fiber fines and PVAc particles follows the motion of water and the deposition is dominated by hydrodynamic force. In addition, stickies also adsorb to fibers/fines, leading to a reduction in PVAc concentration. However, for aeration induced deposition, bubbles selectively attach to hydrophobic PVAc particles, and the measurement results are influenced by surface wettability. The results from new model surface are consistent to the results from current measurement methods, including HDPE deposition and INGEDE Method 4.

5.5 References

[1] Blanco, A.; Negro, C.; Monte, C.; Fuente, H.; Tijero, J., Overview of two major deposit problems in recycling: slime and stickies. Part II: stickies problems in recycling. *Progress in paper recycling* **2002,** *11* (2), 26-37.

[2] Gunnars, S.; Wågberg, L.; Cohen Stuart, M., Model films of cellulose: I. Method development and initial results. *Cellulose* **2002,** *9* (3), 239-249.

[3] Patel, S. N.; Banerjee, S., Deposition of hot melt and wax on surfaces. *Tappi journal* **1999,** *82* (11), 99-103.

[4] Doshi, M.; Jong, R.; Aziz, S. In *Measurement of microstickies*, TAPPI Engineering, Pulping and Environmental Conference 2008, 2008; pp 24-27.

[5] Illergård, J.; Enarsson, L.-E.; Wågberg, L.; Ek, M., Interactions of hydrophobically modified polyvinylamines: adsorption behavior at charged surfaces and the formation of polyelectrolyte multilayers with polyacrylic acid. *ACS applied materials & interfaces* **2010,** *2* (2), 425-433.

[6] Welkener, U.; Hassler, T.; McDermott, M., The effect of furnish components on depositability of pitch and stickies. *Nordic Pulp and Paper Research Journal (Sweden)* **1993**.

[7] Banerjee, S.; Roberts, M. K.; Hutten, M., Interaction among fiber, water and stickies. *Status Report to the Recycled Paper and Surface and Colloid Science* **1996**, 1.

[8] Hutten, I.; Diaz, R.; Roberts, M. K.; Jeffrey, C.; Banerjee, S., Fiber to water distribution of stickies. *Tappi journal* **1997,** *80* (4), 193-197.

[9] Springer, A. M.; Dullforce, J. P.; Wegner, T., The effects of closed white water system contaminants on strength properties of paper produced from secondary fiber. *Tappi J* **1985,** *68* (4), 78-82.

[10] De Jong, R. L.; Aziz, S., The agglomeration of microstickies. *ATIP. Association technique de l'industrie papetière* **2006,** *60* (5), 22-26.

[11] Doshi, M.; Dyer, J.; Aziz, S.; Jackson, K.; Abubakr, S., Quantification of micro stickies. *Paper Recycling Challenge-Process Control&Measurement* **1997**, 119-122.

CHAPTER 6. AGGLOMERATION OF MICROSTICKIES BY ELECTRIC FIELD

6.1 Introduction

Electrocoagulation has been widely used in water treatment processes. The anode metal material is oxidized to destabilize the particles and agglomerate the colloidal particles for sedimentation, filtration or flotation. For example, electrocoagulation removed the virus and other dissolved organic carbon in water[1-2]. Electrocoagulation also has various applications in paper industry. For example, electroflotation and electrocoagulation improved the removal efficiency of flexographic ink due to larger particle size and finer bubbles generated in the process[3-5]. Besides the benefits to deinking, electrocoagulation also improved the quality of the wastewater from paper mills by decreasing COD, BOD, turbidity and AOX through the oxidation mechanism with dissolved metals[6-8].

However, the dissolved metal ions from the oxidation of metal ions is a new kind contaminant in the water system. For example, ferrous ions and aluminum ions cannot precipitate in acidic condition and will remain in the water system. Furthermore, the sacrificial anode material should be replaced periodically to provide metals for electrocoagulation due to the corrosion of metal anode. In this study, electric field treatment was applied to treat microstickies for the colloidal particles agglomeration. And two experiment conditions were chosen to suppress the oxidation of anode and decrease the magnitude of current. First of all, the experiment was conducted in DI water environment to increase the electrical resistance. Secondly, a non-symmetric geometric set-up was

chosen that the surface area of anode is much smaller than cathode. In fact, the anode is a metal rod and the cathode electrode is the surface of the container. Based on the experimental condition of low current density and high voltage, a new agglomeration mechanism was proposed based on the migration of particles under electric field. In addition, effects of different detacky agents and dispersants, including polyvinyl alcohol, PDADMAC and lignosulfonate, on the stability of microstickies and the performance of electric treatment were investigated.

6.2 Materials and Method

6.2.1 Materials

Deionized water from an ion-exchange system with a resistivity of greater than 18 MΩ cm was used in all described experiments. Polyvinyl acetate (PVAc) with molecular weight about 100,000 and methanol were purchased from Fisher Scientific. The filter paper for filtration was quantitative filter paper with coarse porosity (09-790F and 09-790-4F). Poly(diallylmethylammonium chloride) with molecular weight of 200,000 was purchased from Sigma Aldrich. Flexible high-density polyethylene (HDPE) was purchased from Henta Corporation.

6.2.2 Methods

6.2.2.1 Influence of different chemicals to the deposition of PVAc on HDPE [9]

Polyvinyl acetate was dissolved in methanol with mass fraction 1% and 2%. 50g PVAc solution was injected into 300g DI water to generate microstickies. To study the influence of detacky agent and dispersant on the deposition of PVAc, different amounts of PVA,

lignosulfonate and PDADMAC were dissolved in water and shear force was generated to induce the agglomeration and deposition of PVAc on HDPE surfaces. The solution was mixed at 500 rpm for 15min. The surfaces were dried under 70°C for 2 hours and the weights of surfaces were measured before and after deposition.

6.2.2.2 Electric field treatment of microstickies suspension

60g of 1% (w/w) PVAc/methanol solution was injected to 1500g DI water and the solution was treated with electric field under different voltage and chemicals. The change in particle size cannot be measured by dynamic light scattering since the size is much greater than 5 microns. A semi-quantitative method was applied through filtration. The solution was filtrated through 75-micron mesh screen, Q8 filter paper and Q2 filter paper respectively as shown in Figure 6-1. The pore sizes of Q8 and Q2 filter papers are 1-5 microns and 20-25 microns. The turbidity and UV absorbance of the filtrates were measured.

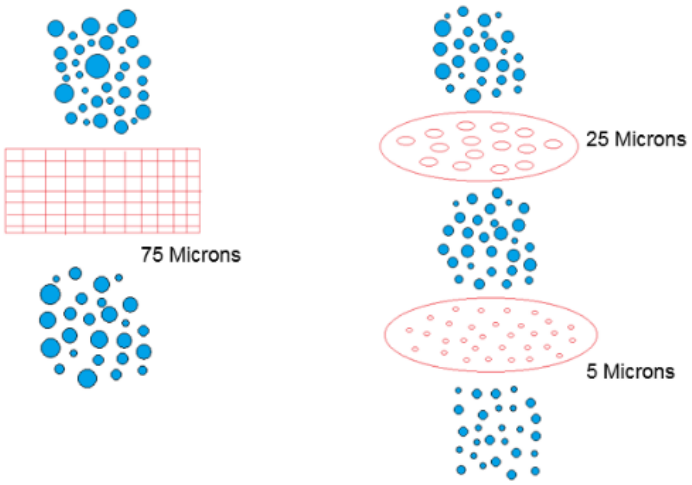

Figure 6-1 Schematic flow chart of the filtration process for filtrate analysis.

6.2.2.3 Macrostickies classifier method for microstickies measurement[10]

50g PVAc/methanol solution (1%) was injected into 300g pulp slurry (0.5% consistency). The solutions before and after agglomeration were put into Pulmac Master Screen with slot size of 100μm. The rejects were collected on a filter paper and measured by INGEDE Method 4. The filter paper prepared by Pulmac Master Screen was dried and dyed by India ink. After that, the entire surface of filter paper was sprinkled with Duralum Special White 220 grit powder, placed in the oven and covered with a steel gravity press for 10 minutes. The samples prepared by INGEDE Method were scanned by the Spec*Scan@2000 setting for Stickies INGEDE BLACK.

6.2.3 Characterization

6.2.3.1 Particle size measurement of PVAc

The particle size of PVAc microparticles was analyzed using a zetasizer (Malvern Zetasizer Nano ZS90, Malvern Instrument Co. Ltd., UK). The particle size was measured every 20 seconds. In order to study the influence of chemicals in the formation of PVAc particles and the agglomeration of formed PVAc particles, two different types of experiments were designed. The PVAc/methanol was injected to chemical additive solutions to investigate the formation process. In the other case, the chemical solution was injected to the PVAc/water suspension after formation.

6.2.3.2 Turbidity and UV-vis spectrometry of filtrates

The turbidity of the filtrates was measured by TC-3000 Trimeter. The instrument was first calibrated through standard turbidity solutions. 30 mL solution was used for each measurement.

The calibration curve of UV-vis spectrometry was prepared by injecting different amount of 1% PVAc solution into water. The calibration curve in Figure 6-2 fits the experimental data linearly with R-square of 0.99. The absorbance of the suspension was measured at 300nm wavelength. The absorbance of the filtrates was measured to study the agglomeration process.

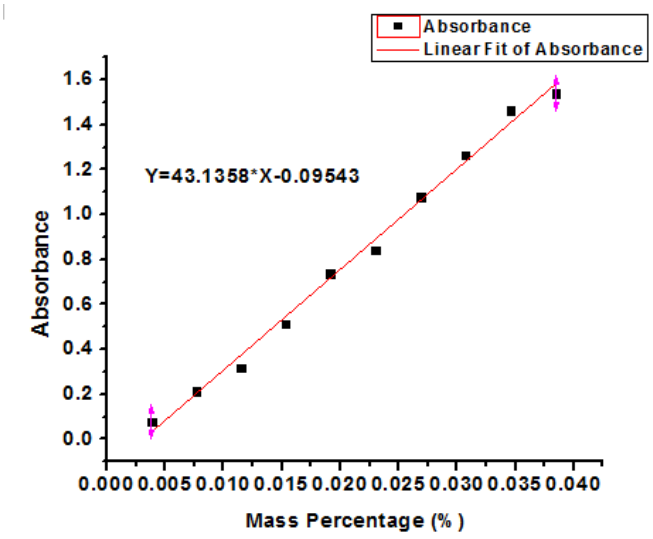

Figure 6-2 Calibration curve of microstickies for UV-Vis spectrometry.

6.3 Results and Discussion

6.3.1 Influence of chemicals on the deposition amount and size of PVAc

Most stickies are hydrophobic in nature and slightly negatively charged in water. In the system with microstickies of PVAc, there are three interactions including electrostatic interaction, van der Waals interaction and hydrophobic interaction. Hydrophobic interaction is the attractive interaction between organic nonpolar molecules. It has been shown that hydrophobic interaction has the same range with van der Waals force, but is about one order of magnitude stronger than van der Waals force[11]. Since PVAc does not

have any ionizable functional groups and the surface potential is -3.1mV[12], hydrophobic interaction dominates the suspension of PVAc. As a result, they have a tendency to agglomerate in water system in order to minimize the surface energy.

Both polyvinyl alcohol (PVA) and poly(diallylmethylammonium chloride) (PDADMAC) are detacky agents widely used in paper industry. Lignosulfonate is a dispersant which stabilizes the particles in water. Although all of them prevent the deposition of PVAc, PVA is nonionic, PDADMAC is cationic and lignosulfonate is anionic. Thus they all have different detacky mechanisms. PVA is the hydrolysis product of PVAc, which has the hydrophobic backbone with hydrophilic hydroxyl group in the side chain. Due to the amphiphilic nature of PVA, it has been applied as a surfactant for nanoparticle synthesis[13-15]. Since PVAc is very hydrophobic in nature, PVA adsorbs onto PVAc to increase the hydrophilicity and stabilize the PVAc particles. In addition, previous research has shown that lignosulfonate is an effective stabilizer for nanoparticles, polymers and dyes due to both electrostatic repulsive forces and steric repulsive forces[16-18]. Lignosulfonate can ionize to negative charge in water. Since most particles in water are also negatively charged, lignosulfonates elevate the negative charge density in the water phase and increase the repulsion force between particles. At last, PDADMAC is a cationic polymer that bridging both the anionic particles itself themselves, the particles with fibers. Thus, PDADMAC destabilizes particles and decreases the stickies concentration through the bridging effect with fiber.

Figure 6-3 shows the deposition amount of PVAc on HDPE with and without chemicals. As expected, all the three chemicals prevented the agglomeration and deposition of stickies. PVA and lignosulfonate had a much smaller deposition amount on HDPE due to

their stabilizer role. However, PDADMAC showed a worse performance than the other two chemicals. As explained previously, PDADMAC acts as a destabilizer and thus induces agglomeration of stickies. However, the deposition amount was still much smaller than control. This is because the agglomeration of stickies in water is a competitive reaction with deposition process and a lower concentration of stickies results in a smaller deposition amount.

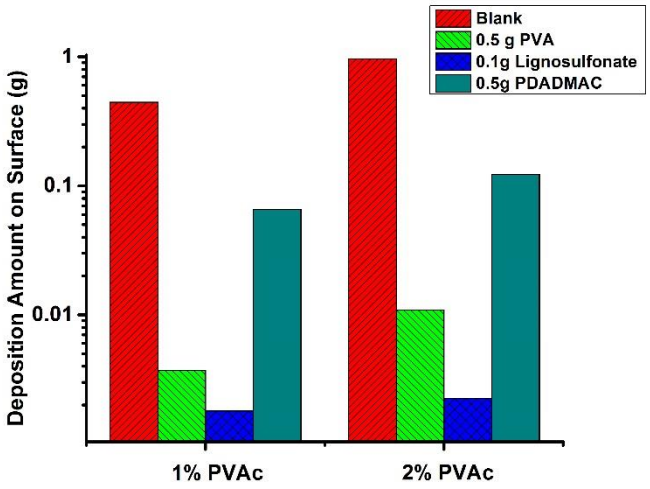

Figure 6-3 Effect of chemical additives on the deposition of microstickies.

The influence of chemical additives to the agglomeration of PVAc was quantified by Malvern zetesizer. These chemicals either affects the formation of stickies or the stickies after formation. The PVAc/methanol solution was injected into solution with different chemical additives to study the stickies formation process, and chemical was injected to microstickies suspension to study the effect of chemicals to formed microstickies. The results from these two processes are shown in Figure 6-4. PDADMAC in solution led to the agglomeration and showed the largest particle size, which is consistent with the mechanism introduced previously. On the other hand, both PVA and lignosulfonate did not

affect the size greatly. Compared with the particle size without any additives, the particles in lignosulfonate solution was slightly smaller, which might come from the dispersant nature of the chemical.

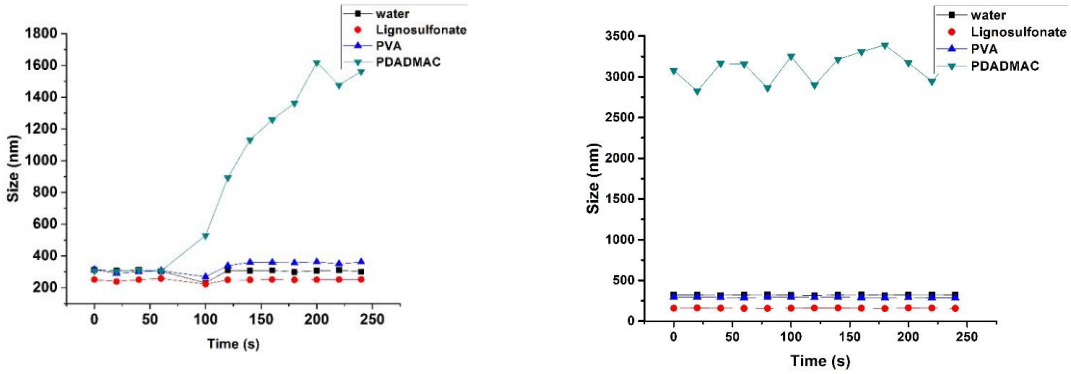

Figure 6-4 Effect of chemical additives on stickies agglomeration (left) during stickies formation and (right) after stickies formation.

6.3.2 Electric field treatment of microstickies

In conventional electrocoagulation processes, the treatment was conducted at relative low voltage (less than 30V) and relative high current density (0.6-6 mA/cm^2)[19-20]. On the other hand, the voltage in this electric treatment is much higher (0.24 kV-2 kV) and the current density is lower (less than 0.06mA/cm^2), as shown in Figure 6-5. The anode is a carbon-coated stainless rod in the center of the container and the cathode is the whole container. The high voltage generates an external electric field in water, inducing the migration of charged microparticles in water and changing the local particles concentration. Since the particles are slightly negatively charged, they are more likely to migrate to the positively charged center anode. As a result, a gradient in the particle concentration is developed from the center of the container to the walls with center having

the highest concentration. With higher local concentration, the distance between particles is shorter and they are more likely to collide with each other through Brownian motion. Furthermore, the external electric field also cancels out the electric repulsion force between particles and reduces the energy barrier for coagulation.

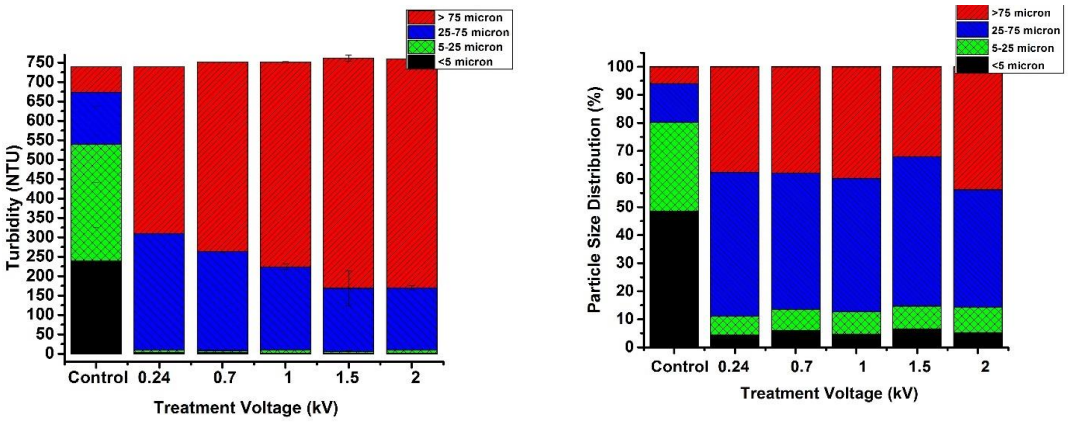

Figure 6-5 Effect of electric treatment on stickies size distribution based on (left) turbidity and (right) UV-Vis spectrometry.

The stickies suspension was treated by electric field at 0.24kV, 0.7kV, 1kV, 1.5kV and 2kV for 10 min. The suspension was then screened through 75-micron mesh screen, 25-micron filter paper and 5-micron filter paper. The absorbance and turbidity of the filtrate were measured. The concentrations of the filtrates were calculated via the calibration curve and the population percentage of particles in each size range was obtained. After treatment, the turbidity of the filtrate through 25-micron filter paper was almost zero, proving that most of the particles were larger than 25 microns after treatment. Furthermore, the screenability of 75-micron mesh screen was also improved greatly. In Figure 6-5, the UV-Vis spectrometer results also proved that more than 90% of the particles were greater than 25 microns compared with only 20% before treatment, which was consistent with the

turbidity data. The turbidity of different treatment voltage showed that the agglomeration was improved with higher voltage. In addition, the absorbance and turbidity results showed that the electric field treatment was very effective even at low voltage, 0.24kV.

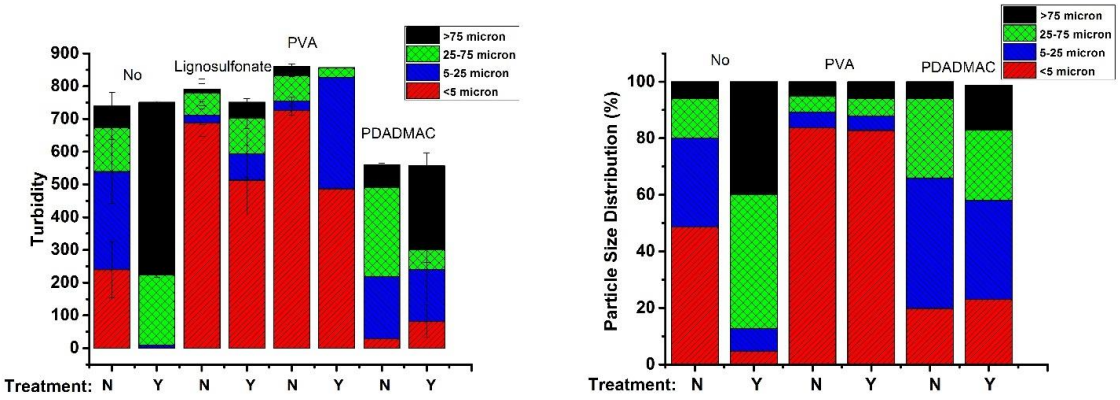

Figure 6-6 Effect of electric treatment on stickies size distribution based on (left) turbidity and (right) UV-Vis spectrometry with the presence of chemical additives.

The influence of chemical additives on the electric field treatment is shown in Figure 6-6. Based on the previous results, lignosulfonate and PVA stabilize the stickies and prevent the agglomeration of stickies. Thus, for the suspensions before electric field treatment, both PVA and lignosulfonate showed higher portion of particles in the size range of smaller than 5 microns. The suspension with PDADMAC had much lower portion of small particles and higher portion of large particles, which was consistent with the cationic nature of the chemical. After electric field treatment, the particle sizes of all the suspensions increased. In the suspensions with PVA and lignosulfonate, the portion of particles smaller than 5 microns decreased after treatment. However, the number of particles with size greater than 75 microns did not increase significantly. Thus, the agglomeration is inhibited by PVA and lignosulfonate compared with the results without additives. While in the suspension with

PDADMAC, the portion of particles greater than 75 microns increased and the screenabilty of mesh screen was also improved.

Because the interference of lignosulfonate to the absorbance, UV-Vis measurement of samples with lignosulfonate was not analyzed here. The results from UV-Vis measurement were similar to those from turbidity measurement. Electric field agglomeration process is not compatible with dispersants because they stabilize the particles. But the treatment of samples with PDADMAC shows shift to larger size distribution.

6.3.3 Image analysis of microstickies agglomeration and comparison with cooking method

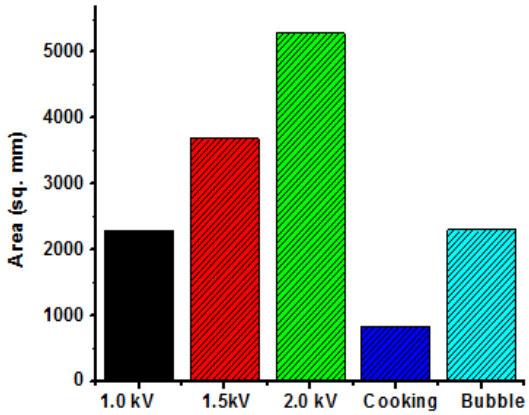

Figure 6-7 Image analysis results of electric treatment, cooking and bubble methods.

The agglomeration of microstickies in fiber suspensions was quantified by INGEDE Method 4 image analysis method. The difference in area before and after agglomeration was calculated to show the treatment performance. As shown in Figure 6-7, detected area by INGEDE Method 4 was significantly increased after electric field treatment. In addition, similar to turbidity and absorbance results, the agglomeration was also enhanced with the

increase of treatment voltage. The same stickies suspension was also treated through temperature elevation for 15min[21] and bubble treatment[9], and the results shows that electric field treatment has a better performance in agglomerating stickies.

6.4 Conclusions

In this chapter, a new agglomeration technology based on electric field treatment was investigated with different detacky agents. Anionic dispersant lignosulfonate and non-ionic detacky agent PVA could stabilize stickies while cationic polymer PDADMAC induced stickies agglomeration. The size distribution and turbidity of the stickies suspension after electric treatment were analyzed. The treatment showed significant increase in particle sizes and improvement in screenability. INGEDE Method 4 image analysis also proved the agglomeration of stickies in the presence of fibers.

6.5 References

[1] Jiang, J.-Q.; Graham, N.; André, C.; Kelsall, G. H.; Brandon, N., Laboratory study of electro-coagulation–flotation for water treatment. *Water research* **2002,** *36* (16), 4064-4078.

[2] Tanneru, C. T.; Rimer, J. D.; Chellam, S., Sweep Flocculation and Adsorption of Viruses on Aluminum Flocs during Electrochemical Treatment Prior to Surface Water Microfiltration. *Environ. Sci. Technol.* **2013,** *47* (9), 4612-4618.

[3] Hsieh, J. In *Review of Patented Electric Field Technology with Application to Non-Impact Printing*, NIP & Digital Fabrication Conference, Society for Imaging Science and Technology: 2008; pp 577-580.

[4] Shemi, A.; Hsieh, J. S., Electroflotation combined with flotation deinking of flexographic newsprint. *Ind. Eng. Chem. Res.* **2010,** *49* (5), 2380-2387.

[5] Shemi, A.; Hsieh, J.; Lee, D., Clarification of flexographic wastewater by electrocoagulation and electroflotation. *Appita Journal: Journal of the Technical Association of the Australian and New Zealand Pulp and Paper Industry* **2014,** *67* (3), 212.

[6] Sridhar, R.; Sivakumar, V.; Immanuel, V. P.; Maran, J. P., Treatment of pulp and paper industry bleaching effluent by electrocoagulant process. *J. Hazard. Mater.* **2011,** *186* (2), 1495-1502.

[7] Bellebia, S.; Kacha, S.; Bouyakoub, A. Z., Experimental investigation of chemical oxygen demand and turbidity removal from cardboard paper mill effluents using combined electrocoagulation and adsorption processes. *Environ. Prog. Sustain. Energy* **2012,** *31* (3), 361-370.

[8] Kamali, M.; Khodaparast, Z., Review on recent developments on pulp and paper mill wastewater treatment. *Ecotoxicol. Environ. Saf.* **2015,** *114*, 326-342.

[9] Du, X.; Hsieh, J. S., Analytical measurement of microstickies on fibers by model surfaces. *Nordic Pulp & Paper Research Journal* **2014,** *29* (2), 232-239.

[10] Doshi, M.; Jong, R.; Aziz, S. In *Measurement of microstickies*, TAPPI Engineering, Pulping and Environmental Conference 2008, 2008; pp 24-27.

[11] Israelachvili, J.; Pashley, R., The hydrophobic interaction is long range, decaying exponentially with distance. *Nature* **1982,** *300* (5890), 341-342.

[12] Jeong, H.-G.; Kim, Y.-E.; Kim, Y.-J., Fabrication of poly (vinyl acetate)/polysaccharide biocomposite nanofibrous membranes for tissue engineering. *Macromolecular Research* **2013,** *21* (11), 1233-1240.

[13] Sahoo, S. K.; Panyam, J.; Prabha, S.; Labhasetwar, V., Residual polyvinyl alcohol associated with poly (D, L-lactide-co-glycolide) nanoparticles affects their physical properties and cellular uptake. *J. Control. Release* **2002,** *82* (1), 105-114.

[14] Wang, Z.; Huang, B.; Liu, X.; Qin, X.; Zhang, X.; Wei, J.; Wang, P.; Yao, S.; Zhang, Q.; Jing, X., Photoluminescence studies from ZnO nanorod arrays synthesized by hydrothermal method with polyvinyl alcohol as surfactant. *Materials Letters* **2008,** *62* (17), 2637-2639.

[15] Yang, M.; Lai, S. K.; Yu, T.; Wang, Y.-Y.; Happe, C.; Zhong, W.; Zhang, M.; Anonuevo, A.; Fridley, C.; Hung, A., Nanoparticle penetration of human cervicovaginal mucus: The effect of polyvinyl alcohol. *J. Control. Release* **2014,** *192*, 202-208.

[16] Li, Z.; Pang, Y.; Ge, Y.; Qiu, X., Evaluation of steric repulsive force in the aqueous dispersion system of dimethomorph powder with lignosulfonates via X-ray photoelectron spectroscopy. *The Journal of Physical Chemistry C* **2011,** *115* (50), 24865-24870.

[17] Lou, H.; Zhu, D.; Yuan, L.; Qiu, X.; Lin, X.; Yang, D.; Li, Y., Fabrication of high-concentration aqueous graphene suspensions dispersed by sodium lignosulfonate and its mechanism. *The Journal of Physical Chemistry C* **2015,** *119* (40), 23221-23230.

[18] Milczarek, G.; Rebis, T.; Fabianska, J., One-step synthesis of lignosulfonate-stabilized silver nanoparticles. *Colloids and Surfaces B: Biointerfaces* **2013,** *105*, 335-341.

[19] Yilmaz, A. E.; Boncukcuoğlu, R.; Kocakerim, M. M.; Keskinler, B., The investigation of parameters affecting boron removal by electrocoagulation method. *J. Hazard. Mater.* **2005,** *125* (1), 160-165.

[20] İrdemez, Ş.; Demircioğlu, N.; Yıldız, Y. Ş.; Bingül, Z., The effects of current density and phosphate concentration on phosphate removal from wastewater by electrocoagulation using aluminum and iron plate electrodes. *Separation and Purification Technology* **2006,** *52* (2), 218-223.

[21] Ben, Y.; Ricard, M.; Dorris, G., Quantifying microstickies via a new agglomeration technique. *Tappi Journal* **2014,** *13* (9), 27-38.

CHAPTER 7. CONCLUSIONS AND FUTURE WORK

7.1 Conclusions

Paper recycling industry is facing new challenges from contaminants that are not compatible with fiber cleaning processes. And the paper products from unclean fiber sources suffer from problems in optical properties and physical strength. The residual contaminants in water stream also cause poor process runnability like web break in paper machine. The most notorious contaminants are hydrophilic inks and microstickies. Hydrophilic inks originate from the new generation aqueous inks to avoid toxic organic solvents and are widely applied in inkjet printers for offices and homes. The long shelf life and high printing quality are other advantages over traditional hydrophobic inks. However, the ink formula and composition that contribute to the exceptional printing quality are also the root cause for deinking problems. Specifically, the submicron ink particles redeposit into the fiber lumen irreversibly which make the problem more complex. Microstickies from glues, tapes in packaging industry both deposit to paper machines and fiber surfaces. And they are dispersed in water and destabilized under external stimulus like pH, temperature, shear force, etc. Thus it is difficult to quantify them, and remove them from pulp slurry.

First of all, we developed a method to distinguish “bound ink” and “redeposited ink”, and quantify the contribution of bound ink and redeposited ink to the residual ink on fiber surfaces after pulping. The method shows that about 16% of original ink is bounded on fiber surface, 33% redeposits to fiber surface, and 50% stays in water phase as free ink after pulping, which guides us to prioritize redeposited ink over bound ink. With this newly

developed method, we also studied the effect of pulping conditions on the relative ratio of bound ink and redeposited ink, and found residual ink on fiber shifts from bound ink to redeposited ink with higher pulping consistency. This find allows us to remove bound ink and redeposited ink simultaneously. As long as a method to control redeposited ink can be established, the bound ink is not a concern because it can be removed by increasing pulping consistency. Adsorption deinking is a potential solution for redeposited ink control and chitosan can adsorb ink particles both from aqueous phase and pulp slurry. The paper ISO% Brightness was 5 point higher and ERIC was 70ppm lower with chitosan adsorption deinking.

Secondly, we investigated the effect of electric treatment on ink removal from pulp slurry as a complimentary to traditional flotation or washing deinking. The electric treatment alone showed high selectivity of ink over fiber through electroflotation mechanism and the ERIC was reduced by 20%. Graphite is a better material as anode material than stainless steel because electrocoagulation by stainless steel leads to ink redeposition during electric pretreatment, and higher yield loss during flotation. However, the flotation itself shows a similar deinking efficiency with electric pretreatment followed by flotation. Thus the benefits from electric pretreatment disappears during flotation, and it is important to be cautious about this problem when applying electric pretreatment.

Thirdly, another alternative modification to flotation, oil-coated bubble flotation, was studied fundamentally and its application in hydrophilic ink deinking was proved qualitatively. There are three fundamental benefits from oil-coated bubble, including fluid dynamics like bubble shape and velocity, thermodynamics that particles show favourable wettability at interfaces, and kinetics that the energy barrier for particle adsorption is

smaller. We focused on the kinetics in this study because the life of a bubble in flotation is short and the adsorption process is kinetically controlled. The particle adsorption kinetics was probed by dynamic interfacial tension measurement and oil-water interface always shows a faster adsorption kinetics, and lower energy barrier for all conditions studied in this thesis. The different in energy barrier between air-water interface and oil-water interface is driven by van der Waals interactions because they are repulsive forces for particle adsorption on air-water interface, and attractive forces for oil-water interface. This fundamentally study illustrates an alternative method to improve flotation efficiency by modifying air bubbles instead of modifying the properties of ink particles. The application of this concept in deinking was demonstrated by a house-made flotation cell and a better deinking performance was observed for oil-coated bubble flotation.

Besides challenges in hydrophilic inks, we also investigated the measurement and removal of microstickies. Specifically, we focused on the deposition of stickies on cellulose fiber and measured it by a model cellulose surface. An agglomeration method based on electric treatment was developed and it improved the screenability of microstickies by 50%.

7.2 Future work

7.2.1 Fundamental study of energy barrier for particle adsorption at fluid-fluid interfaces

The most important aspect in particle adsorption kinetics study is the methodology establishment. As shown in Appendix C, there are two gaps in developing the methodology to analyze dynamic interfacial tension. The first one is the difficulty in determining the

early stage where the ½ power law between γ and t is followed. The second one is the significantly different results from different kinetics models.

For the first problem, log-log plot shows some potentials but the analysis is very sensitive to the value of γ_0. A criterion for early stage determination was developed for surfactant systems[1]. But the conclusion cannot be applied to particle system because one parameter in the criterion is related to the Langmuir isotherm, and the assumption of reversible adsorption in Langmuir isotherm is contradictory with the irreversible adsorption of particles.

For the second problem, it is clearly shown in Appendix C that the early stage energy barrier, i.e. the energy barrier between particles and pristine interfaces, as extracted from experimental tension data, is dependent on the model used. Sometimes even negative energy barriers were obtained. Thus, it is necessary to understand the similarities and differences between different modelling methods and choose the one that fits specific experimental conditions. Additionally, the negative energy barrier problem can possibly be fixed with more accurate measurement of particle size and particle contact angle at interfaces, especially in-situ measurement methods that focus on microscopic individual particles instead of a macroscopic bulk average.

If the previously described gaps are bridged, or even if not, it is worthwhile to revisit the particle adsorption kinetics with a different particle-oil system, or the same particle-oil system with different pH, that show a higher energy barrier. The current energy barrier in Chapter 4 is not significantly greater than zero (the apparent energy barriers are negative), and it is difficult to directly determine different components in energy barrier like

electrostatic double layer induced energy barrier, image force induced energy barrier and van der Waals force induced energy barrier. However, special attention has to be invested in adjusting the energy barrier into a reasonable value where the reduction in interfacial tension by particle adsorption can be measured accurately, given the standard error of pendant droplet method. For example, if the adsorption kinetics is too slow, the change in interfacial tension will be very small and it is difficult to distinguish the signal from background noise.

7.2.2 Oil coated bubble flotation deinking

One of the most important challenges in oil-coated bubble flotation is the failure in froth formation by oil itself. As a result, oil with ink particles adsorbed on the oil-water interface cannot stay on the surface of ink suspension and oil droplets with ink will recirculate back into the ink suspension. Appendix D showed some efforts to solve this problem by adding CTAB into the system, and the surfactant prevents the particles from adsorbing on oil-water interface if the CTAB concentration is greater than 0.1mM. Thus, it is important to find a surfactant that can stabilize air-water interface while keeping oil-water interface active. The particle adsorption on interfaces with the presence of surfactants is a complex problem that contradictory effects were observed by previous publications[2-5]. In some cases, there is a synergistic effect between particles and surfactants, but in other cases they compete with each other. Therefore, a fundamental study in particle adsorption at interfaces with the presence of surfactants is necessary to generate froth without preventing particles from adsorption.

7.2.3 Adsorption deinking

It was shown in Figure 2-7 that the time required to reach equilibrium for chitosan was over double the time frame of deinking. For chitosan, the adsorption is driven by electrostatic interaction between amine group and negatively charged ink particles. Thus, it is important to develop a relationship between functional groups and adsorption kinetics, and synthesize new materials with those specific functional groups to improve the adsorption kinetics as well as adsorption kinetics. Another area to improve is the regeneration of adsorbents. For polymer beads, they can be regenerated after hydrophobic ink deinking by surfactants[6]. But it is still unknown for hydrophilic ink deinking. Surfactant solutions with cationic surfactants or amine-based surfactants like CTAB, EDTA are more likely to succeed.

7.3 References

[1] Casandra, A.; Ismadji, S.; Noskov, B. A.; Liggieri, L.; Lin, S.-Y., A study on the method of short-time approximation–Criteria for applicability. *International Journal of Heat and Mass Transfer* **2015,** *90*, 752-760.

[2] Lan, Q.; Yang, F.; Zhang, S.; Liu, S.; Xu, J.; Sun, D., Synergistic effect of silica nanoparticle and cetyltrimethyl ammonium bromide on the stabilization of O/W emulsions. *Colloids and Surfaces A: Physicochemical and Engineering Aspects* **2007,** *302* (1), 126-135.

[3] Pichot, R.; Spyropoulos, F.; Norton, I., Competitive adsorption of surfactants and hydrophilic silica particles at the oil–water interface: interfacial tension and contact angle studies. *J. Colloid Interface Sci.* **2012,** *377* (1), 396-405.

[4] Ravera, F.; Ferrari, M.; Liggieri, L.; Loglio, G.; Santini, E.; Zanobini, A., Liquid–liquid interfacial properties of mixed nanoparticle–surfactant systems. *Colloids and Surfaces A: Physicochemical and Engineering Aspects* **2008,** *323* (1), 99-108.

[5] Ravera, F.; Santini, E.; Loglio, G.; Ferrari, M.; Liggieri, L., Effect of nanoparticles on the interfacial properties of liquid/liquid and liquid/air surface layers. *The Journal of Physical Chemistry B* **2006,** *110* (39), 19543-19551.

[6] Schwarz, S.; Petzold, G.; Oelmann, M. Cleaning particles from waste paper recycling process, involves introducing particle having impurities on its surface to water, and adding surfactant material before, simultaneously or after introducing step and then realizing energy input. DE102012208219 A1, 2013.

APPENDIX A. LATE STAGE ENERGY BARRIER ANALYSIS

Appendix A shows the fitted curve of late stage dynamic interfacial tension and the calculated energy barrier based on Equation 1.9 and Equation 1.12. At late stage, the energy barrier is dominated by the blocking effect of adsorbed particles.

A.1 Fitted curve of late stage dynamic interfacial tension

The fitted curves of late stage dynamic surface tension at air-water interface is shown in Figure A-1 and dynamic interfacial tension at oil-water interface is shown in Figure A-2.

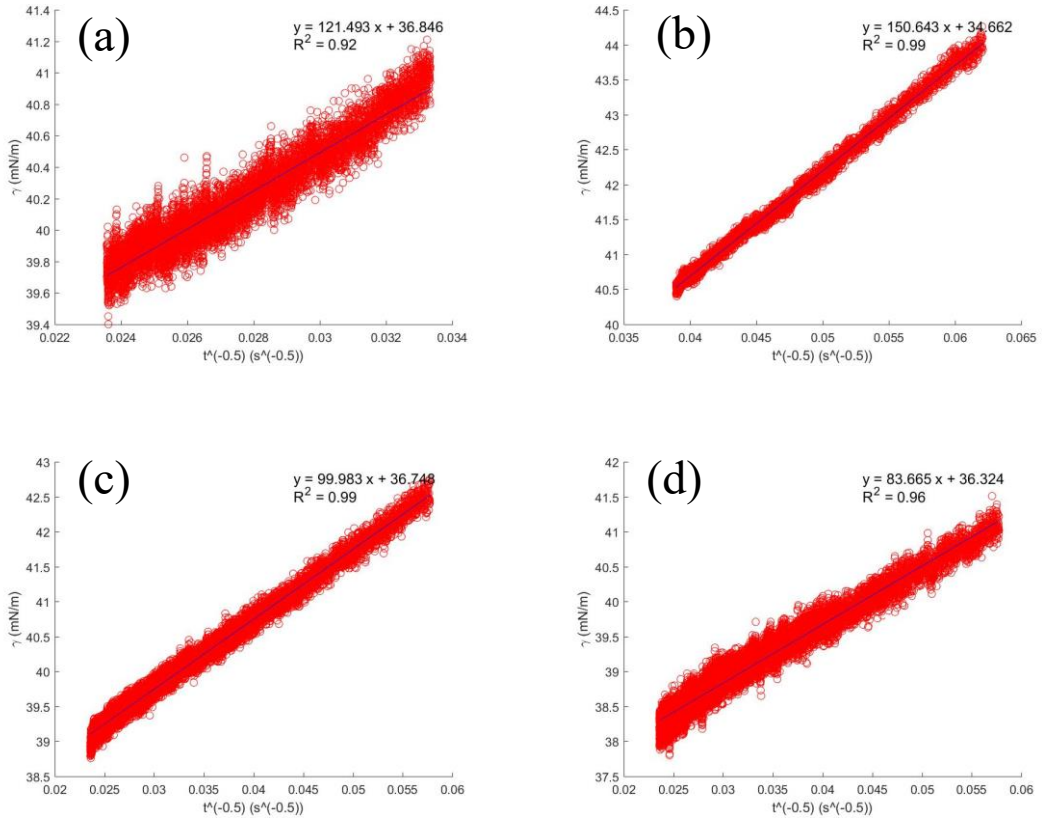

Figure A-1 Plots of late stage dynamic surface tension data (a) 0.05% EC 0.2mM NaCl (b) 0.05% EC 10mM NaCl (c) 0.08% EC 0.2mM NaCl (d) 0.08% EC 10mM NaCl. Solid blue lines are linear regression with parameters indicated in each panel.

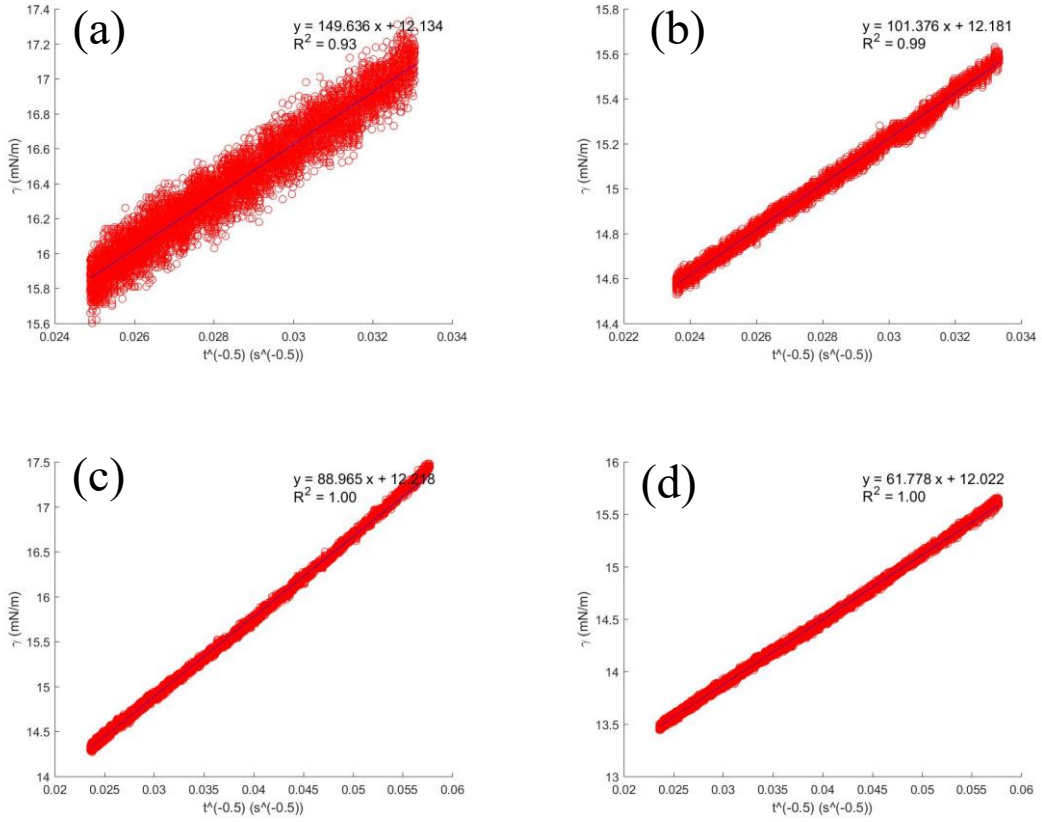

Figure A-2 Plots of late stage dynamic interfacial tension data (a) 0.05% EC 0.2mM NaCl (b) 0.05% EC 10mM NaCl (c) 0.08% EC 0.2mM NaCl (d) 0.08% EC 10mM NaCl. Solid blue lines are linear regression with parameters indicated in each panel.

A.2 Late stage energy barrier analysis

The energy barrier was calculated by comparing the effective diffusion coefficient from Equation 1.9 and Stokes-Einstein diffusion coefficient, as shown in Equation 1.12. Θ_{max} was assumed to be 0.91 to in order to calculate molar surface concentration Γ_{∞} in Equation 1.12. The late stage energy barrier is 17kT for all the different conditions, indicating that

the adsorption kinetics is not dependent on the properties of pristine interface because the interface is covered by particles.

Table A-1 Fitted slope and computed late stage energy barrier from Equation 1.9 and Equation 1.12. The actual diffusion coefficient of EC particle is 1.7×10^{-12} m^2 s^{-1}.

Mass concentration (g/L)	Salt concentration (mM)	Type of interface	$\frac{d\gamma}{d\sqrt{1/t}}$ ($N\ m^{-1}\ s^{0.5}$)	ΔE (kT)
0.5	0.2	air-water	1.39E-01	1.80E+01
0.5	10		1.48E-01	1.81E+01
0.8	0.2		1.00E-01	1.83E+01
0.8	10		8.36E-02	1.79E+01
0.5	0.2	oil-water	1.46E-01	1.81E+01
0.5	10		1.06E-01	1.74E+01
0.8	0.2		8.66E-02	1.80E+01
0.8	10		6.29E-02	1.74E+01

APPENDIX B. EARLY STAGE SLOPE ANALYSIS

This appendix illustrates the statistical analysis of slopes from early stage adsorption under different conditions. Specifically, t-test analysis was performed to understand if there are significant differences between results from different experimental conditions with a significance level of 0.05. If the p-value is less than 0.05, the null hypothesis is rejected and there are statistically significant differences between two conditions. On the contrary, if the p-value is greater than 0.05, the null hypothesis is accepted.

B.1 Air-water interface

Table B-1 EC 0.05% 0.2mM vs. 10mM t-test.

	0.2mM	10mM
Mean	-3.69E-01	-4.77E-01
Variance	1.91E-03	1.40E-03
Observations	1.00E+01	5.30E+01
Hypothesized Mean Difference	0.00E+00	
P(T<=t) two-tail	**8.97E-06**	

Table B-2 EC 0.05% 10mM vs. 20mM t-test.

	10mM	20mM
Mean	-4.77E-01	-4.81E-01
Variance	1.40E-03	8.54E-03
Observations	5.30E+01	1.90E+01
Hypothesized Mean Difference	0.00E+00	
P(T<=t) two-tail	**8.63E-01**	

Table B-3 EC 0.08% 0.2mM vs. 10mM t-test.

	0.2mM	10mM
Mean	-6.25E-01	-7.68E-01
Variance	5.07E-03	7.19E-03
Observations	1.20E+01	1.70E+01
Hypothesized Mean Difference	0.00E+00	
P(T<=t) two-tail	**4.08E-05**	

Table B-4 EC 0.2mM 0.05% vs. 0.08% t-test.

	0.05%	0.08%
Mean	-3.69E-01	-6.25E-01
Variance	1.91E-03	5.07E-03
Observations	1.00E+01	1.20E+01
Hypothesized Mean Difference	0.00E+00	
P(T<=t) two-tail	**3.16E-09**	

Table B-5 EC 10mM 0.05% vs. 0.08% t-test.

	0.05%	0.08%
Mean	-4.77E-01	-7.68E-01
Variance	1.40E-03	7.19E-03
Observations	5.30E+01	1.70E+01
Hypothesized Mean Difference	0.00E+00	
P(T<=t) two-tail	**5.74E-11**	

B.2 Silicone oil-water interface

Table B-6 EC 0.05% 0.2mM vs. 10mM t-test.

	0.2mM	10mM
Mean	-5.46E-01	-6.66E-01
Variance	3.71E-03	7.23E-03
Observations	9.00E+00	2.10E+01
Hypothesized Mean Difference	0.00E+00	
P(T<=t) two-tail	**2.75E-04**	

Table B-7 EC 0.05% 10mM vs. 20mM t-test.

	10mM	20mM
Mean	-6.66E-01	-6.46E-01
Variance	7.23E-03	3.01E-03
Observations	2.10E+01	1.90E+01
Hypothesized Mean Difference	0.00E+00	
P(T<=t) two-tail	**3.86E-01**	

Table B-8 EC 0.08% 0.2mM vs. 10mM t-test.

	0.2mM	10mM
Mean	-9.23E-01	-1.15E+00
Variance	1.82E-02	2.47E-02
Observations	9.00E+00	1.10E+01
Hypothesized Mean Difference	0.00E+00	
P(T<=t) two-tail	**2.48E-03**	

Table B-9 EC 0.2mM 0.05% vs. 0.08% t-test.

	0.05%	0.08%
Mean	-5.46E-01	-9.23E-01
Variance	3.71E-03	1.82E-02
Observations	9.00E+00	9.00E+00
Hypothesized Mean Difference	0.00E+00	
P(T<=t) two-tail	**1.02E-05**	

Table B-10 EC 10mM 0.05% vs. 0.08% t-test.

	0.05%	0.08%
Mean	-6.66E-01	-1.15E+00
Variance	7.23E-03	2.47E-02
Observations	2.10E+01	1.10E+01
Hypothesized Mean Difference	0.00E+00	
P(T<=t) two-tail	**3.03E-07**	

B.3 Air-water vs. Silicone oil-water interface

Table B-11 EC 0.05% 0.2mM air vs. silicone oil t test.

	Air	Silicone oil
Mean	-3.69E-01	-5.46E-01
Variance	1.91E-03	3.71E-03
Observations	1.00E+01	9.00E+00
Hypothesized Mean Difference	0.00E+00	
P(T<=t) two-tail	**4.55E-06**	

Table B-12 EC 0.05% 10mM air vs. silicone oil t test.

	Air	Silicone oil
Mean	-4.77E-01	-6.66E-01
Variance	1.40E-03	7.23E-03
Observations	5.30E+01	2.10E+01
Hypothesized Mean Difference	0.00E+00	
P(T<=t) two-tail	**1.12E-09**	

Table B-13 EC 0.05% 20mM air vs. silicone oil t test.

	Air	Silicone oil
Mean	-4.81E-01	-6.46E-01
Variance	8.54E-03	3.01E-03
Observations	1.90E+01	1.90E+01
Hypothesized Mean Difference	0.00E+00	
P(T<=t) two-tail	**2.41E-07**	

Table B-14 EC 0.08% 0.2mM air vs. silicone oil t test.

	Air	Silicone oil
Mean	-6.25E-01	-9.23E-01
Variance	5.07E-03	1.82E-02
Observations	1.20E+01	9.00E+00
Hypothesized Mean Difference	0.00E+00	
P(T<=t) two-tail	**8.58E-05**	

Table B-15 EC 0.08% 10mM air vs. silicone oil t test.

	Air	Silicone oil
Mean	-7.68E-01	-1.15E+00
Variance	7.19E-03	2.47E-02
Observations	1.70E+01	1.10E+01
Hypothesized Mean Difference	0.00E+00	
P(T<=t) two-tail	**3.14E-06**	

APPENDIX C. REVIEW AND COMPARSION OF DIFFERENT KINETICS MODELS FOR PARTICLE ADSORPTION

Although different authors applied the same method to estimate late stage energy barrier from dynamic interfacial tension (Equation 1.9 and 1.12), there are three kinetics models in determining early stage energy barrier. Method a (Equation 1.25 and 1.26) was recently developed by Bizmark based on generalized random sequencing adsorption theory on solid-fluid interfaces. The model relies on slopes from late stage dynamic interfacial tension to estimate early-stage energy barrier. The limitation of this method is the failure of taking DLVO interactions between adsorbed and unadsorbed particles. Method b (Equation 1.12 and 1.13) relies on the early adsorption kinetics to estimate energy barrier by comparing effective diffusion coefficient with Stokes Einstein diffusion coefficient. It is very similar to Method c (Equation 1.5 and 1.12) which was originally developed to study surfactant adsorption kinetics and works well for particle systems when the desorption energy is in the same order of magnitude of kT.

In addition, another challenge in utilizing Method b and c is that a clear criterion to determine the "early stage" is missing. Thus, it is difficult to figure out the time regime when the dynamic interfacial tension follows model predictions.

In this section, a review and comparison is summarized to show the dramatic difference in particle adsorption kinetics when the same data set was fitted to different models. Secondly, Method a is applied to analyze the data reported in Chapter 4 and Appendix A and the results are compared with Method b which is chosen to study the particle adsorption

kinetics in Chapter 4. Finally, the advantages and limitations of log-log plot in determining the "early stage" time regime is discussed.

C.1 Summary and comparison of different kinetics models

Table C-1 summarizes the most recent study in adsorption kinetics through dynamic interfacial tension measurement. The column "early ΔE" shows the energy barrier from the paper and the superscript represents the data analysis method chosen by the authors. And the energy barrier was reanalzyed by Method b based on the information provided in the publications. The papers by Kutuzov and Ferdous were not reanalzyed because Method b and Method c are identical if desorption energy is similar to kT. The early energy barriers from Method b are consistently smaller than the ones from Method a, and negative energy barriers are observed based on data from Bizmark and Fang. Another important finding is the lack of criterion to determine early stage. The fitted time regime ranges from 4s to over 100s without explanations about why this time regime was chosen.

Table C-1 Summary of previous publications in particle adsorption kinetics at fluid-fluid interfaces.

Particle	Desorption Energy (k_BT)	Type of interface	Early stage fitting time regime (s)	Early ΔE (k_BT)	Early ΔE (method b) (k_BT)	Ref
EC	10^4	Air-water	10-100s	5.9[a]	-5[b]	Bizmark[1]
PEG-Iron oxide	10^3	Water-decane	4s	5.6-10.6[a]	1[b]	Nelson[2]

Table C-1 Summary of previous publications in particle adsorption kinetics at fluid-fluid interfaces(continued).

Silica	45	Water-decane	100-250s	8[b]		Dugyala[3]
Poly(lactic-co-glycolic acid)	10^4	Air-water Water-octane	120-180s	5[b]		Gyulai[4]
TOPO-CdSe	3.3-13	Water-toluene	N/A	1.5[c]		Kutuzov[5]
alkanethiol-capped gold	kT	Water-hexane	N/A	0.3-7.7[c]		Ferdous[6]
Graphene oxide	N/A	Water-toluene	16s	N/A	-2[b]	Fang[7]
Poly(NiPAAm) based microgel	Irreversible	Water-heptane	100s-3600s	N/A		Li[8]

[a]The energy barriers were calculated from Equation 1.25 and 1.26.

[b]The energy barriers were calculated from Equation 1.12 and 1.13.

[c]The energy barriers were calculated from Equation 1.5 and 1.12.

An example of data analysis is shown in Table C-2 and the original data comes from the paper by Bizmark. This paper also investigated the adsorption of EC on air-water interfaces, which is the same particle system studied in this thesis and this is the reason why this paper was chosen. Again, negative energy barriers were obtained when the EC concentration is greater than 0.4g/L, the same as the data reported in Chapter 4 of this thesis.

Table C-2 Early stage energy barrier by applying Method b to analyze data from Bizmark. The diameter is 89.1nm and diffusion coefficient is 4.84×10^{-12} m^2s^{-1}.

Mass concentration (g/L)	Type of interface	$\frac{d\gamma}{d\sqrt{t}}$ ($N\,m^{-1}\,s^{-0.5}$)	ΔE (kT)	ΔG (kT)	ΔE (kT)
0.1	air-water	-6.50E-05	9.40E-01[b]	4.30E+04	3.1[a]
0.2		-2.03E-04	5.11E-02[b]		
0.4		-4.19E-04	-3.88E-02[b]		
0.6		-8.02E-04	-5.00E-01[b]		
0.8		-1.04E-03	-4.53E-01[b]		
1.8		-1.38E-03	-5.67E-01[b]		

C.2 Analysis of data in Chapter 4 by Method a

In order to compare Method a and Method c completely, the data set from Chapter 4 and Appendix A was also reanalzyed following Method a and the results are shown in Table C-3. Now similar to results reported by Bizmark, all the energy barriers are positive if analyzed by Method a. Thus, it can be concluded that the mathematical formulas of Method a always ensure a positive energy barrier can be obtained.

Additionally, the energy barriers for particle adsorption at oil-water interfaces are always smaller, or equal to the barrier at air-water interfaces, which is consistent with the conclusions from Chapter 4.

Table C-3 Early stage energy barrier by applying Method a to analyze data from Chapter 4 and Appendix A.

Mass concentration (g/L)	Salt concentration (mM)	Type of interface	$\frac{d\gamma}{d\sqrt{1/t}}$ ($N\ m^{-1}\ s^{0.5}$)	K_1	k_a ($m\ s^{-1}$)	ΔE (kT)	ΔG (kT)
0.5	0.2	air-water	1.39E-01	1.28E-02	4.02E-06	1.3[a]	4.65E+05
0.5	10		1.48E-01	1.36E-02	3.56E-06	1.5[a]	
0.8	0.2		1.00E-01	1.47E-02	4.85E-06	0.5[a]	
0.8	10		8.36E-02	1.23E-02	6.96E-06	0.5[a]	
0.5	0.2	oil-water	1.46E-01	1.42E-02	3.25E-06	1[a]	4.40E+05
0.5	10		1.06E-01	1.02E-02	6.24E-06	0.5[a]	
0.8	0.2		8.66E-02	1.34E-02	5.81E-06	0.5[a]	
0.8	10		6.29E-02	9.75E-03	1.10E-05	0.5[a]	

C.3 Log-log plot for early stage fitting regime identification

The following equation can be obtained by restructuring Equation 1.13

$$\log_{10}(\gamma_0 - \gamma(t)) = \log_{10}(2N_A|\Delta E|c_{eq}\sqrt{\frac{D}{\pi}}) + \frac{1}{2}\log_{10}(t) \quad \textbf{(C.1)}$$

And the early stage can be defined as the time regime when the slope of $\log_{10}(\gamma_0 - \gamma(t))\ vs.\log_{10}(t)$ equals to ½. As shown in Figure C-1, the initial slope increased from 0.289 to 0.469 when the fitted time regime changed from 8s to 15s. Thus,

15s can be approximately taken as the time regime for early-stage fitting because the ½ power law predicted by theoretical models is followed. This method provides an option to define the length of fitted region for early stage kinetics study. However, as shown in Figure C-1(d), this method is very sensitive to γ_0. The value of γ_0 in (a) (b) and (c) is 72.8 mN/m, and the value in (d) is 71.5 mN/m. And the minor difference leads to a dramatic difference in the slope, the intercept, and the duration of early stage to ensure ½ slope. Thus, the log-log plot is not a reliable method to determine the time regime for early stage fitting unless the limitation is solved.

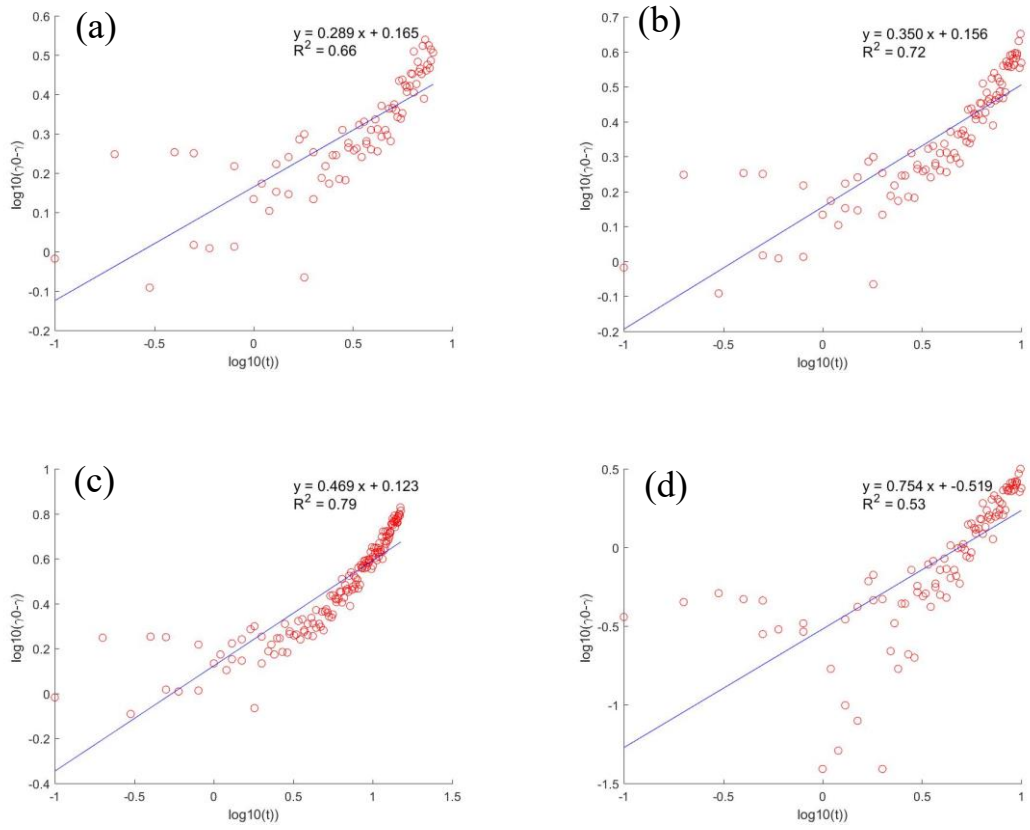

Figure C-1 Log-log plot with (a) 8s (b) 10s (c) 15s (d) 10s as fitting time regime. The γ_0 of (a)(b)(c) is 72.8 mN/m, and the γ_0 of (d) is the average of first five measurements.

C.4 References

[1] Bizmark, N.; Ioannidis, M. A.; Henneke, D. E., Irreversible adsorption-driven assembly of nanoparticles at fluid interfaces revealed by a dynamic surface tension probe. *Langmuir* **2014,** *30* (3), 710-717.

[2] Nelson, A.; Wang, D.; Koynov, K.; Isa, L., A multiscale approach to the adsorption of core–shell nanoparticles at fluid interfaces. *Soft matter* **2015,** *11* (1), 118-129.

[3] Dugyala, V. R.; Muthukuru, J. S.; Mani, E.; Basavaraj, M. G., Role of electrostatic interactions in the adsorption kinetics of nanoparticles at fluid-fluid interfaces. *Physical Chemistry Chemical Physics* **2016,** *18* (7), 5499-5508.

[4] Gyulai, G.; Kiss, É., Interaction of poly (lactic-co-glycolic acid) nanoparticles at fluid interfaces. *Journal of Colloid and Interface Science* **2017,** *500*, 9-19.

[5] Kutuzov, S.; He, J.; Tangirala, R.; Emrick, T.; Russell, T.; Böker, A., On the kinetics of nanoparticle self-assembly at liquid/liquid interfaces. *Physical Chemistry Chemical Physics* **2007,** *9* (48), 6351-6358.

[6] Ferdous, S.; Ioannidis, M. A.; Henneke, D., Adsorption kinetics of alkanethiol-capped gold nanoparticles at the hexane–water interface. *Journal of Nanoparticle Research* **2011,** *13* (12), 6579-6589.

[7] Fang, S.; Chen, T.; Chen, B.; Xiong, Y.; Zhu, Y.; Duan, M., Graphene oxide at oil-water interfaces: Adsorption, assembly & demulsification. *Colloids and Surfaces A: Physicochemical and Engineering Aspects* **2016,** *511*, 47-54.

[8] Li, Z.; Geisel, K.; Richtering, W.; Ngai, T., Poly (N-isopropylacrylamide) microgels at the oil–water interface: adsorption kinetics. *Soft Matter* **2013,** *9* (41), 9939-9946.

APPENDIX D. CHALLENGES IN OIL-COATED BUBBLE FLOTATION WITH PRELIMINARY STUDIES

There are still some challenges associated with the flotation deinking and the most important one is the failure in froth formation by oil itself. As a result, oil with ink particles adsorbed on the oil-water interface cannot stay on the surface of ink suspension and oil droplets with ink will recirculate back into the ink suspension. This appendix shows some efforts in solving the problem.

D.1 Dynamic interfacial tension

Figure D-1 shows dynamic interfacial tension of ink suspension-air and ink suspension-silicone oil interfaces. The surface tension didn't show any significant decrease, indicating that ink particles cannot adsorb to air-water interface. However, oil-water interface tension dropped significantly in the first 100s. This further proves that ink particles can only adsorb to oil-water interface.

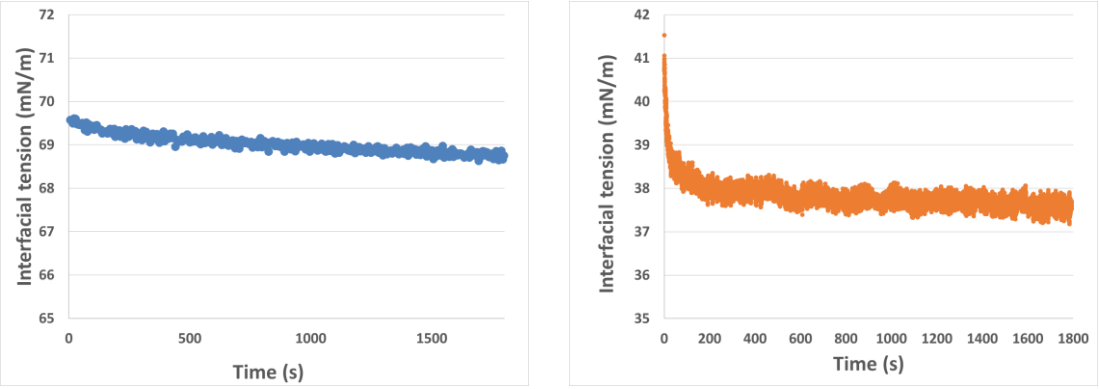

Figure D-1 The effect of ink particles adsorption on (left) air-water surface tension and (right) oil-water interface tension.

D.2 Effect of CTAB on particle size, particle zeta-potential

In order to generate froth during flotation, surfactant CTAB was added to ink suspensions and its impact on ink stability and ink adsorption on oil-water interfaces is shown in Table D-1. CTAB, a cationic surfactant was chosen, because surfactants have a larger diffusion coefficient than particles and adsorb to interface faster. CTAB at interface can reduce the adsorption energy barrier by attracting negatively charged ink particles onto interface. In most of conditions in Table D-1, the stability of ink particles is a good indicator for its adsorption on oil-water interface. If the ink particles are destabilized by CTAB or NaCl, they will agglomerate because the interparticle electrostatic repulsion forces are screened. In the meantime, particle-interface electrostatic repulsion forces are also screened which leads to the ink particle adsorption to interface. The only exceptions are when CTAB concentration is greater than 0.1mM. In these conditions, in particles cannot adsorb to oil-water interface even if particles are destabilized. One possibility is the competition between CTAB and ink particles that there is no space left on interface for particle adsorption. Thus it is important to find a surfactant that can stabilize froth (air-water interface) while allowing particle adsorption on oil-water interface. Another alternative solution is to dissolve surfactants or other chemicals that have specific interactions with ink particles, and can stabilize froth, into oil phase.

Table D-1 The effect of CTAB and NaCl concentration on ink size, zeta-potential and adsorption on oil-water interface.

CTAB concentration (mM)	Salt concentration (mM)	Size (nm)	Zeta-potential (mV)	Precipitation observed?	Adsorb on oil-water interface?
0	0	150	-65	N	N
0	100	450	-25	Y	Not clear
0	200	N/A	N/A	Y	Y
0.005	0	140	-24	N	N
0.005	100	1126	-12.3	Y	Y
0.01	0	1000	-7	Y	Y
0.05	0	170	30	N	N
0.05	100	1400	16.9	Y	Not clear
0.05	1000	N/A	N/A	Y	Y
0.1	0	140	20.5	N	N
0.1	100	1226	13.2	Y	N
0.2	400	N/A	N/A	Y	N